Articles provided:

. Luis Gonçalves, Rui Martins, António Ferrari, Realtime Parallel Software Implementation of a DS-CDMA Multiuser Detector, published online, in Microprocessors and Microsystems, Elsevier, July 2021. **First realtime implementation of a complex DS-CDMA detector involving inversion of matrices.**
https://doi.org/10.1016/j.micpro.2021.104051

. Luís Gonçalves, Diogo Cunha, Method to Determine the Delay between Measurements in two or more Spectrum Analyzers or Power Meters, Recent Advances in Communications and Networking Technology, Bentham Science Publishers, Volume 5, Issue 2, August 2016. **English version of the patent. New method to measure time delays through measure of powers with a linear conversion from the latter on the former.**
http://dx.doi.org/10.2174/2215081105666161128142559

. Deepaknath Tandur, Jonathan Duplicy, Kamran Arshad, David Depierre, Janne Lehtomäki, Keith Briggs, Luis Gonçalves, Atilio Gameiro, MME Approach for Cognitive Radio Systems Evaluation: Measurement, Modeling and Emulation in IEEE Vehicular Technology Magazine (special issue on applications of cognitive radio networks), Volume 7, Issue 2, pages 77-84, June 2012.
Article output from project FP7 – QoSMOS. First Triennium FCT PostDoc.
http://ieeexplore.ieee.org/stamp/stamp.jsp?tp=&arnumber=6182685

. L. Mendes, L. Gonçalves, A. Gameiro, GSM Downlink Spectrum Occupancy Modeling in IEEE International Symposium on Personal, Indoor and Mobile Radio Communications (PIMRC'11), Toronto, Canada, 10-14 September 2011 Interesting Analysis of the Measurement Setup. Modeling of GSM Spectrum Occupancy. **Article of Spectrum Occupancy that states that Time between opportunities distribution and Time period of opportunities distribution has a decay Exponential Distribution.**
http://ieeexplore.ieee.org/stamp/stamp.jsp?tp=&arnumber=6140021

. L. Gonçalves, A. Gameiro, *Erratum: Multi-Sensor Frequency Domain Multiple Access Interference Canceller for DS-CDMA Systems*, European Transactions on Telecommunications, Wiley & Sons, Volume 19, Issue 4, Page 495, June 2008, **Article with several crucial corrections to ETT article principally in several equations. These equations were used by other authors articles a posteriori.**
http://doi.wiley.com/10.1002/ett.1297

. L. Gonçalves, A. Gameiro, Multi-Sensor Frequency Domain Multiple Access Interference Canceller for DS-CDMA Systems in European Transactions on Telecommunications (ETT), Wiley & Sons, Volume 18, Issue 3, Pages 263–273, April 2007, **Article of Reference of the use of Fresh Filters in Frequency Domain in Multiuser Detection in DS-CDMA Systems. This detector has advantages in relation to MMSE detector in an implementation in WCDMA-TDD or TD-CDMA (Popular Republic of China)**.
http://doi.wiley.com/10.1002/ett.1146

Realtime Parallel Software Implementation of a DS-CDMA Multiuser Detector

Luís Carlos Gonçalves*, Rui Escadas Martins†,
António Brito Ferrari†
*Instituto de Telecomunicações, 3810-193 Aveiro, Portugal
†Instituto de Engenharia Electrónica e Telemática de Aveiro (IEETA), Universidade de Aveiro, 3810-193 Aveiro, Portugal
Emails: lgoncalves@av.it.pt, rmm@ua.pt, ferrari@ua.pt
Link DOI: https://doi.org/10.1016/j.micpro.2021.104051

***Abstract*—In this article the complexity and runtime performance of two Multiuser Detectors for Direct Sequence-Code Division Multiple Access were evaluated in two different hardware platforms. The innovation and aim is to take advantage of present parallel hardware to bring Multiuser technology to present and future Base Stations in order to increase the capacity of the overall system, to reduce the transmission power by the mobile stations and to reduce base station hardware requirements, in Universal Mobile Telecommunications System. The detectors are based on the Frequency Shift Canceller concatenated with a Parallel Interference Canceller. This detector implies the inversion of multiple identical size small matrices and because of that it is very scalable contrary to other solutions/detectors that only permit a sequential implementation despite their lower complexity. Implementations for the Time Division-Code Division Multiple Access, in two software platforms one in OpenMP and the other in CUDA were done taking into account the carrier and doppler frequency offsets (offset different for each user). The result shows that this deployment aware real-time implementation of the Multiuser Detectors is possible with a Graphics Processor Unit being three times faster than required.**

***Index Terms*—Heterogeneous Computing, Real Time Implementation, High Performance Computing, Frequency Shift Canceller, Parallel Interference Canceller, Multiuser Detection**

I. Introduction

Third Generation Universal Mobile Telecommunications System-Time Division Duplex (UMTS-TDD) specs define three chip rates for transmission: 7.68MChips/s, 3.84MChips/s and 1.28MChips/s. The latter is the one used in the People's Republic of China since 2007 with 1.28Mchips/s and it is named Time Division-Synchronous Code Division Multiple Access (TD-SCDMA).

The hardware of the base stations are actually upgraded several times during a decade to meet the technology advances. Better Multiuser Detection (MUD) has the potential to increase the spectral efficiency and wireless network coverage in the uplink of base stations, as to increase the energy efficiency in mobile stations. It can also decrease the number of diversity antennas in the base station, thereby decreasing costs in hardware and also increasing energy efficiency. Depending on the age and provider of those base stations the upgrade can be done through a board connected to a backplane or connected through optic fiber to a standalone card or computer.

MUD algorithms could be deployed in mobile station receivers and base stations receivers from the UMTS-TDD standard in all chip rates: 1.28 MChips/s, 3.84 MChips/s and 7.68 MChips/s. In this work a possible implementation in base stations, in uplink is studied. MUD application to the uplink is transparent to the mobile stations with the specifications having no restrictions about using it.

At uplink the signal received at the base station has passed through different (transmission) channels. MUD is used in the receiver and acts over the sampled spread signal at baseband with the goal of cancelling the other user's signals (Multiuser Access Interference (MAI)) to recover the user of interest.

The use of MUD includes some single user detector functionality because it needs to deal with the channel distortion of the portion of the received signal related to the user of interest. The MUD detectors like the Minimum Mean Square Error Detector (MMSE) and the Frequency Shift Canceller (FSC) can be integrated in a RAKE [1] (composed structures) and can be concatenated with a Parallel Interference Canceller (PIC) or a Serial Interference Canceller (SIC) to improve even more its performance. The concatenation with a SIC is more appropriate for downlink because of the power differences of the users' signals components of the signal received in each mobile station and with a PIC for uplink because of similar receiving signals power of the different users in the base station. In [2]–[4] such composite structures with multiuser, single user and spatial processing using configurations including the FSC concatenated with a PIC were studied.

The order of complexity of the optimal multiuser detector (OMUD) [5], or maximum likelihood detector, is exponential and hence not physically realizable. Different algorithms to reduce the complexity and find solutions whose Bit Error Rate (BER) comes close to the optimum have been proposed.

The FSC belongs to the category of Frequency Shift Filters (FRESH) [6] which has structures that use the existing correlation between frequency bands of man-made signals.

The MMSE detector [7]–[9] implies the inversion of a large diagonal matrix typically with LsUxLsU size (Ls is the number of symbols in a slot and U the number of

users). This is in an ideal case, as typically the upsampling and channel length must also be taken into account. It is to be expected that much larger memory resources would be needed for the implementation of such algorithm. Also the MMSE Algorithm is not so scalable as the FSC given the latter has decoupled user processing and multiple small matrix inversions.

Despite Iterative Multiuser Detection being claimed as a less complex solution [10], it is an iterative procedure and so its implementation must be sequential (serial). Also, it might not converge to the right solution.

Genetic Algorithms-based multiuser detectors have been proposed by a number of authors ([11], [12] and citations within). These algorithms are not as scalable in terms of parallel computation because the software code used to recover concurrently DS-CDMA users diverges. To the best of our knowledge, no implementations of such algorithms that satisfy the strict timing requirements have been reported.

With the emergence of integrated parallel processor architectures and the availability of parallel extensions to programming languages [13], [14] (like OpenMP, and CUDA both extensions of C) many algorithms that were previously too complex can now be efficiently implemented in software. This paper reports on the implementation of DS-CDMA MUD in multicore processors and in parallel heterogeneous architectures with GPUs. There has been previous work reported on the use of GPUs for interference cancellation in CDMA communications [15]. The execution times reported are in the range of seconds to tens of seconds for 20,000 bits, whereas a real-time implementation requires a maximum execution time of 1.4ms for 1,408 bits.

As far as is the knowledge of the authors, this work is innovative in the sense that it is the first realtime implementation of DS-CDMA MUD in parallel architectures with Graphical Processor Units (GPUs), making possible their incorporation in base stations.

In [16], [17] can be found single elementar tasks than can be done by GPUs and in [18] with other Parallel Architectures like the Intel Xeon Phi. In [19], [20] can be found full algorithms implemented in GPUs.

In the past, simpler Multiuser Detectors (PICs and Sequential Detectors) were implemented in Field-Programmable Gate Arrays (FPGAs) [21]–[23] and GPUs [15]. And signal processing algorithms applied to Radars were explored in [24].

Previous work of the authors, concerning this subject was presented in [25].

In Section II the basics of DS-CDMA systems, and details of the MUD detectors implemented, are presented. In Section III the implementation done of the Multiusers Detectors, in OpenMP and CUDA are described. In Section IV the complexity and performance analysis are analyzed. And finally in Section V, the main conclusions are stated.

II. Detectors with the Frequency Shift Canceller

A baseband Direct Sequence-Spread Spectrum (DS-SS) signal, for one user and spreading sequences of spreading factor of Q_{max}, is represented at the receiver (base station) by

$$s_i^l(t) = \sum_k a_{kD+l}^i \, g_i^l(t - kT) \tag{1}$$

where $\{a_{kD+l}^i\}$ is the information symbol sequence, l is the index of the spreading sequence , i is the user index, $1/T$ is the symbol rate and $g_i^l(t)$ is the *signature waveform*. $g_i^l(t)$ is given by

$$g_i^l(t) = \sum_{q=0}^{Q_{\max}-1} \widetilde{c}_i^l p(t - qT_c) * h_i(t) \tag{2}$$

for the maximum spreading factor of the system (SF=Q_{max}), where $\{\widetilde{c}_i^l\}$ is the spreading sequence of index l, $p(t)$ the normalized elementary pulse[1], T_c is the chip period, $h_i(t)$ is a linear filter representing the impulsional response of the transmission channel and the symbol * represents the convolution operation.

Multiple signals $s_i^l(t)$, of multiple transmitting users and corresponding spreading sequences, are received and are superimposed in the time and frequency in the base station.

Table I
Simulation Parameters

Number of Users	16
Number of Antennas	2
Number of Taps per antenna	2
Spreading Factor	16
Chip Rate	1.28 MChips/s
Modulation	QPSK
Channel	GBSBEM [26], [27]
Mobiles Speed	50 Km/h
PathLoss Exponent	3.8
Maximum Delay Spread	4.0 μs
UpSampling Factor	8
Line of Sight Distance of Mobiles	600 m
Number of bits simulated	10 Million

A Data Symbol is a complex number and it can represent several bits encoded in phase and amplitude. The mapping of Bits in Symbols is named modulation *i.e.* Quadrature Phase Shift Keying (QPSK), 8-Phase Shift Keying (8-PSK), 16-Quadrature Amplitude Modulation (16-QAM) with different mapping each one.

For proper operation of the Multiuser Detector a discrete version of the signature sequence represented by $g_i^l(t)$ must be generated/replicated in the receiver.

The mobile stations are commanded in such way that the signals in the base station in one uplink slot are superimposed and due to non-ideal conditions not totally synchronized. The policy of a Multiuser Detector is to cancel the interfering users signals, named Multiple Access Interference (MAI) from the user of interest. Due to the effect of the Transmission Channels even with synchronism the user's signals are not orthogonal. Such detectors also

[1]Impulse Response of the Raised Cosine

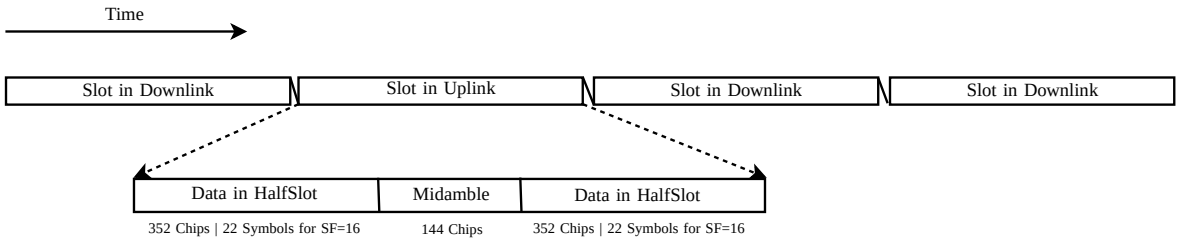

Figure 1. Transmission in Slots. Definition of HalfSlots. Information for 1.28MChips/s

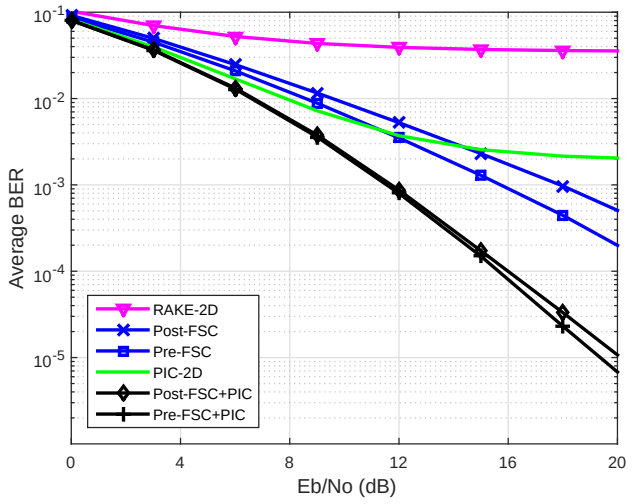

Figure 2. Performance (BER) for QPSK, SF=16 and 2 receiver diversity antennas.

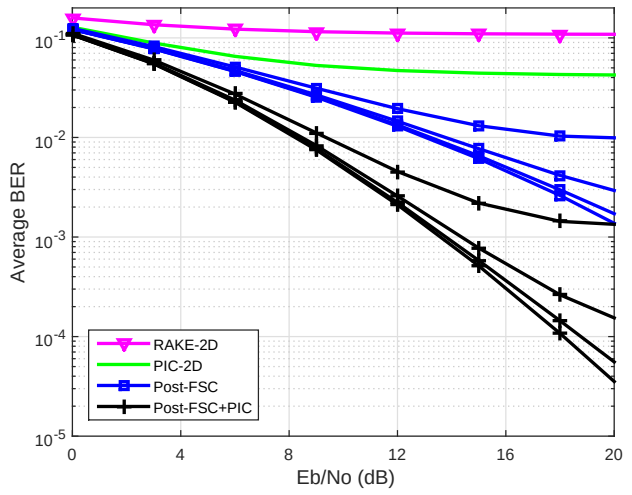

Figure 3. Performance (BER) for QPSK, SF=16 and 2 receiver diversity antennas with different upsamples in the receiver. Curves with decreasing performance (upwards) of Post-FSC and Post-FSC+PIC: non-degradation (or ideal) case, upsample of 16, 8 and 4. The curves of the RAKE and PIC are for non-degradation (or ideal) case.

have some single user functionality (*i.e.* RAKE) that reduces the impairment introduced by the Transmission Channel of the user of interest.

The signal to noise ratio can also be improved by having several receiving antennas in the base station.

The format of a slot in a TD-SCDMA frame is depicted in Figure 1. In [2]–[4], [25] are defined two configurations for the Multiuser detector one named Pre-FSC [25, Fig. 1] and the other Post-FSC [25, Fig. 2] either concatenated with a Hard-PIC [25, Fig. 3]. These schematics are reflected in Algorithm 1 and Algorithm 2 respectively. A good description of the FSC canceler can be found in [2].

In the case of a standalone implementation, the Frequency Shift Algorithm is well adapted to single user processing (different from joint detection in MMSE where all users must be detected at the same time) because the processing is decoupled from the other users even if it needs to know which users are active. The algorithm proposed in [2]–[4] does not need large matrix inversions (18x18 for 1.28 Mchips (China) and 3.84Mchips/s (Europe)).

The proposed implementation is for 1.28MChips/s but it is easily configurable for 3.84MChips/s. Despite the fact that in this work, the case of 16 users of spreading factor (SF) of 16 is treated, the detector supports the mix of other lower spreading factors. For example, one user of spreading factor 4 is treated as 4 users (16/SF=4) of spreading factor 16 [2]–[4], in both the FSC and the PIC. Also the detector allows a mix of QPSK, 8PSK and 16-QAM modulations.

This detector is valid for Beamforming and for Spatial Diversity if it is given the correspondent channel to do the processing. The frequency offset impairment between the carrier in the transmitter plus the doppler offset due to movement and the reference carrier in the receiver can be compensated at the end of the receiver chain because each user spread spectrum signal remains cyclostationary with that offset. It is considered that the doppler offset is equal for the paths in each user transmission channel. Because the midamble interval (Figure 1) and the Carrier Frequency Offset, the bits on each side of the slot must be recovered separately. In the case of joining the two sides, each user signal looses the cyclostationary.

Simulations of the BER versus the Energy of the Bit to Noise Ratio (Eb/N0) were performed with the parameters given by Table I, for the Pre-FSC and Post-FSC configurations. These parameters were chosen in order to reflect a medium size cell (600m line of sight, $4\mu s$ Maximum Delay Spread) in a typical high damping scenario (3.8 Path Loss Exponent). Figure 2 depicts the results. All the taps are aligned with the samples by default (non-degradation (or ideal) of performance case) and the upsample is the same in the whole simulation chain. While the Pre-FSC in standalone performs slight better than the Post-FSC, when concatenated with the PIC the performance is significantly better and both configurations, Pre-FSC+PIC and Post-FSC+PIC, have similar performances.

In real conditions the first tap, with greater amplitude,

Algorithm 1 Multiuser Detector Code Description of Pre-FSC+PIC Configuration

```
Load data (Burst, Channel)
Generate Signatures Waveforms in Discrete Fourier domain without Channel impairment
Generate Fast Fourier Transform (FFT) of Root Raised Cosine(RRC) and Raised Cosine
Start statistics, Start counting time
Filter with Root Raised Cosine the input Burst (one for each antenna), It is kept a discrete time domain and a discrete frequency domain copy, BURSTANTn (discrete time domain)
Generate the Noise Power Density at the input of the FSCs (from the estimate of the noise power, number of symbols per user in a half slot and the RRC filter)
Parallel begin nusers
    Generate Signatures Waveforms with Channel Impairment for the user correspondent to the thread and each antenna
    Barrier
    for nantennas do
        Frequency Shift Canceller
        Matching Filter to user channel at the antenna
        Accumulate
    end for
    Downsampling (correspondent operation in Discrete Fourier domain) by the upsampling factor
    Matching Filter to the Spreading Code
    Downsampling(correspondent operation in Discrete Fourier domain)by the Maximum Spreading Factor of the system
    Inverse Fast Fourier Transform
    Symbol Demodulation
    Reconstruction of the user signal with Channel impairment from the bits for each antenna, USERiANTn
    Barrier
    Sum of the all users reconstructed signals for each antenna and with channel impairment, SUMANTn (operation divided by the threads equally). Each thread sum, one subset of the samples, through the users at each antenna.
    Barrier
    for nantennas do
        Cancellation (BURSTANTn-SUMANTn+USERiANTn)
        Matching Filter (discrete time domain operation) to the antenna user channel
        Accumulate
    end for
    Downsampling by the upsampling factor
    Correlation (equivalent to Matching Filter) to the Spreading Code
    Downsampling by the Maximum Spreading Factor of the system
    Symbol Demodulation
Parallel end
Stop statistics, Stop counting time
```

Algorithm 2 Multiuser Detector Code Description of Post-FSC+PIC Configuration. Only shown the diferences from Algorithm 1

```
...
...
Parallel begin nusers
    Generate Signatures Waveforms with Channel Impairment (the channel includes Maximum Ratio Combining before FSC) correspondent to the thread (nusers signatures each thread)
    for nantennas do
        Matching Filter to user channel at the antenna
        Accumulate
    end for
    Frequency Shift Canceller
    ...
    ...
Parallel end
...
```

of each user's channel are not aligned[2] between the users, causing an increase in the BER. Figure 3 shows how the BER improves when upsampling factors of 4, 8 and 16 are used for the Post-FSC and Post-FSC+PIC. Contrary to the simulations in Figure 2 the profile of each user transmission channel suffers a delay with an uniform distribution between zero (0) and 4 Chips ($3.125\mu s$) representing the imprecision of the time advance[3]. In this simulation chain the sampling factor of the Transmitter and the Channel was 128 (8x16) increasing the Channel time representation precision. Figure 3 shows that with an upsampling of 16 the BER curve is very close to the "ideal" case, represented by the bottom curve. It also shows that for Eb/No < 12 an upsampling of 8 virtually has no degradation in BER, *i.e.* in such conditions there is no advantage in using higher upsampling factors. The curves of the performance of the RAKE and the PIC are for the case when the taps are aligned with the samples by default (ideal). The curves for the Pre-FSC(+PIC) are not represented because they are similar, but not equal, to the Post-FSC(+PIC).

[2]The others taps are already not aligned.

[3]The advance in time that each mobile station must provide in transmission in order that all users signals are synchronized (by leading tap) in the base station.

III. Implementation

Both the Pre-FSC+PIC and Post-FSC+PIC were implemented in serial code, in OpenMP and in CUDA (version 10.0) in a computer with a i9-9900K CPU (8 cores, with AVX2) with a RTX2070 Graphic Processing Unit (GPU) and a computer with i7-8750H Processor (6 cores, AVX2) with a GTX1050Ti GPU. Both CPUs feature hyperthreading. Eclipse with *gcc* was used in both platforms. The CPUs and GPUs are connected through a PCIe3 bus in both platforms.

Nvidia GPU architecture has evolved through several generations, featuring increased GFlops ratings and faster and more unified CPU-GPU memory models. The RTX2070, based in the Turing architecture features 36 Streaming Multiprocessors (SMXs) each with 64 streaming processor (SP) cores. The 4 MByte Outer Cache is common to all the SMXs. The GTX1050Ti is based on the Pascal architecture. It has 6 SMXs, each with 128 SP cores, and a 1MByte outer cache.

The serial code was used to measure the complexity in Millions of Single Precision Floating Point Operations with PAPI[4] and to take the reference runtime in both machines. The serial code runtimes were taken at maximum/Turbo 5GHz Clock of the i9-9900K and at maximum/Turbo 4.1GHz Clock of the i7-8750H.

The comparison between the single precision and the double precision versions showed that single precision had less than 1% relative error in the symbols (before quantization) recovered by the FSC and the PIC. Hence, single precision was used for the computations.

The target time to recover both Half Slots (HSs) is about 1.4ms considering one single carrier with half of the slots used for the uplink. In order to take full advantage of the parallel processing power of the GPUs, instead of processing 1 HS at a time a set of 36 half slots were acquired to be processed simultaneously. This maximizes the use of the SMXs present in each architecture while keeping the extra delay introduced within bounds that do not affect the quality of the communications, corresponding to a maximum latency of 25.7ms[5] which added to the processing time must be below 150ms, the maximum acceptable delay in one way call path. The latency of acquiring the HSs for the processing will be shorter in the case of a basestation with multiple carriers or/and multiple scrambling codes where the 36 HSs can be obtained faster. The serial code was evaluated for 1 HS, the runtime for 36 HSs being 36x higher.

OpenMP was used to parallelize the code in both platforms. Algorithm 1 presents the description of the Multiuser Detector Code for the Pre-FSC+PIC configuration and Algorithm 2 shows the differences from Algorithm 1 for the Post-FSC+PIC configuration. The implementation is the same for the i9 and the i7. Because the processing for recovering each user in the detector with FSC is (almost) decoupled of the processing to recover the other users, 16 threads, one for each user, were created. The PIC has an identical structure to the Pre-FSC but the equivalent operations between the two are made in the time domain instead. As can be seen inside the parallel section of the code of both algorithms there are barrier instructions to synchronize the data between threads. The first barrier, present only in Algorithm 1, guarantees that the Channel Impaired Signature Waveforms of each user (thread) needed by all threads are all generated when needed. The second barrier, in both Algorithms, guarantees that the reconstruction of each spread signal (in each thread) from the bits detected by the detector with FSC is completed when needed. This operation is part of the PIC detector. The third and last barrier, also in the PIC code, guarantees the generation of the sum of all reconstructed users when needed.

The algorithms were also implemented using CUDA. The implementations made for the RTX2070 and GTX1050Ti were the same with no differences in the grid and block sizes because the number of SMXs in the RTX2070 is a multiple of the number in the GTX1050Ti. The implementation was made with more than 20 kernels for each implementation (two Pre-FSC+PIC implementations and two Post-FSC+PIC implementations). Each kernel is called once, and does the processing for the 16 users, 36 HSs at once. There is only one copy from host (CPU) to device (GPU) with the initial data and another from device to host with the final bits (data of all 36 HSs). Between host to device kernel calls the data remains all the time in the GPU external memory. Synchronization between the kernels (like the barriers in OpenMP) was not needed. Since there is no CPU code between kernels, consecutive kernels in the same CUDA stream are serialized. The block sizes for the kernels were dimensioned in order to use the maximum number of SMX registers with the active warps[6]. Generally, a maximum block size of 128 (1024 possible) was used, mostly for simple wide equal operations kernels like the combining or accumulate. A reduction of more than 10% in global execution time was achieved with this kind of optimizations. With more complex kernels (like the FSC) and high degree of parallelism the amount of L1 cache used by each thread is very small and has little impact on the performance. For the case of 1HS it was necessary to reduce the block size and increase the number of blocks in order to have a better distribution of the processing through all the SMXs. It was not necessary to use atomic operations. Also there is little code divergence[7] accross the kernels. There was no runtime advantage to use nested parallelism either in CUDA or in OpenMP. In the case of the Post-FSC+PIC implementations, given that the Downsamplings and Matched Filter had the same grid and block sizes, they were included in the FSC kernel with almost no increase in the runtime relative to the FSC when processed alone, due to the reduction of time in passing the data to the next kernel.

In the Pre-FSC configuration the number of signatures generated (in each HS), which are discrete frequency sig-

[4] *http://icl.cs.utk.edu/papi/*

[5] 14 slots allocated to uplink in 2 frames and 4 slots of a third frame for a total of 25.7ms, totalizing 36 HSs.

[6] A warp is set of 32 synchronous threads that are executed at same time with the same code.

[7] Divergence means, in synchronous threads running the same code, some need to follow a different code path and the others wait that path converges with the own *e.g.* an *if else*

nals, is equal to the number of users times the number of antennas (see Algorithm 1) and in the Post-FSC configuration the number of signatures generated is equal to the number of users squared (see Algorithm 2). Hence, in the latter the number of signature waveforms does not increase with the number of antennas, but they are more demanding to compute because their number is higher. The Post-FSC was implemented in two configurations, one in which the impaired signature waveforms are generated directly in the discrete frequency domain[8] (with transcendental functions, sine and cosine) from previously ones generated offline without the impairment (in the frequency domain but through FFTs in the time domain) and the other in which the signature waveforms are generated from scratch in the time domain and then they are converted to the discrete frequency domain by the FFTs. The former is less complex but the latter permits to do the cancellation with the users signals affected with carrier plus doppler frequency offsets making it more suitable in practice. Affecting the signature waveforms with the carrier plus doppler frequency offsets must be done in the discrete time domain because in the discrete frequency domain the offset is a fraction of a sample. In the time domain the phase of (signature waveforms) samples must be affected by a linear increasing or decreasing angle.

In both implementations (OpenMP and CUDA) the code for the inversion of the matrices was taken from CLAPACK[9]. The code was inlined and cleaned of redundancy to make a single block of code embedded in the FSC function or kernel. The functions used from CLAPACK were *cpptrf* and *cpptri*. The first does the Cholesky decomposition in single precision and the latter finds the invert of the matrix having the result of the decomposition. Only the lower part of the matrices are stored. Other approaches of CUDA implementations of matrix inversions with Cholesky decomposition can be seen in [28], [29]. This solution has better performance than the native CUDA matrix inversion functions because when using them it is necessary to split the FSC in several kernels originating more accesses to the video main memory to pass the data between the kernels thereby increasing the latency.

In the CPUs there is some runtime warm-up between consecutive runs. For the serial code (with 1HS) the data and code fits in the L3 cache. In the case of the GPUs there is practically no warm-up as the data is everytime moved from CPU to GPU. There is warm-up related to transfer of the compiled kernels code in the first run and not in the subsequent runs.

IV. Complexity Results and Performance Discussion

Tables II and III show the complexity in Millions Floating Point Instructions, runtime (Wall time) for serial code for the i9 and i7 and runtime for CUDA for the RTX2070 and GTX1050Ti. The execution time of the serial implementations largely exceeds the 0.7ms (half of 1.4ms) target for 1 HS for all the different algorithms and configurations, with the execution times for the Post-FSC+PIC more or almost than double the times for the Pre-FSC+PIC.

Figure 4 shows the results of the profiling of the simultaneous CPU cores usage (CPU time which is different from Wall time) in the i7, with OpenMP, given by Intel's VTune profiler. The profile shows that the average CPU usage is about 7.5, which is a value typical for applications with an average amount of parallelism. This compares with a theoretical maximum of 12 that corresponds to the 6 cores running 2 simultaneous threads each. Figure 4 shows that during a significant part of the overall processing time less than 4 threads are executing. This is due to the fact that 16 threads are launched with the processor supporting a maximum of 12 threads running concurrently. However execution times feature a large variance, incompatible with the real-time requirements of the application.

When the GPUs are used the speedup achieved over the correspondent serial implementation figures also in Tables II and III both for 36 HSs and for a single one. When processing 1 HS at a time, the RTX 2070 and the GTX1050Ti do not achieve real time for the detectors that are implementation aware (Time Domain Sig. Wave. generation). Comparing the speedups achieved by the GPUs for 1HS they are of the same order of magnitude in both GPUs. Despite the RTX2070 be a much powerful GPU, the resources required to process 1HS is a small set of those resources and because of that the GTX1050Ti rivalizes with it in processing power. The full potential of the RTX2070 is revealed with the processing of simultaneous 36 HS. The joint processing of 36 HS roughly doubles the speedup in relation to the 1HS case for the GTX1050Ti, while the speedup increase for the RTX 2070 is much higher, reaching 104.2 times in relation to single thread CPU case for the Post-FSC+PIC with Time Domain Signatures Generation and 2 antennas.

In CUDA, the runtime includes the data transfer time between the CPU and GPU and back needed in a real-time implementation as well as the small CPU runtime. The arrays from the FSC kernel are stored in the GPU main memory. The amount of available cache memory (principally L2) correspondent to this main memory is important because the FSC kernel has many no coalescent accesses. The shortest execution times were achieved with a single thread program invoking the kernels. In all implementations, each time the FSC is called, 32 x 16 x nHS matrix inversions are made (nHS - number of HalfSlots), for 1.28MChips/s, for 16 users and 1 antenna. This number of matrix inversions is multiplied by the number of antennas for the Pre-FSC+PIC configuration whereas it remains constant in the configuration Post-FSC+PIC.

In CUDA with 36 HSs processing, the Post-FSC+PIC with Time Domain Signatures Generation, despite being more complex than correspondent Pre-FSC+PIC for 2 antennas, has better runtimes because it has only half of the threads (and half of the matrix inversions) launched by the FSC kernel and so less L2 cache constraints. That does not happen for 36HSs, 1 antenna where the Pre-FSC+PIC has better runtimes.

In the case of Post-FSC+PIC with Time Domain Signa-

[8]The FSC needs the signature waveforms in the frequency domain
[9]*http://www.netlib.org/clapack/*

		MFPI	i9 (Serial)		RTX2070 CUDA	
1 ant, 1HS	Pre+PIC, Time Domain Sig Gen	52.7	7.4ms	1x	1.22ms	6.1x
	Pre+PIC, Transcendentals	47.31	6.6ms	1x	1.2ms	5.5x
	Post+PIC, Time Domain Sig Gen	138.1	23.2ms	1x	1.3ms	17.8x
	Post+PIC, Transcendentals	58.1	11.9ms	1x	0.69ms	17.2x
1 ant, 36HS	Pre+PIC, Time Domain Sig Gen	1897.2	0.2664s	1x	5.1ms	52.2x
	Pre+PIC,Transcendentals	1703.2	0.2376s	1x	4.9ms	48.5x
	Post+PIC, Time Domain Sig Gen	4971.6	0.8352s	1x	7.8ms	107.1x
	Post+PIC,Transcendentals	2091.6	0.4284s	1x	5.4ms	79.3x
2 ant, 1HS	Pre+PIC, Time Domain Sig Gen	93.38	12.7ms	1x	1.24ms	10.2x
	Pre+PIC, Trancendentals	82.61	11.0ms	1x	1.23ms	8.9x
	Post+PIC, Time Domain Sig Gen	144.0	24.6ms	1x	1.4ms	17.6x
	Post+PIC,Trancendentals	73.1	20.0ms	1x	0.72ms	27.8x
2 ant, 36HS	Pre+PIC, Time Domain Sig Gen	3361.7	0.4572s	1x	9.4ms	48.6x
	Pre+PIC, Transcendentals	2964.0	0.396s	1x	10.6ms	37.4x
	Post+PIC, Time Domain Sig Gen	5184	0.8856s	1x	8.5ms	104.2x
	Post+PIC, Transcendentals	2631.6	0.720s	1x	6.0ms	120.0x

Table II

PERFORMANCE DATA. RTX2070. UPSAMPLE EQUAL TO 8 AND THE NUMBER OF TAPS EQUAL TO 2. IT IS ASSUMED THAT THE COMPLEXITY FOR 36HS IS 36X OF THE 1HS. IT IS ASSUMED ALSO THAT THE TIME FOR SERIAL FOR 36HS IS 36X OF THE 1HS. HS - HALF SLOTS, MFPI - MILLION FLOATING POINT INSTRUCTIONS. . THE I9 IS A 8 CORE HYPERTHREADING CPU A MAXIMUM/TURBO 5GHZ CLOCK AND A 16MBYTES L3 CACHE

		MFPI	i7 (Serial)		GTX1050Ti CUDA	
1 ant, 1HS	Pre+PIC, Time Domain Sig Gen	52.7	9.55ms	1x	1.12ms	8.5x
	Pre+PIC, Transcendentals	47.31	8.4ms	1x	1.11ms	7.6x
	Post+PIC, Time Domain Sig Gen	138.1	28.9ms	1x	1.67ms	17.3x
	Post+PIC, Transcendentals	58.1	15.1ms	1x	1.35ms	11.2x
1 ant, 36HS	Pre+PIC, Time Domain Sig Gen	1897.2	0.3438s	1x	20.4ms	16.9x
	Pre+PIC,Transcendentals	1703.2	0.3024s	1x	19.9ms	15.2x
	Post+PIC, Time Domain Sig Gen	4971.6	1.0404s	1x	30.6ms	34.0x
	Post+PIC,Transcendentals	2091.6	0.5436s	1x	21.6ms	25.2x
2 ant, 1HS	Pre+PIC, Time Domain Sig Gen	93.38	16.3ms	1x	1.69ms	9.6x
	Pre+PIC, Trancendentals	82.61	14.1ms	1x	1.66ms	8.5x
	Post+PIC, Time Domain Sig Gen	144.0	30.4ms	1x	1.75ms	17.4x
	Post+PIC,Trancendentals	73.1	25.0ms	1x	1.43ms	17.5x
2 ant, 36HS	Pre+PIC, Time Domain Sig Gen	3361.7	0.5868s	1x	38.7ms	15.2x
	Pre+PIC, Transcendentals	2964.0	0.5076s	1x	37.5ms	13.5x
	Post+PIC, Time Domain Sig Gen	5184	1.0944s	1x	32.9ms	33.3x
	Post+PIC, Transcendentals	2631.6	0.900s	1x	24.2ms	37.2x

Table III

PERFORMANCE DATA. GTX1050TI. UPSAMPLE EQUAL TO 8 AND THE NUMBER OF TAPS EQUAL TO 2. IT IS ASSUMED THAT THE COMPLEXITY FOR 36HS IS 36X OF THE 1HS. IT IS ASSUMED ALSO THAT THE TIME FOR SERIAL FOR 36HS IS 36X OF THE 1HS. HS - HALF SLOTS, MFPI - MILLION FLOATING POINT INSTRUCTIONS. . THE I7 IS A 6 CORE HYPERTHREADING CPU WITH A MAXIMUM/TURBO 4.1GHZ CLOCK AND A 9MBYTES L3 CACHE

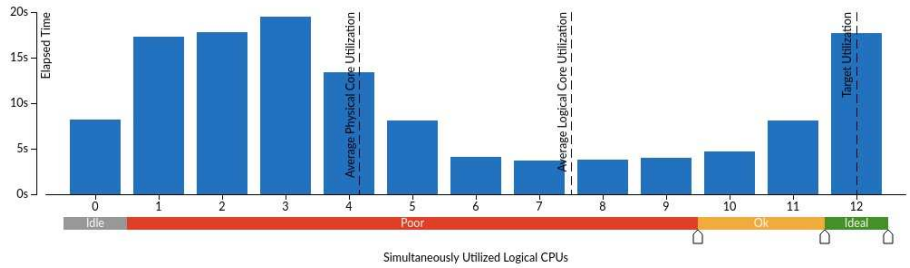

Figure 4. Bar Diagram given by Intel's Vtune profiler for Post-FSC+PIC, Time Domain Sig Gen, 2 antennas, 1HS with OpenMP on the i7 and 10000 continuous iterations. CPU with six Physical Cores and twelve Logical Cores.

Kernels	GTX1050Ti	RTX2070
FSC (Op. Ratio 66.6%)	84.7%	86.1%
FFTs Signatures(Op. Ratio 11.8%)	3.2%	3.3%
PIC Cancellation+Max-Rat-Comb (Op. Ratio 3.2%)	3.8%	2.4%
PIC Signals Reconstruction from Pre-FSC bits(Op. Ratio 2.2%)	2.5%	2.1%

Table IV

PERCENTAGE OF THE RUNTIME OF THE SEVERAL KERNELS IN PRE-FSC+PIC (WITH TIME DOMAIN SIGNATURES GENERATION), 2 ANT, 2 TAPS, UPS=8

Kernels	GTX1050Ti	RTX2070
FSC (Op. Ratio 75.1%)	86.1%	89.3%
PIC Cancellation+Max-Rat-Comb (Op. Ratio 3.6%)	3.9%	2.3%
PIC Signals Reconstruction from Pre-FSC bits (Op. Ratio 2.5%)	2.6%	1.9%

Table V

PERCENTAGE OF THE RUNTIME OF THE SEVERAL KERNELS IN PRE-FSC+PIC (WITH TRANSCENDENTALS), 2 ANT, 2 TAPS, UPS=8

tures Generation (for any number of antennas) more than half of the operations are from FFTs and they are done with a much optimized library *cuFFT* from Nvidia. As a consequence, one of the highest speedups relative to the serial implementation and highest performance in GFlops are achieved by the Post-FSC+PIC with Time Domain Signatures Generation.

Because the number of taps of the transmission channel concatenated with Combining, that is seen by the FSC block in the Post-FSC is larger (compared with the Pre-FSC

Kernels	GTX1050Ti	RTX2070
FSC+DownS+MatchedF+DownS (Op. Ratio 21.7%)	57.2%	58.9%
FFTs Signatures(Op. Ratio 61.4%)	23.0%	24.1%
PIC Cancellation+Max-Rat-Comb (Op. Ratio 2.1%)	4.9%	3.3%

Table VI
PERCENTAGE OF THE RUNTIME OF THE SEVERAL KERNELS IN POST-FSC+PIC (WITH TIME DOMAIN SIGNATURES GENERATION), 2 ANT, 2 TAPS, UPS=8

Kernels	GTX1050Ti	RTX2070
FSC+DownS+MatchedF+DownS (Op. Ratio 42.7%)	69.6%	73.4%
Signature Waveforms Generation (Op. Ratio 28.8%)	10.3%	8.2%
PIC Cancellation+Max-Rat-Comb (Op. Ratio 4.1%)	5.9%	4.0%
PIC Signals Reconstruction from Post-FSC bits (Op. Ratio 2.9%)	4.0%	3.4%

Table VII
PERCENTAGE OF THE RUNTIME OF THE SEVERAL KERNELS IN POST-FSC+PIC (WITH TRANSCENDENTALS), 2 ANT, 2 TAPS, UPS=8

that only sees the taps of the channel) and the number of transcendental operations (in Post-FSC+PIC with transcendentals) are proportional to that number, the Post-FSC+PIC (with transcendentals) has less performance (GFlops) with the sequential program in the i9 and i7. Those operations, beyond being slower ones, are not (auto)vectorized in Intel CPUs because the vectorization hardware does not support them. That does not happen in CUDA where the latency is hidden with the switching of *Warps*. That explains the great speedup of the Post-FSC+PIC with transcendentals, with CUDA with 36 HSs.

For the Post-FSC+PIC and Pre-FSC+PIC configurations (with two antennas, Time Domain Signatures Generation (deployment aware) and upsample of 8) the processing of the 36 HSs takes less than 25.7ms in the RTX2070, satisfying the time specifications of UMTS-TDD. In the same conditions the GTX1050Ti does not achieve the goal to process 36 HSs in less that 25.7ms making, in this situation, a embedded solution with a single GPU not viable.

The speedups achieved in the GPUs are mainly limited by the available memory bandwidth. The necessary external GPU memory for the FSC kernel to run for 36HS, 16 users, 18x18 size matrix inversions (redundant bands), is about 32.4MBytes of temporary memory (for the PostFSC) far more than the 4 MBytes of the Level 2 cache of the RTX 2070. The higher memory bandwidth available in the RTX2070 jointly with greater number of cores is the main reason of achieving higher speedups than the GTX1050Ti. On the other hand, performance being limited by the memory bandwidth and not by the amount of parallel execution engines, implies that increasing the number of HSs processed in parallel brings no performance advantage.

Tables IV, V, VI and VII give the percentage of runtime of the most time consuming kernels reported by the profiler together with the percentage of floating point operations in each kernel for the RTX2070 and the GTX1050Ti. It can be noticed in Table VI how *cuFFT* library (see the FFTs Kernel) is optimized, certainly with low level programming, by the high percentage of operations corresponding to lower percentage of the total runtime.

It was found that the RTX2070 with the Post-FSC+PIC with Signatures Generation from time domain, 2 antennas, 2 taps, 36HS, upsample of 8 in continuous run consumes about 149W (with a stable temperature of 73°C) on a maximum of 175W. In these conditions, the RTX2070 is running at 609.9GFlops. The GTX1050Ti with the same settings runs at 157.6GFlops. For achieving realtime processing, with the same settings, is needed at least 201.7GFlops.

V. CONCLUSIONS

The complexity and runtime of a deployment aware Multiuser Detector for uplink that takes into account the carrier plus doppler frequency offsets was evaluated to investigate the possibility of its deployment in UMTS-TDD Base Stations. It was shown that when the detectors are implemented on i9 or i7 platforms the execution times achieved largely exceed the timing deadlines of UMTS-TDD. On the other hand, heterogeneous CPU+GPU architectures deliver a real-time solution, in particular when the amount of parallelism of the GPU architectures is fully taken into profit by processing several UMTS-TDD Half Slots in parallel. The results presented show that execution times with the RTX2070 satisfy the time constraints for base stations with either 1 or 2 antennas for any implementation of the two detection algorithms. The GTX1050Ti is also a solution for base stations with a single antenna if the Pre-FSC+PIC detector, with Time Domain Signatures Generation, is used. A significantly increased performance can be expected with increased memory access bandwidth.

The high processing scalability of the proposed Multiuser Detector, due to the existence of many small equal size matrices to be inverted, must be highlighted making it a good candidate for deployment. That permits to increase the capacity of the system, to reduce the power emitted by the mobile stations or to use less hardware in the base station. This solution can be provided by the base stations manufacturers to the operator with several versions featuring increased upsampling rates.

The detectors were validated in a simulation chain, that gave the Bit Error versus the Energy of bit over noise spectral density (Eb/No), showing similar performances between them and showing the degradation of performance with the sampling rate in one of them. The BER curves show a detection quality similar to the best achieved by other algorithms reported in the literature of which no real-time implementation is known.

Future work in the case of commercial use, includes the implementation of these algorithms on FPGA[10] [30] to achieve better energy efficiency [31].

ACKNOWLEDGMENTS

The core of the work presented here was done while the first author was a post-doctoral researcher within IEETA/University of Aveiro with a grant from Fundação para a Ciência e Tecnologia (FCT), Portugal supported by POPH/FSE. Thanks are due to Prof Atilio Gameiro and to Instituto de Telecomunicações of Aveiro for providing the computers with the GPUs, to Prof Paulo Dias and IrisLab both from University of Aveiro, to Massive Lab from INESC TEC and to Eng Paulo Ribeiro from Vodafone Portugal.

[10]With new FPGAs, programmed in OpenCL, that have floating point units in each cell.

References

[1] J. G. Proakis and M. Salehi, *Digital Communications*. McGraw-Hill, Inc, Fifth ed., 2007.

[2] L. Gonçalves and A. Gameiro, "Multi-Sensor Frequency Domain Multiple Access Interference Canceller for DS-CDMA Systems," *European Transactions on Telecommunications, John Wiley & Sons, Ltd*, vol. 18, pp. 263–273, April 2007. http://doi.wiley.com/10.1002/ett.1146.

[3] L. Gonçalves and A. Gameiro, "Erratum: Multi-Sensor Frequency Domain Multiple Access Interference Canceller for DS-CDMA Systems," *European Transactions on Telecommunications, John Wiley & Sons, Ltd*, vol. 19, p. 495, June 2008. http://doi.wiley.com/10.1002/ett.1297.

[4] L. Gonçalves, *Detecção Multiutilizador no Domínio da Frequência para Sistemas DS-CDMA*. Ph. D. Thesis, Departamento de Electrónica, Telecomunicações e Informática, Universidade de Aveiro, Aveiro, Portugal, 2009. http://ria.ua.pt/bitstream/10773/2225/3/2010000093.pdf.

[5] S. Verdú, "Minimum Probability of Error for Asynchronous Gaussian Multiple-Access Channels," *IEEE Transactions of Information Theory*, January 1986. http://ieeexplore.ieee.org/document/1057121/?arnumber=1057121.

[6] W. A. Gardner, "Cyclic Wiener Filtering: Theory and Method," *IEEE Transactions on Communications*, vol. 41, January 1993. http://ieeexplore.ieee.org/document/212375/?arnumber=212375.

[7] A. Klein and P. W. Baier, "Linear Unbiased Data Estimation in Mobile Radio Systems Applying CDMA," *IEEE Journal of Selected Areas in Communications*, September 1993. http://ieeexplore.ieee.org/xpl/freeabs_all.jsp?arnumber=233218.

[8] A. Host-Madsen and K.-S. Cho, "MMSE/PIC multiuser detection for DS/CDMA systems with inter- and intra-cell interference," *IEEE Transactions on Communications*, vol. 47, pp. 291–299, February 1999. http://ieeexplore.ieee.org/xpl/freeabs_all.jsp?arnumber=752135.

[9] M. Vollmer, M. Haardt, and J. Götze, "Comparative Study of Joint-Detection Techniques for TD-CDMA Based Mobile Radio Systems," *IEEE Journal on Selected Areas in Communications*, vol. 19, August 2001. http://ieeexplore.ieee.org/xpl/freeabs_all.jsp?arnumber=942509.

[10] E.-L. Kuan and L. Hanzo, "Burst-by-Burst Adaptive Multiuser Detection CDMA: A Framework for Existing and Future Wireless Standards," *Proceedings of the IEEE*, vol. 91, pp. 278–302, February 2003. http://ieeexplore.ieee.org/xpl/freeabs_all.jsp?arnumber=1182063.

[11] A. Zahedi and H. Bakhshi, "Multiuser Detection Based on Adaptive LMS and Modified Genetic Algorithm in DS-CDMA Communication Systems," *Wireless Personal Communications, Springer*, vol. 73, pp. 931–947, 2013. https://doi.org/10.1007/s11277-013-1224-7.

[12] A. Zahedi, S. Rajamand, S. Jafari, and M. Rajati, "A Novel Multiuser Detector Based on Restricted Search Space and Depth-First Tree Search Method in DS/CDMA Communication Systems," *Wireless Personal Communications, Springer*, vol. 82, pp. 1531–1545, 2015. https://doi.org/10.1007/s11277-015-2297-2.

[13] M. D. McCool, "Scalable Programming Models for Massively Multicore Processors," *Proceedings of IEEE*, vol. 96, pp. 816–831, May 2008. http://ieeexplore.ieee.org/xpl/freeabs_all.jsp?arnumber=4490125.

[14] O. Schenk, M. Christen, and H. Burkhart, "Algorithmic performance studies on graphics processing units," *Journal of Parallel and Distributed Computing*, vol. 68, pp. 1360–1369, October 2008. https://doi.org/10.1016/j.jpdc.2008.05.008.

[15] F. Arguello, D. Heras, and M. Boo, "GPU detectors for interference cancellation in chaos-based CDMA communications," *Electronic Letters*, vol. 46, pp. 727–729, 13th May 2010. http://dx.doi.org/10.1049/el.2010.0915.

[16] X. Chen, L. Ren, Y. Wang, and H. Yang, "GPU-Accelerated Sparse LU Factorization for Circuit Simulation with Performance Modeling," *IEEE Transactions on Parallel and Distributed Systems*, vol. 26, pp. 786–795, March 2015. http://ieeexplore.ieee.org/xpl/freeabs_all.jsp?arnumber=6774937.

[17] G. Jo, J. Nah, J. Lee, J. Kim, and J. Lee, "Accelerating LINPACK with MPI-OpenCL on Clusters of Multi-GPU Nodes," *IEEE Transactions on Parallel and Distributed Systems*, vol. 26, pp. 1814–1825, July 2015. http://ieeexplore.ieee.org/xpl/freeabs_all.jsp?arnumber=6846313.

[18] M. Lu, Y. Liang, H. P. Huynh, Z. Ong, B. He, and R. S. M. Goh, "MrPhi: An Optimized MapReduce Framework on Intel Xeon Phi Coprocessors," *IEEE Transactions on Parallel and Distributed Systems*, vol. 26, pp. 3066–3078, November 2015. http://ieeexplore.ieee.org/xpl/freeabs_all.jsp?arnumber=6939728.

[19] C. G. Kim and Y. S. Choi, "Exploiting Multi -and Many-core Parallelism for Accelerating Image Compression," in *2011 Fifth FTRA International Conference on Multimedia and Ubiquitous Engineering*, (Crete, Greece), 28-30 June 2011. http://ieeexplore.ieee.org/stamp/stamp.jsp?tp=&arnumber=5992185.

[20] H. Su, C. Zhang, J. Chai, M. Wen, N. Wu, and J. Ren, "A High-Efficient Software Parallel CAVCL Encoder Based on GPU," in *2011 34th International Conference on Telecommunications and Signal Processing (TSP)*, (Budapest, Hungary), 18-20 Aug 2011. http://ieeexplore.ieee.org/stamp/stamp.jsp?tp=&arnumber=6043672.

[21] S. F. Swanchara, *An FPGA–Based Multiuser Receiver Employing Parallel Interference Cancellation*. Master of Science in Electrical Engineering, Faculty of the Virginia Polytechnic Institute and State University, Blacksburg, Virginia, July 22, 1998. https://vtechworks.lib.vt.edu/bitstream/handle/10919/36983/THESIS.pdf.

[22] A. O. Dahmane and L. Mejri, "FPGA Implementation of Block Parallel DF-MPIC Detectors for DS-CDMA Systems in Frequency-Nonselective Channels," *Journal of Electrical and Computer Engineering, Hindawi Limited*, 2008. http://dx.doi.org/10.1155/2008/435756.

[23] Z. Quan, J. Liu, and Y. Zakharov, "FPGA Implementation of DCD Based CDMA Multiuser Detector," in *2007 15th International Conference on Digital Signal Processing*, (Cardiff, UK), 1-4 July 2007. http://ieeexplore.ieee.org/stamp/stamp.jsp?tp=&arnumber=4288583.

[24] R. S. Perdana, B. Sitohang, and A. B. Suksmono, "A survey of graphics processing unit (GPU) utilization for radar signal and data processing system," in *2017 6th International Conference on Electrical Engineering and Informatics (ICEEI)*, pp. 1–6, Nov 2017. http://ieeexplore.ieee.org/document/8312430/?arnumber=8312430.

[25] L. C. Gonçalves, R. E. Martins, and A. B. Ferrari, "Software Parallel Implementation of a DS-CDMA Multiuser Detector," in *The 23rd International Conference on Software, Telecommunications and Computer Networks (SoftCOM 2015)*, (Split-Bol (Island of Brac), Croatia), 16-18 September 2015. http://ieeexplore.ieee.org/xpl/freeabs_all.jsp?arnumber=7314124.

[26] J. C. Liberti and T. S. Rappaport, "A Geometrically based Model for Line-of-Sight Multipath Radio Channels," in *IEEE 46^{th} Vehicular Technology Conference (VTC'96)*, (Atlanta, USA), 28 April - 1 May 1996. http://ieeexplore.ieee.org/xpl/freeabs_all.jsp?arnumber=501430.

[27] J. C. Liberti and T. S. Rappaport, *Smart Antennas for Wireless Communications: IS-95 and Third Generation CDMA Applications*. Prentice Hall, 1999.

[28] J. Kurzak, H. Anzt, M. Gates, and J. Dongarra, "Implementation and Tuning of Batched Cholesky Factorization and Solve for NVIDIA GPUs," *IEEE Transactions on Parallel and Distributed Systems*, vol. 27, pp. 2036 – 2048, July 2016. http://ieeexplore.ieee.org/xpl/freeabs_all.jsp?arnumber=7275187.

[29] A. Haidar, A. Abdelfattah, M. Zounon, S. Tomov, and J. Dongarra, "A Guide for Achieving High Performance with Very Small Matrices on GPU: A Case Study of Batched LU and Cholesky Factorizations," *IEEE Transactions on Parallel and Distributed Systems*, vol. 29, pp. 973–984, May 2018. http://ieeexplore.ieee.org/document/8214236/?arnumber=8214236.

[30] A. J. Maier and B. F. Cockburn, "Optimization of Low-Density Parity Check decoder performance for OpenCL designs synthesized to FPGAs," *Journal of Parallel and Distributed Computing*, vol. 107, pp. 134–145, September 2017. http://dx.doi.org/10.1016/j.jpdc.2017.04.001.

[31] K. Nagasu, K. Sano, F. Kono, and N. Nakasato, "FPGA-based tsunami simulation: Performance comparison with GPUs, and roofline model for scalability analysis," *Journal of Parallel and Distributed Computing*, vol. 106, pp. 153–169, August 2017. https://doi.org/10.1016/j.jpdc.2016.12.015.

Send Orders for Reprints to reprints@benthamscience.net

Method to Determine the Delay between Measurements in two or more Spectrum Analyzers or Power Meters

Luis Carlos Gonçalves[a*], Diogo Fernandes da Cunha[b]

[a] *Instituto de Engenharia Electrónica e Telemática de Aveiro, University of Aveiro, Aveiro, Portugal;* [b]*Marine Instruments S.A., Vigo, Spain;*

Abstract: The aim is to compute the time delay between the set of measurements in each of two or more Spectrum Analyzers using a linear relation between two dimensions (power and time). This method of time measurement implies to input in each Spectrum Analyzer two identical and synchronized Amplitude Shift Keying signals, each one modulated by a square wave of duty cycle of 50%. It is also valid with Direct Current. Instead of an input of an Amplitude Shift Keying signal (Radio Frequency /Microwaves) it is input a square wave and the power is measured with a Direct Current power meter with trigger.

Keyword: Amplitude Shift Keying (ASK), Direct Current, Power Meter, trigger by software, trigger by hardware, Spectrum Analyzer (SA), Spectrum Occupancy, Fusion

1. INTRODUCTION

The present invention is related with the computation of the time difference, between the start of the set of measurements of power (in one sweep) in two or more Spectrum Analyzers triggered by hardware, software or mix. The time difference is computed from the power measurement sets of the SAs. The difference between the time delays of the triggers on the SAs is the computed time. Those delay differences may be due to the hardware or software of the Spectrum Analyzers or because the signals of the triggers are not synchronized at first place.

In case of SAs with precise timings, this method can be used for computing the difference of delays of the signals of trigger generated by external circuits. That can be used, for example, to measure the difference of transmission time in two transmission lines or absolute transmission time in a single one and by that way to measure the length of a transmission line. It also allows measuring the degree of synchronization between simultaneous measurements in multiple SAs.

In order to verify the method or in other applications of the method, the SAs can be replaced by other power meters of Radio Frequency, Microwave or Direct Current, (DC) all with triggers.

This method of measurement implies the input of identical synchronous Amplitude Shift Keying signals resulted from the modulation of a carrier by a square wave of 50% duty cycle.

If the SAs are located far apart from each other the ASK signals must be synchronized in some way, *i.e.*, by Global Positioning System (GPS). If co-located, a common ASK signal can be split in equally powered signals by a signal splitter/divisor. The method permits the correction of the computed time difference in case the ASK signals do not have the same measured power due to calibration errors on the SAs or unbalanced signal division on the splitter. The computed signal, from all sweep points, representing time, shows a good precision, in case of having a periodic maximum top flatness representing the true delay difference. That precision happens when the period of time computed is much greater than the temporal imprecisions of the instruments, and in the case of the computed time be about the period of the ASK signal divided by 4. The method is also applicable in DC with a positive square wave with duty cycle of 50% and with DC power meters with trigger. All the theory is applicable the same way.

In Section 2 is presented the functionality of the main apparatus of this work, the Spectrum Analyzer. The main theoretical work, which final result is the computed time equation, is presented in Section 3. In Section 4, the theoretical determination of the precision of the method is done. In Section 5, the applicability of the method is presented. The experiment to test the method is described in Section 6. The results obtained by applying the method are presented in Section 7. Finally, the conclusions are outlined in Section 8.

*Address correspondence to this author at the Instituto de Engenharia Electrónica e Telemática de Aveiro, University of Aveiro, Aveiro, Portugal; E-mail: luisgo@ua.pt

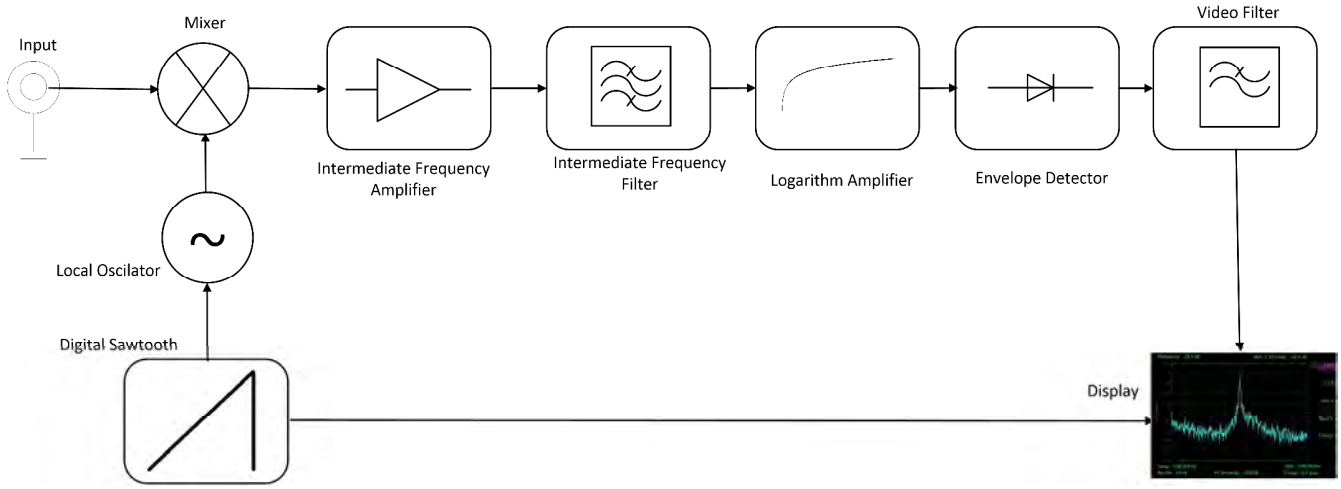

Figure 1 Heterodyne Spectrum Analyzer

2. SPECTRUM ANALYZERS

The main component of the measuring setup in this work is the Spectrum Analyzer. This section will give insight about this apparatus. Figure 1 shows a simplified conceptual schematic of a heterodyne Spectrum Analyzer used in this work. The information on the input signal's level is contained in the level (in its envelope) of the Intermediate Frequency (IF) signal. For this reason, after Intermediate Frequency Filter (Resolution Filter with Resolution Bandwidth (RBW)) be performed, this IF signal's envelope is determined. The procedure for doing this is comparable to the demodulation of an AM signal, which means that it is possible, for instance, to employ an analog envelope demodulator. The filtered IF signal is rectified and the RF signal components can be eliminated by a lowpass filter named Video Filter. After the envelope smoothed by the Video Filter, it is displayed **[1]**. The logarithm filter before the rectifier permits to increase the range of the signal to be displayed.

In modern Spectrum Analyzers the signal is sampled at Intermediate Frequency and all forward processing is done digitally. Before sampling the Spectrum Analyzer has several cascaded Intermediate Frequency stages, with decreased IF thru that chain.

Then it is enumerated the main parameters to set in a Spectrum Analyzer

- Number of equal spaced frequency points of the sweep: This is a setting that only can take some predefined values (*i.e.* 501, 1001, 2001, later represented by *I* points). Usually is an odd number to include both limits of the band. In this work, a set of *I* sweep points is named as a *section*.
- Pair: Start and Stop Frequency (StartBand and StopBand respectively) or Pair: Center Frequency and Frequency Span (CenterFrequency and SPAN respectively). Determines the bandwidth in which the sweep points are spanned.

$$StartBAND = CenterFreq - SPAN/2 \quad , \quad StopBAND = CenterFreq + SPAN/2$$

  In case of SPAN=0 all measurements points are made at the same frequency
- Resolution Bandwidth (RBW) . Bandwidth of the measurement in turn of the frequency of the sweep point. Better practice is to made

$$(I-1)*RBW = StopBAND - StartBAND$$

- Video Bandwidth (VBW) – Filter to smooth the IF envelope. Must be, in our case, 3-10 times the bandwidth of the Resolution Filter.
- Sweep Time – It is the accumulated time of the measurements, in all sweep points. It takes in account the settling times of the filters (RBW Filter and VBW Filter). Then the sweep time in each point is not the total sweep time divided by the number of sweep points. That only happens for SPAN=0.
- Detector Type (*i.e.* RMS) The detector used in this work is the RMS that gives information of the power.

3. DETAILED DESCRIPTION OF THE INVENTION

In Figure 2, one example of a setup for indirect measurement of the time difference between the start time of the measurements (A8) of two SAs (B4 and B5, Figure 2, Figure 3, Figure 4) is shown. In this setup (Figure 2), the trigger is made by hardware in one SA and in software in the other. The time instant of the start of the measurement, in the SA with trigger by hardware is deterministic. In the SA with trigger by software the instant of time of measurement start is randomness.

In Figure 3, the setup with two SAs triggered by software (triggered through commands transmitted through Ethernet) and in Figure 4, another setup with two SAs triggered by hardware (with the trigger inputs), from one Card commanded and Power supplied by USB (Universal Serial Bus) with digital TTL outputs (B8, acronym CARD) are shown. The Card is programmed by USB by a Portable Computer (B1).

In each SA, one ASK signal of equal power (which are not really equal due to asymmetries in the signal splitter) is injected thru a Signal Splitter (B3). The measurement is made with the SAs central frequency setting equal to the carrier frequency and SPAN equal to zero. The Resolution Bandwidth setting in the SAs must be such that it includes in excess the bandwidth of the ASK signal which it must be determined from visualization of the ASK signal in the SA, with adequate SPAN and Resolution bandwidth.

In Figure 5, the ASK wave with two time measurement windows of power, each representing one point of the sweep in each SA, is shown.

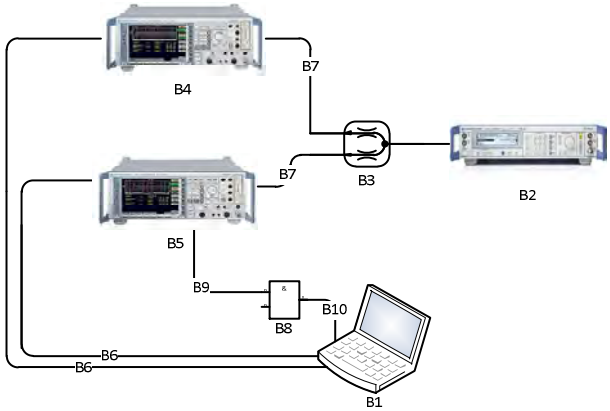

Figure 2 Measurement Setup 1 (one), B1– Portable Computer, B2 – Signal Generator (ASK generator), B3 – Signal Splitter, B4, B5 – Spectrum Analyzers, B6 – Ethernet Connection (Double Port Ethernet Card), B7 – SMA Cable, B8 – Card of TTL digital outputs commanded and Power supplied by USB (Universal Serial Bus), B9 – Cable connected to the trigger input of the Spectrum Analyzer, B10 – USB Cable.

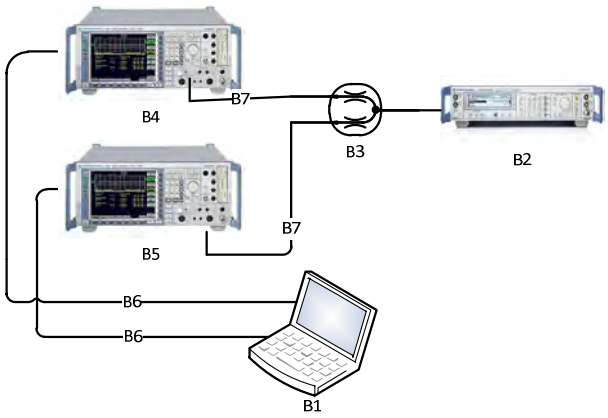

Figure 3 Measurement Setup 2 (two), B1 – Portable Computer, B2 – Signal Generator (ASK generator), B3 – Signal Splitter, B4,B5 – Spectrum Analyzers, B6 – Ethernet Connection (Double Port Ethernet Card), B7 – SMA Cable

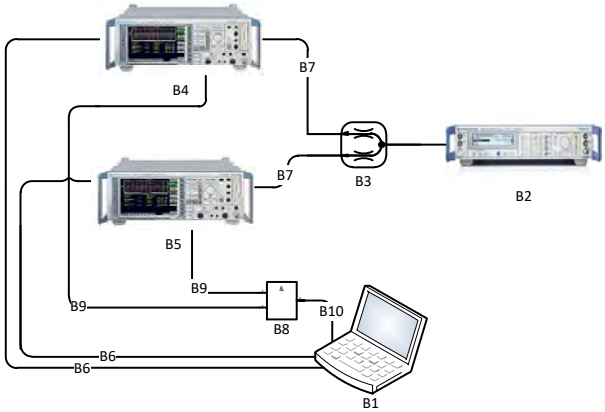

Figure 4 Measurement Setup 3 (three), B1 – Portable Computer, B2 – Signal Generator (ASK generator), B3 – Signal Splitter, B4,B5 – Spectrum Analyzers, B6 – Ethernet Connection (Double Port Ethernet Card), B7 – SMA Cable, B8 – Card of TTL digital outputs commanded and Power supplied by USB (*Universal Serial Bus*), B9 – Cable connected to the trigger input of the Spectrum Analyzer, B10 – USB Cable

Initially, the sweep point time (T_{sw_p}, A7) is set as half of the period of the ASK signal ($T_{ASK}/2$, A9). Notice that in each SA the sweep time will be the number of sweep points multiplied by such time ($T_{ASK}/2$, A9). For SPAN equal to zero the settling times of the Resolution and Video Filters are zero [2] in page 76.

In approximation it can be considered that at each sweep point the SA measures the energy and then it is divided by the interval of time of the measurement to compute the power.

In this case, the value of the time difference in the SAs (given in Figure 5 by T_{Δ_i}, A8) is linearly related to the Energy difference between them (as states Figure 5). In this perfect scenario, with $T_{sw\_p} = T_{ASK}/2$, from each sweep point is obtained the same result for T_{Δ_i} for all *i*. The wave

representing time computed from all sweep points is a flat line.

T_{Δ_i} corresponds to the energy $T_{sw\_p}\left|P^i_{SA_1}-P^i_{SA_2}\right|$, $T_{ASK}/2$ corresponds to energy $T_{ASK}P_{ASK}$:

$$T_{\Delta_i}=\frac{T_{sw\_p}\left|P^i_{SA_1}-P^i_{SA_2}\right|}{T_{ASK}P_{ASK}}\frac{T_{ASK}}{2}=\frac{\left|P^i_{SA_1}-P^i_{SA_2}\right|}{2P_{ASK}}T_{sw\_p} \quad (1)$$

where $P^i_{SA_1}$ and $P^i_{SA_2}$ are the measured powers (linear, if the measurements are made in a logarithm scale as dBm they must be converted to Watt) in each sweep point *i* in each SA (SA_1 and SA_2, B4 and B5). P_{ASK} is the power of the ASK signal injected in each SA. The other variables are displayed in Figure 5.

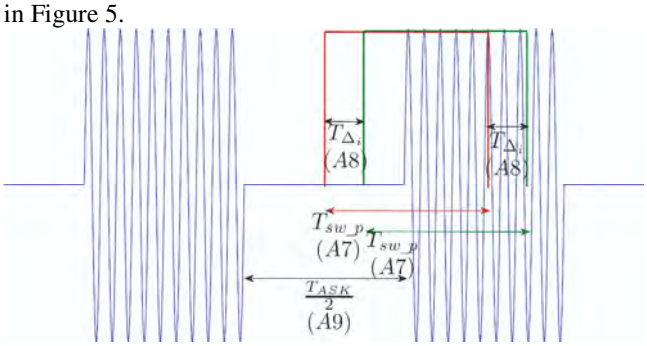

Figure 5 Rectangles – Measurement temporal Windows in two SAs in one point of the sweep, Sine wave of 50% Duty Cycle – ASK Signal.

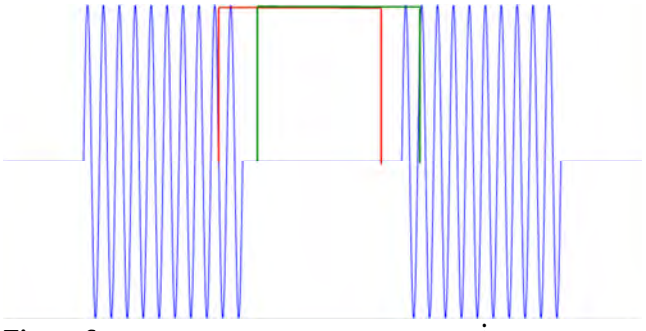

Figure 6 Case in which T_{Δ_i} is about zero for all i.

It may happen that the relative time phase of the measurements to be of Figure 6 and in that case the power difference and computed time is zero for all *i*. One way to solve this problem is to make the measurement time in each sweep point slightly greater than half period of ASK signal in such way that the relative time phase will change through the sweep points. The time between time instants of the start of the measurement in the two SAs continues to be given by Equation 1. The value of Equation 1 through *i* index of the sweep points changes periodically from zero to a maximum, differently from before in which the values kept constant. The maximum is the difference between the time instants.

P_{ASK} can be directly measured in each sweep *section* (because $T_{sw\_p}>T_{ASK}/2$). There is a equality relation of the measured energy $T_{sw\_p}\underset{i\in\{1,\ldots,I\}}{\mathrm{MAX}}(P^i_{SA_1})$ and the energy of the ASK wave which gives

$$P_{ASK}=\frac{T_{sw\_p}\underset{i\in\{1,\ldots,I\}}{\mathrm{MAX}}(P^i_{SA_1})}{T_{ASK}} \quad (2)$$

where $\underset{i\in\{1,\ldots,I\}}{\mathrm{MAX}}(P^i_{SA_1})$ represents the maximum of the measured power in each *section* in the SA_1 (the SA chosen is irrelevant).

From here on, $i\in\{1,\ldots,I\}$ will be omitted from the equations.

Different calibration errors on the SAs and unbalanced attenuations in the signal splitter can be compensated (it is important to compensate one SA in relation to the other because the real values of variables involved are not available) with the following gain in power in the SA_2

$$G_\Delta=\frac{\mathrm{MAX}(P^i_{SA_1})}{\mathrm{MAX}(P^i_{SA_2})} \quad (3)$$

Replacing Equation 2 in Equation 1 and replacing the Equation 3 in Equation 1 it is obtained

$$T_{\Delta_i}=\frac{\left|P^i_{SA_1}-P^i_{SA_2}G_\Delta\right|}{\mathrm{MAX}(P^i_{SA_1})}\frac{T_{ASK}}{2} \quad (4)$$

In the expression $\left|P^i_{SA_1}-P^i_{SA_2}G_\Delta\right|/\mathrm{MAX}(P^i_{SA_1})$, the calibration errors of SA_1 are cancelled if the error is modelled with a gain.

4. PRECISION OF THE METHOD

The relative error of function F, in function of the errors of its variables, is given by

$$\frac{\Delta F}{F(x_1,x_2,\ldots.x_n)}=\frac{\sum_{j=1}^{n}\frac{dF}{dx_j}\Delta x_j}{F(x_1,x_2,\ldots.x_n)} \quad (5)$$

Thus, if there is a high precision the variables involving time and $P^i_{AS_1}-P^i_{AS_2}G_\Delta>0$ is reached to absolute error on computing the time difference

$$\Delta T_{\Delta_i}=\frac{T_{ASK}}{2}\frac{P^i_{SA_1}(\varepsilon_{11}-\varepsilon_{12})}{\mathrm{MAX}(P^i_{SA_1})}+\frac{T_{ASK}}{2}\frac{P^i_{SA_2}(\varepsilon_{22}-\varepsilon_{21})}{\mathrm{MAX}(P^i_{SA_2})} \quad (6)$$

where ε_{11} - Relative Error in the measurement of $P^i_{SA_1}$, ε_{12} - Relative Error in the measurement of $MAX\left(P^i_{SA_1}\right)$, ε_{21} - Relative Error in the measurement of $P^i_{SA_2}$, ε_{22} - Relative Error in the measurement of $MAX\left(P^i_{SA_2}\right)$.

Notice that in the same SA, the relative error can have the same signal and thus it can be an error cancellation effect.

Considering that the standard deviation of the relative error of measured power in the SAs is ε_r (best case [3], [4] typically 1.5%/100, but it was found in internet sites reporting errors as low as 0.4%) and for the worst case $\varepsilon_{12} = -\varepsilon_{11} = -\varepsilon_r$ and $\varepsilon_{21} = -\varepsilon_{22} = -\varepsilon_r$ thus

$$\left|\Delta T_{\Delta_i}\right| = \varepsilon_r T_{ASK}\left(\frac{P^i_{SA_1}}{\mathrm{MAX}\left(P^i_{SA_1}\right)} + \frac{P^i_{SA_2}}{\mathrm{MAX}\left(P^i_{SA_2}\right)}\right) \tag{7}$$

$$\frac{\left|\Delta T_{\Delta_i}\right|}{T_{\Delta_i}} = 2\varepsilon_r\left(\frac{P^i_{SA_1}\mathrm{MAX}\left(P^i_{SA_2}\right) + P^i_{SA_2}\mathrm{MAX}\left(P^i_{SA_1}\right)}{\left|P^i_{SA_1}\mathrm{MAX}\left(P^i_{SA_2}\right) - P^i_{SA_2}\mathrm{MAX}\left(P^i_{SA_1}\right)\right|}\right) \tag{8}$$

The theoretical relative error given by Equation 8, with $T_{ASK}/2 \cong 2T_\Delta$, being T_Δ the difference of time instants of the start of measurements (A8), is approximately 5% (for 1.5% of relative error of the power measurements). This is the worst case. Also the real relative error can be smaller if it is a cancelling effect of the error or if the precision of the SAs are better. The precision decreases with the increase of $T_{ASK}/2$ (A9) in relation to $2T_\Delta$. $T_{ASK}/2$ (A9) must be chosen big enough in order to compute the time instants difference expected but not too much in order to guarantee the precision. It is recommended that

$$\begin{gathered} T_\Delta < \tfrac{1}{2}\left(T_{ASK} - T_{sw\_p}\right) \\ T_{sw\_p} = \frac{T_{ASK}}{2}\left(1 + \frac{\delta}{100}\right) \\ \delta > 5 \\ \delta < 15 \end{gathered} \tag{9}$$

This set of Equations 9 calculates the period of ASK wave in function of the time to be computed. By Equations 9 the time to be computed must be smaller than approximately one quarter of the period of the ASK wave.

δ is a parameter which defines the percentage in which the point sweep time is greater to half of the period of the ASK wave. As defined by Equations 9 it is recommended that this percentage to be between 5 and 15.

These simultaneous conditions, expressed by Equations 9, guarantees that the waves presented in the Results (Section 7), have sufficiently large tops.

5. APPLICATION EXAMPLES

In the study of signal fusion in Cognitive Radio is necessary to do synchronous power measurements with two positions separated two hundred meters between measurement sets in order to measure shadow conditions. This is the follow up of measurement with a single setup [5] of Spectrum Occupancy with Global System for Mobile communications (GSM) bands. In Figure 7, the measurement campaign scenario for Cognitive Radio is shown. $P(t, s_1)$ (A5) is the power measured in SA_1.

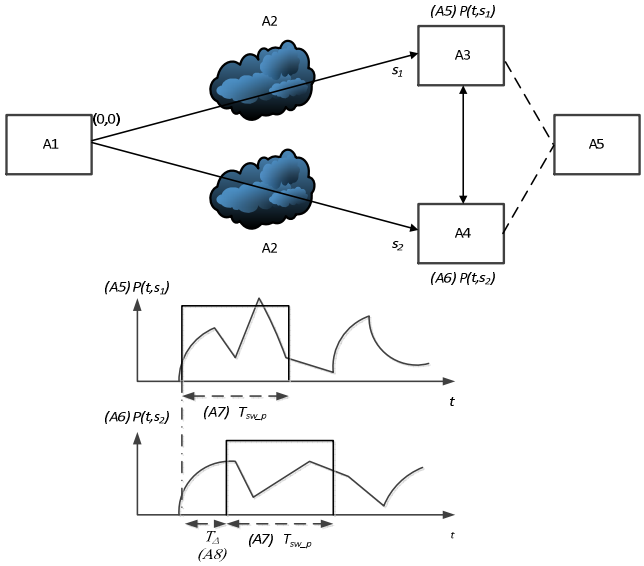

Figure 7 Measurement Campaign Scenario for Cognitive Radio. A1 – Base Station, A2 – Obstacles, A3 - Sensor (SA_1) with $P(t,s_1)$, A4 - Sensor (SA_2) with $P(t,s_2)$, A5 – Computer. The distance between sensors is less than 200 meters.

Each rectangle shows the temporal window of a sweep point measurement. For the measurements to be useful it is necessary that they are synchronized on the two or more SAs. The difference between time instants T_Δ (A8) is found with the proposed method. To obtain a good synchronism it is needed that $T_\Delta \ll T_{sw\_fusion}$ ([1] T_{sw_fusion} - measurement time period in each sweep point to do later the fusion). In [5] the sweep point time was 4.62ms, equal to the time of one frame of GSM. It was found that the time period between the start of the measurements in the SAs with hardware triggers (T_Δ, A8) was about $8\mu s$ which it is a good synchronism for the sweep point time equal to the GSM

[1] Do not make confusion with the sweep point time in the method to compute T_Δ (A8).

frame. This repeatable $8\mu s$ can be compensated with a manual command or by a software command doing a delay to the response to the trigger on the SA in advance.

Previous work on Spectrum Occupancy, with or without data fusion, was made by synchronism obtained by GPS [6] which it does not permit flexibility in the choice of the sweep time and it does not permit continuous measurements without time lapses. In other cases, the time measurement is made in computer networks, usually back to back in Media Access Control (MAC) layer and it involves considerable technological resources [7], [8]. In our case the method simplifies because the original system includes SAs that can measure power with precision.

This invention might origin Application Notes for brands of SAs as Rohde-Schwarz, Keysight, Tektronix, etc. One group of companies that can be interested in the industrialization of the invention are manufacturers of instruments to measure the delay difference in two (or more) transmissions lines. It can also measure absolute delays in transmission lines if one Input/Output TTL line is connected directly to the trigger of one SAs (or power meter) and the other Input/Output TTL line is connected to the transmission line in which the delay must be measured. This delay can be used to measure the length of transmission lines.

The invention can be enlarged to include Power Meters in Direct Current, with a squared wave instead the ASK wave. Thus, much more companies can be interested. A Power Meter of Direct Current has a much simpler technology and it broadens the applicability.

6. DESCRIPTION OF THE EXPERIMENT WITH TRIGGER BY HARDWARE IN BOTH SPECTRUM ANALYSERS

Mount the setup of Figure 4.

In the extremities of RG58 Cables (B9, Figure 4), each one with 90 meters, do the connections of Figure 8. The shield of the RG58 cable is connected to the 0V of the CARD (I3, Figure 8). In the SAs sides the shield is connected to the external of the connector of the trigger input (I4, Figure 8). Both cable terminations are protected from overshoot and undershoot voltages, with Schottky Diodes (I1, I2, I5, Figure 8) and one Zener Diode (I6, Figure 8). In the CARD (B8) side (L1, Figure 8) are protected with two Schottky Diodes (I1, I2, Figure 8, BAT85S model) because there is access to the Power Supply connections. In the SAs sides (triggers inputs, L2, Figure 8) are protected with Schottky Diode (I5, Figure 8) and a Zener Diode (I6, Figure 8, BZX79–C5V6 model) because there is no access to the higher voltage of Power Supply of the SAs.

Program manually the signal generator (B2, R&S, SMU200A, R&S®SMU-B9/-B10/-B1 options) to generate the ASK wave with the pretended period, changing the rate of Symbols/Bits in the Baseband Block. Greater periods of the modulating squared wave can be obtained with Data Patterns (selecting Patterns in Baseband window) with consecutive 1s, followed by consecutive 0s. The period of ASK wave can be found by Equations 9.

Not known in advance the time to compute T_{Δ}, the ASK signal period (T_{ASK}) must be tried till the right measurement is achieved. T_{ASK} must be chosen in order to compute in excess the expected time. One way to test the period of the ASK signal (T_{ASK}), it is to change it one small percentage and if it gives a different computed time it is because T_{ASK} is not the right one yet.

Program also the ASK modulation on the signal generator, ASK modulation index of 100%, rectangular filter in baseband with internal clock and internal data. In the Radio Frequency (RF) section of the signal generator define the carrier frequency, and the power level of the carrier in order that all the signal (total power, including all the bandwidth of the ASK signal) to be at least 30dB higher than the noise power, but not too high in order to respect the linear response of the SAs, signal generator and splitter.

Run the Labview program in the Portable Computer (B1) to program the SAs (B4, B5. Rhode & Schwarz, FSP40 and FSQ8 models) with the sweep time (T_{sw_p} times the number of sweep points), number of sweep points (this parameter can only take certain values determined by SAs maker), RMS measurements, SPAN=0, carrier frequency, resolution bandwidth (measure previously manually the bandwidth of the signal ASK with a SA, with the setting SPAN different from zero) and the video bandwidth (3-10 times the measurement bandwidth) and put the SAs in waiting mode of a hardware trigger. This programming is done by the Portable Computer through two Ethernet Cables (B6, STP – Shielded Twisted Pair, direct connection without repeaters) with more than 90 meters (< 100 meters), one to each SA. In the Portable Computer side there is a double Ethernet Card (with two ports, 100BaseT).

Then the Labview program switches simultaneous the two lines of Output TTL (B8, same byte Output) of the CARD (with Push-Pull outputs), from approximately 0V to 5V. The two SAs must do the measurement due to the trigger (signal trough RG58 cables, D9). The voltage level in which the SAs do the trigger must be equal in both SAs and in the Positive Edge or Negative Edge (in this case the switch must be done from 5V to 0V) in both.

Read the measurements (group of sweep points, named as *sections*, in floating point format) from the SAs through the Ethernet connections, to the Portable Computer and save them to the disk.

Compute Equation 4 for each sweep point and obtain each *section* of Figure 10 ahead (using all the points). It can be used the same Portable Computer that it reads the measurements from the SAs to make the computations and generate the graphics with a program as the Matlab.

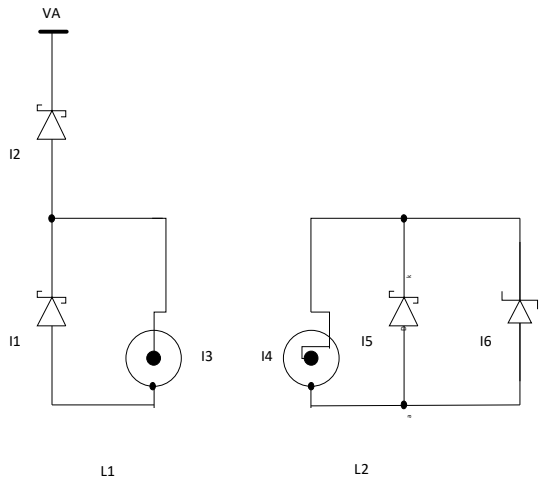

Figure 8 Connections of the Zener Diode and Schottky Diodes for the voltage limitation in both ends of the cable RG58 in which is transmitted the trigger signal. I1,I2,I5 – Schottky Diodes, I6 – Zener Diode, I3,I4 – Endings of RG58 cables. L1 – Card of TTL digital outputs commanded and Power supplied by USB (*Universal Serial Bus*) end side, L2 – Spectrum Analyser end side, VA – 5 Volts from Card commanded and Power supplied by USB (*Universal Serial Bus*) of TTL digital outputs.

The measurements can be made with more than 2 SAs (*n* SAs). Thus it is generated the trigger in $n > 2$ TTL Outputs (the signal splitter has *n* outputs also). Read the measurement sets with *n* Ethernet Cables connected to *n* SAs. But the computations are made in groups of 2 measurements (sets) (2 at a time) from 2 SAs until cover all SAs.

7. RESULTS

In Figure 9, several *sections*, each representing one sweep, of computed time difference from power measurements in two SAs (B4, B5) triggered by software (scenario of Figure 3) are presented. It represents four *sections* of 501 sweep points each. The parameters are $T_{sw\_p} = 21ms$, $T_{ASK} = 40ms$ and $P_{ASK} = 0.44\mu W$ ($-33.56dBm$). As it can be seen, the difference of time instants (A8) is given by the maximum which does not change during one *section*. The real relative error can be considered small taking in consideration the flat tops of the *section* waves. No repeatable computed times (in different *sections*) can be due to time differences in the processing on the SAs and lack of synchronism sending the commands, through Ethernet Cables (B6), by the computer.

Figure 10 shows the measures in a scenario of two SAs (B4, B5) triggered by hardware (scenario Figure 4). To compute the difference of instant of time of approximately $8\mu s$, it was used $T_{ASK} / 2 = 100\mu s$. The trigger voltage levels in the two SAs were 1.4V, positive edge. The computed time can be due to different delays in response to trigger signals of the SAs and to different delays introduced by the external circuits to the SAs. Despite the lack of flat tops of the *section* waves, the measured value has better repeatability than in the experiment with triggers by software (see the tops between *sections*). The lack of flat tops is due to the fact that the computed difference of time instants is no longer far greater than the time precision of the SAs and for the time computed ($8\mu s$) and for the chosen ASK signal period ($100\mu s$) the relative error given by Equation 8 is far greater (about 45%).

This method gives the relative delay between the start of the measurements on multiple SAs but it does not give which triggers first. That can be found, in the case of the experiment with triggers by software, doing a delay (by software, a fraction of the delay computed) in the software trigger command in one of the SAs. If the medium delay increases then this is the SA more delayed. In other way it is the SA in advance. In case of the experiment with triggers by hardware, the delay can be introduced in one of the outputs of the CARD (B8) that makes the trigger in one SA. Other way is introducing a delay to the reaction to the hardware trigger in one SA through a software command to SA (from the computer) or manually programming in the SA.

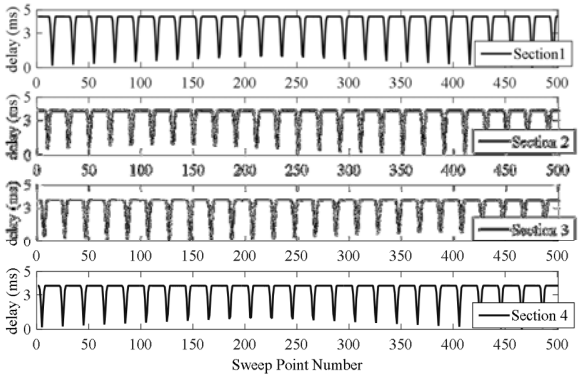

Figure 9 Computation Results of the difference between time instants of the start of the power measurements (in a sweep) between two SAs (Trigger by Software).

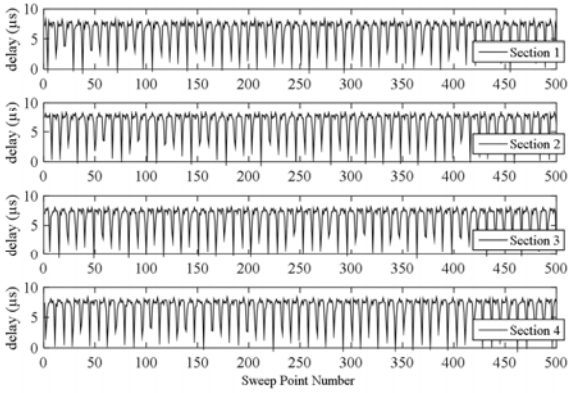

Figure 10 Computation Results of the difference between time instants of the start of the power measurements (in a sweep) between two SAs (Trigger by Hardware).

8. CONCLUSION

A new method to compute the time between the start of measurements in two or more SAs was presented. The method can have applications beyond the aim of the authors that it was to find out the better methods of trigger of SAs in order to achieve a better synchronism between measurements for spectrum occupancy for cognitive radio. Other application, it is to measure delays in transmission lines and so it length.

In the case of the time computed is far greater to the time imprecisions of the instruments and in case of the time computed be approximately one fourth of the ASK signal period, the computed time precision shows better results than the theoretical error reports. Beyond the fact that the theoretical error is for the worst case, the discrepancy can also be explained by the fact that in determination of the time, exists an error cancellation effect or/and the SAs precision, to measure power, is better than the specifications.

CONFLICT OF INTEREST

None.

ACKNOWLEDGEMENTS

We want to acknowledge the Portuguese Patent Reviewer and also from this Journal. Also to be acknowledged is the chair of the project QoSMOS at Institute of Telecommunications at Aveiro and Associate Professor at University of Aveiro, Prof. Atilio Gameiro.

This research was done during the stay of the authors in Institute of Telecommunications at Aveiro. This research was supported by Fundação para a Ciência e Tecnologia, Portugal and FP7, European Project QoSMOS and it gave up Portuguese Patent 107293.

References

[1] D. Liebl, Measuring with Modern Spectrum Analyzers, Educational Note, Rohde & Schwarz, Feb. 2013 .

[2] C. Rauscher, V. Janssen e R. Minihold, Fundamentals of Spectrum Analysis, Sixth ed., Rohde & Schwarz, 2008.

[3] *R&S FSQ Signal Analyzer Specifications,* Rhode & Schwarz.

[4] *Agilent PSA Series Spectrum Analyzers,* Data Sheet.

[5] L. Mendes, L. Gonçalves and A. Gameiro, "GSM Downlink Spectrum Occupancy Modeling," in *IEEE International Symposium on Personal, Indoor and Mobile Radio Communications (PIMRC'11)*, Toronto, Canada, 2011.

[6] M. Wellens, J. Riihijärvi, M. Gordziel e P. Mähönen, "Evaluation of Cooperative Spectrum Sensing Based on Large Scale Measurement," em *Third IEEE International Symposium on New Frontiers in Dynamic Spectrum Access Networks (DySPAN)*, Chicago, Illinois, USA, 2008.

[7] B. Ngamwongwattan e R. Thompson, "Measuring One-way Delay of VoIP Packets without Clock Synchronization," em *IEEE Instrumentation and Measurement Technology Conference (I2MTC 2009)*, Singapure, 2009.

[8] A. Hernandez e E. Magafia, "One-Way Delay Measurement and Characterization," em *Third International Conference on Networking and Services (ICNS 2007)*, Athens, Greece, 2007.

Received: Revised: Accepted:

COGNITIVE RADIO SYSTEMS EVALUATION

Measurement, modeling, and emulation approach

Deepaknath Tandur, Jonathan Duplicy, Kamran Arshad, David Depierre, Klaus Moessner, Janne Lehtomäki, Keith Briggs, Luis Gonçalves, and Atílio Gameiro

A vertically integrated approach is presented to evaluate the performance of cognitive radio (CR) systems. The approach consists of three pillars: measurement, modeling, and emulation (MME). This integrated approach enables the reproduction of the radio environment in laboratory conditions and aims to guarantee the same performance results as one would obtain in the field. This article provides a detailed explanation for each pillar along with state-of-the-art overviews. Finally, a test bed based on the MME approach is presented.

MME Approach

In today's wireless industry, it is generally accepted that the spectrum scarcity faced by the operators can be significantly alleviated by employing CR technology [1]. However, CR technology is still not mature, and it creates many challenges that have so far prevented its wide commercial deployment. Thus, it is critical that all stakeholders interested in CR, such as operators, device manufacturers, and regulators, have a clear understanding of the limitations and possibilities of this technology. An accurate characterization of the radio environment is therefore an essential task, as it will aid in understanding CR limitations.

In this article, we propose a new approach to bring realism into the technology assessment. The MME approach of the radio environment is shown in Figure 1. In general, the radio frequency (RF) scene is first measured over a range of frequencies, time instants, and locations. The data collected can then be converted to a mathematical model, which can further be emulated in a controlled environment either in software or hardware. It should be noted that, besides this sequence (Flow 1), it is possible that models are built from the scratch and then confirmed or fine-tuned through measurements, before being finally emulated (Flow 2). Finally, it is also possible that the modeling block is completely bypassed (Flow 3). The last sequence is called the deterministic case, where the measurement is immediately followed by emulation of the measured signals.

The timescale and target of Flows 1 and 2 are different from the one from Flow 3. In the first two cases, a system-level evaluation is targeted, and its aim is to evaluate the capacity of CR systems or the macrospectrum occupancy

Digital Object Identifier 10.1109/MVT.2012.2190219
Date of publication: 13 April 2012

 1556-6072/12/$31.00©2012IEEE

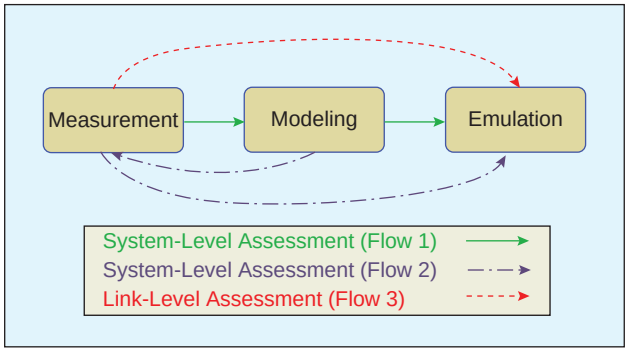

FIGURE 1 MME-integrated approach.

pattern. In particular, this methodology should assist designers in evaluating the potential of CR system in various bands and locations. This activity will require measurements over multiple periods and may involve days or weeks. In the last case (Flow 3), a link-level evaluation is targeted. Typically, short radio scenes are captured and then directly replayed in the laboratory to evaluate CR-sensing algorithms. The timescale in this case can be considered to be in the order of a fraction of seconds. The MME-integrated approach brings the real-world environment to the laboratory and aims to offer fully trustable results to the various CR stakeholders.

MME: Measurement

Since the CR concept emerged in 1999 [1], numerous measurement campaigns have been performed in diverse locations and for different scenarios. The measurements have typically covered a wide range of frequencies, from a few tens of megahertz to a few gigahertz. Table 1 summarizes some of the recent campaigns. The main conclusions are always consistent. They show a low usage of the overall spectrum with vacant spectrum bands, spatially and temporally. This implies that CR technology has the potential to significantly improve the spectrum usage by exploiting these spectrum holes.

The most commonly used measurement method is the energy/power detection scheme. In [6], it was shown that, depending on the selected parameter such as the frequency span, measurement period, location, and antenna polarization, the measurements results can lead to a different conclusion about spectrum occupancy. However, the most significant parameter is the decision threshold, which may have a huge impact on perceived spectrum occupancy.

Figure 2 shows an example of a measurement result that compares the sensitivity of the signal occupancy in percentage to the decision threshold variation for the industrial, scientific, and medical (ISM) band in 2.4–2.4835-GHz frequency. The results are obtained at 2:00 p.m. and 8:00 a.m. for an entire week, with the outcome for Wednesday afternoon at 2.00 p.m. highlighted. These measurements were done at the University of Oulu in downtown Oulu, Finland, in June 2011. The setup consisted of an ISM-band antenna, ISM-band filter, a low-noise amplifier (LNA), and Agilent N6841A RF sensor. Frequency bin separation was set to 109.375 kHz. The figure shows that the average occupancy is typically low. Similar low-occupancy results for ISM bands have also been reported in [3] and [7]. Figure 2 also shows a different occupancy result as the threshold is varied. Thus, if the selected threshold is too high, it will lead to an underestimation on the spectrum occupancy, and if it is too low, it will lead to an overestimation. The selection of the correct threshold value is therefore an important criterion. There are classically three ways to select a threshold [6].

- *Maximum Noise Criterion*: This takes the maximum recorded noise level as the threshold. Its main drawback is that it may underestimate the occupancy because of weak signal samples lying below the maximum noise level.
- *Probability of False Alarm (PFA)*: The threshold is selected such that only a fraction of the noise samples are above the threshold. The PFA is classically set to 1%, which is considered to be the best tradeoff.
- *m-dB Criterion*: This adds *m* dB to the average noise floor.

The criterion for threshold selection is dependent on the application use case. However, the selected threshold value should result in the most accurate picture of the occupancy scenario.

In Figure 3, we compare the occupancy result based on power measurements, with the access point (AP) logs taken from the public access network OULU (panOULU). This figure has been obtained after a one-week measurement in the Tellus library at the University of Oulu in

TABLE 1 *Characteristics of some recent measurement campaigns for spectrum usage evaluation.*

Location	*Instigator*	*Type*	*Frequency Range*	*Reference*
Denver, San Diego, Los Angeles	National Telecommunications and Information Administration	Outdoor	108 MHz–19.7 GHz	[2]
Singapore	Institute for Infocomm Research	Outdoor	80 MHz–5.85 GHz	[3]
Auckland, New Zealand	University of Auckland	Indoor/outdoor	806 MHz–2.75 GHz	[4]
Aachen, Germany	Rheinisch-Westfaelische Technische Hochschule Aachen University	Indoor/outdoor	20 MHz–6 GHz	[5]

January 2011. The power measurement results were obtained by a fast Fourier transform (FFT)-based spectrum analyzer that performs at least 200 measurements per second for a 156-kHz frequency bin separation in 2.4–2.5-GHz ISM band. The threshold is set to 20 dB above the noise floor, which is approximately −95 dBm in this case. The high threshold value is selected so as to avoid any false alarm due to internal noise of the receiver. In the figure, the log-based traffic information has been scaled and shifted up according to a regression analysis. The comparison is made for only one wireless LAN (WLAN) channel with a closeby AP. The figure shows that there is a good agreement with the actual WLAN activity logs. The slight deviation from the logs may be due to nonpanOULU WLAN traffic, nontraffic beacon signals, and other interferences.

Similar occupancy results for global system for mobile communication (GSM) carriers for one working day were obtained at the University of Aveiro campus in Portugal [8]. Figure 4 shows the variation of the spectrum occupancy of a single 200-kHz GSM 1800 channel consisting of eight time-division multiple access (TDMA) slots. The measurement period is set equal to the GSM frame duration of 4.62 ms. The measurement here is continuous compared with the typically discontinuous wideband (WB) measurements undertaken in Table 1. In the result, a channel is considered occupied if at least one of the eight time slots in the frame is used. From the figure, we see that, during the business hours, the occupancy is at most 70%, whereas during the night hours, there is considerably more availability of the spectrum.

So far, we have considered only the spectrum occupancy criterion, but for certain radio access technologies, the spectral resource is used even when no user is actually transmitting, for example, in downlink code-division multiple access (CDMA) systems. Even with GSM systems, a huge difference exists between spectrum occupancy and real traffic occupancy. This can be due to two factors:

- an increase in number of frequency channels used as broadcast channels (BCHs)
- an increase in occupancy due to frequency-hopping functionality.

Thus, the concept of traffic occupancy gives a much better image of how spectral resources are actually used. In the GSM case, it can be defined as the average occupancy over the TDMA time slots on each of the traffic channels (TCHs), which can be potentially used by the user equipment (UE). To this end, a measurement campaign was undertaken by Thales Communications and Security in a business area in the suburbs of Paris in February 2011. The campaign was conducted to quantify the difference that exists between the spectrum and traffic occupancies on GSM 900 bands. On each of the 124

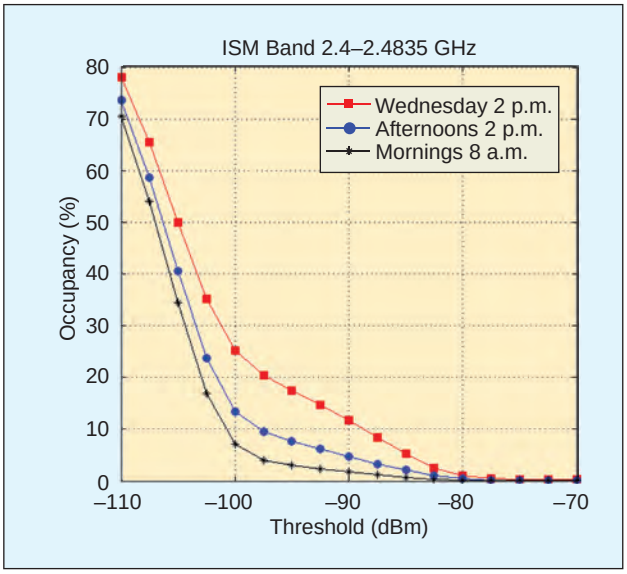

FIGURE 2 Impact of the decision threshold on the spectrum occupancy of ISM band.

channels of the band, a detection algorithm was implemented to detect and decode the BCHs and detect the TCHs and estimate their time-slot occupancy.

Figure 5 illustrates the evolution of both occupancies during 24 h for France Telecom (FT) Orange network operator. This figure emphasizes the existing difference between the spectrum occupancy and its actual usage on GSM bands. One can observe that the spectrum occupancy is much higher than the traffic occupancy. The results highlight that there is much more potential opportunity in the available spectrum space, which can be exploited by the CR system.

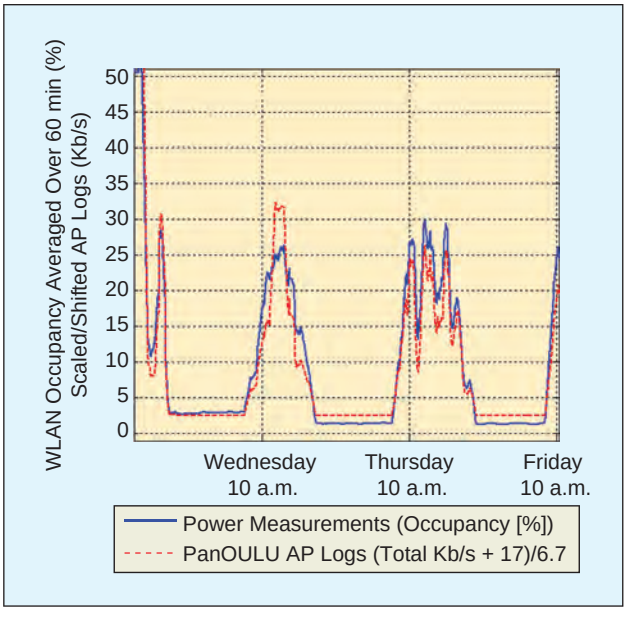

FIGURE 3 Power measurement versus AP logs (time series) with a sliding window of 60 min.

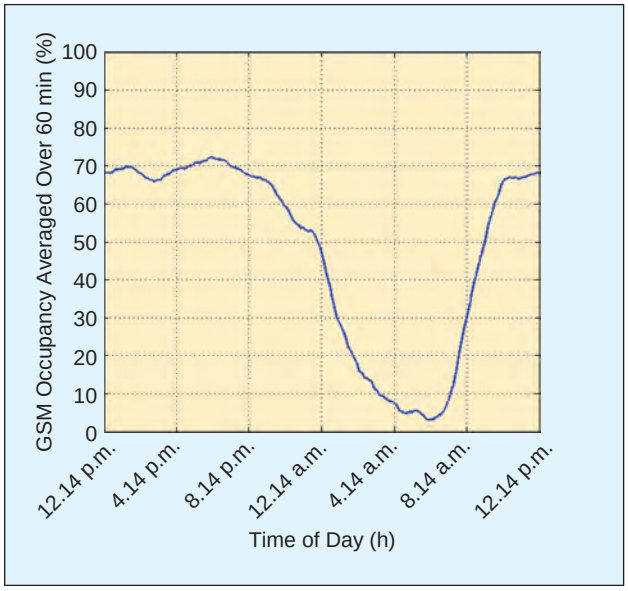

FIGURE 4 A single 200-kHz GSM 1800 channel occupancy measured over a single day at Aveiro, Portugal, with a sliding window of 60 min.

It should be noted that Figures 3–5 provide the measurement results for a 60-min window period and mainly emphasize on system-level evaluation. The results from these measurements are first fed to the modeling block, and then based on statistical studies, the emulation block plays the radio scene to evaluate the capacity of CR systems. This corresponds to Flow 1 within the MME framework.

Similarly, shorter measurement periods in the order of fraction of seconds or minutes can also be estimated. In this case, short radio scenes are captured and then directly fed to the emulation block to evaluate the CR sensing algorithms. This corresponds to Flow 3 within the MME framework. The aim here is to evaluate and validate

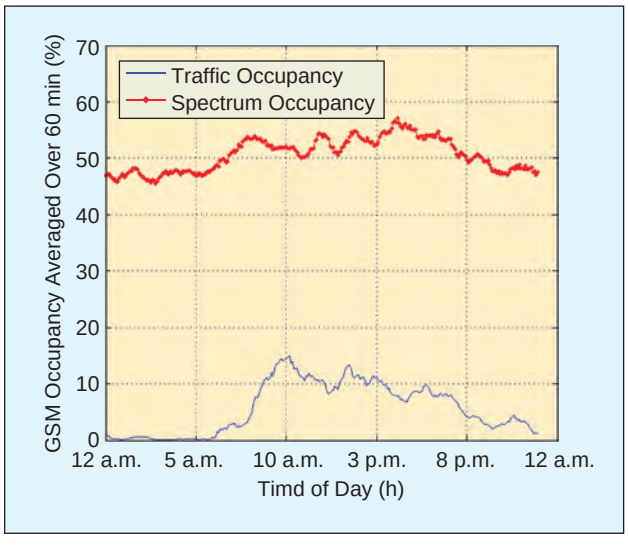

FIGURE 5 Spectrum and traffic occupancies during a single day for a French operator at Colombes, Paris, with a sliding window of 60 min.

the link-level evaluation of the CR system. We may now consider the second item that is the modeling block in our three-pillar process.

MME: Modeling

To enable spectrum-sharing techniques based on CR technology, it is also crucial to understand and model incumbent user behavior. Therefore, we provide an overview of modeling task within the MME framework. The approach is divided into statistical modeling and database modeling. While the statistical approach models the dynamic behavior of the incumbents, the database approach focuses on the static environment, such as the television white space (TVWS) bands.

Statistical Modeling

The measurement results shown in the previous section cannot be extended directly to other locations, spectrum bands, and time intervals, and this is because of variations in the incumbent usage pattern; hence, in theory, separate measurements are needed at each time and place. To provide a representative usage of an incumbent, a statistical-based modeling approach can be considered as an attractive solution. Here, the first- and second-order statistical parameters are employed on the measurement results to develop the spectrum occupancy model of the incumbent users. Then the radio scene corresponding to this occupancy model is finally played by the emulator for the system-level evaluation. It should be noted that, within the MME framework, this corresponds to Flow 1.

A quick survey of literature shows that the statistical modeling is a very active area in research. The different approaches that have been considered for modeling the incumbent usage pattern in time, frequency, and space domain are discussed below.

In the time domain, spectrum occupancy models are widely based on discrete- or continuous-time Markov chain (CTMC) schemes. The basic principle of Markov chain is that the spectrum usage in each channel can be modeled by two states, with one state indicating that the channel is occupied and therefore not available to the opportunistic user while the other state indicates that the channel is free and available to the opportunistic users. In CTMC model, the channel remains in one state for a random period of time. This state-holding time can be modeled based on empirical results as a generalized Pareto, or as geometric or log-normal distributions [9]. In real systems (e.g., cellular systems), occupancy of a channel is a consequence of a large number of random factors such as traffic load, resource management policies, specific location, mobile operator packages, and so on; as a result, channel usage is itself a complex stochastic process and still an open research question. Recently, Wang and Salous [10] analyzed the spectrum occupancy in GSM bands by applying time-series models. To analyze the data, an

autoregressive integrated moving average (ARIMA) model was fitted to the data in GSM bands in Durham, United Kingdom [10]. A time-varying spectrum occupancy model was also proposed in [11]. Here, the statistical spectrum occupancy model is based on a combination of several probability density functions (PDFs).

In the frequency domain, the statistical distribution of channel occupancy is shown to follow a beta distribution [12]. The use of Poisson and Poisson-normal distributions for the characterization of channel occupancy has also been presented in [13]. In the spatial domain, the models characterize the spectrum occupancy patterns at different locations. Spatial distribution of the power spectral density of incumbent user signal has been studied in [14] using random field theory. Most recently, a more sophisticated approach to model spectrum occupancy in a realistic urban environment (at a ground level, inside buildings, and on rooftops) was presented in [15].

Based on the incumbent user's channel access dynamics for specific location and time, it is also possible to derive statistical information, such as the total number of spectrum opportunities in terms of the probability of each channel being free. In previous work [16], the exact and approximate probability distributions for the total number of free channels not being used by the incumbent users was derived. Figure 6 compares the exact and the various approximate probability distribution functions in a scenario when the channels are most likely occupied by the incumbent users. It is seen from Figure 6 that Camp–Paulson approximation provides the most accurate curve.

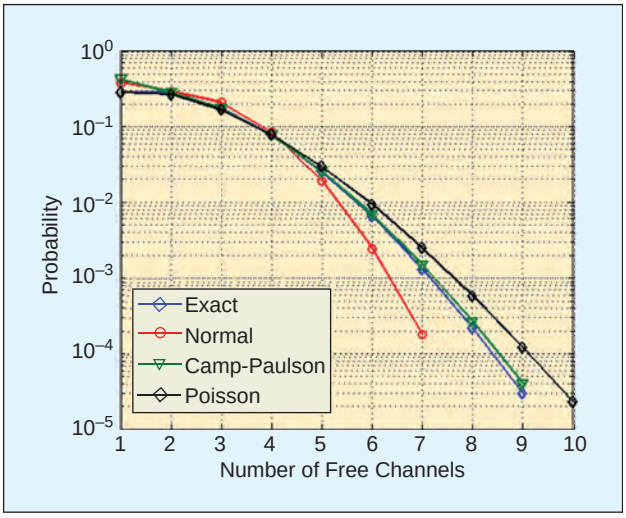

FIGURE 6 Probability distribution function of total number of opportunities.

Database Modeling

In static radio environments, CR systems are envisaged to have access to a database of incumbent spectrum occupancy to minimize the risk of interference and reduce the sensing requirements. In TVWS bands, such a database will contain signal strength information from TV transmitters as well as wireless microphone data. The computation of such a database is a large computational task. It needs two main inputs:

- The first input is a list of TV transmitter data, which is usually provided by national regulators.
- The second input is the terrain data required by propagation models. The propagation models used are often of the irregular terrain Longley–Rice type, which include empirical models of diffraction effects over hills.

Additionally, a protocol is required for remote communication with the database; various proposals are currently being evaluated. Security will be a basic requirement here. Upon receipt of a query, the database will provide a channel (or channels) and an allowed power level and register the channel as in use at the specified locations and for the specified period. In the United Kingdom, the Ofcom regulator has published consultation documents on design issues [17]. Such databases are starting to be offered as a commercial service [18]. Figures 7 and 8 show the typical database computation outputs for the United Kingdom. Figure 7 shows a square of size 6° longitude and 6° latitude covering most of England, with spectral colors indicating minimum channel occupancy (dark blue) to maximum (red). It will be seen that there is considerable spatial variation, proving that the database does provide useful information.

From the database, statistical summary information may also be computed. The most useful is population-density weighted so that we gain estimates of the distribution of the amount of free spectrum per user. Figure 8 shows a typical cumulative distribution computed this way for the whole of the United Kingdom. It will be seen that 50% of the population has six channels available, i.e., 48 MHz.

Within the MME framework, the database computations derived from TV transmitter and propagation data can eventually be fed to the measurement block (Flow 2) for further verification and refinement of the model. Once the verification is complete, the computed data can then be fed to the emulation block.

MME: Emulation

Emulation is the third pillar of the MME-integrated approach. It is worth noting that this test bed can be implemented either in hardware or software. It is the core of the proposed CR test bed shown in Figure 9. The emulator consists of a WB signal generator that stimulates the sensing engine of a CR device with a set of waveforms derived from the measurement-modeling (MM) stages of the MME approach. As discussed in the "MME Approach" section, the emulation involves two cases with different time scales: deterministic and model based.

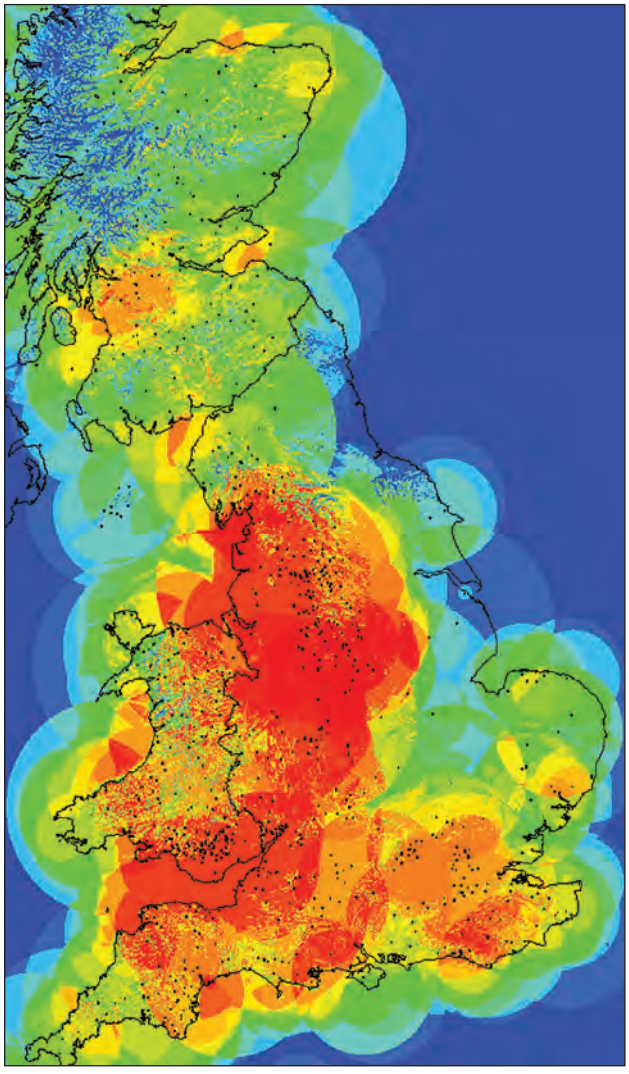

FIGURE 7 The TV band occupancy density for United Kingdom. (Image courtesy of BT Innovate & Design.)

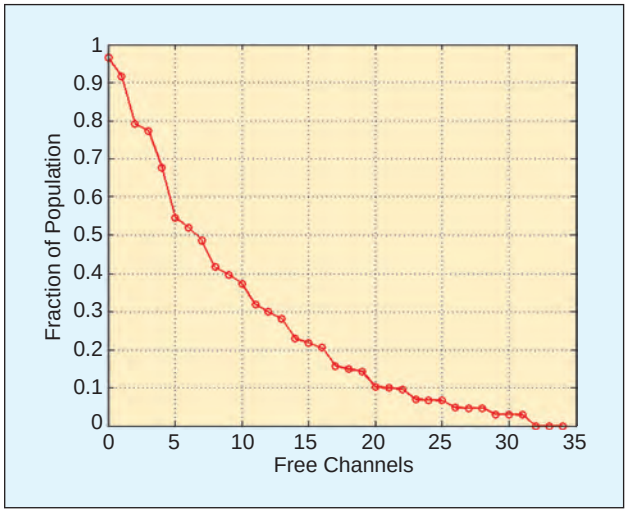

FIGURE 8 The TV band white space availability for the whole of the United Kingdom.

In the first deterministic case, the modeling block is skipped and the recorded sequences obtained from the measurement campaign are directly replayed on the emulator without any changes. The incumbent usage pattern (on/off) is emulated without the need for any channel emulation. This emulation scenario serves the link-level performance evaluation and, in particular, the sensing engine performance study.

In the second model-based case, both statistical and database approaches are considered. Here, the incumbent usage pattern emulation is combined with the channel emulation to accurately reproduce the actual RF scene. This emulation scenario serves the system-level performance evaluation.

Figure 9 shows that, in the test bed, the sensing estimates of the CR device can be compared with the source to evaluate the performance of the sensing engine. Metrics such as probabilities of detection, false alarm, or the detection speed can be evaluated in this manner. On the other hand, the CR device can also make decisions about the available opportunities based on the sensing engine outputs. In this case, the transmitter of the CR device (secondary) can start transmitting on the available spectrum holes. The output of the secondary transmitter is then added to the stimulus signal and later fed to CR device receiver as well as the incumbent systems receiver. Through bit error rate (BER) measurements (as an example), both the quality of the secondary transmission and its impact on the incumbent systems can be evaluated. As depicted in the figure, a CR test bed can also include channel emulation blocks. Adding these blocks between the receivers and the modeled (or emulated) transmit sources will enable the inclusion of fading and Doppler effects in the radio scene. A true radio scene experienced by the mobile device is then emulated; hence, both the static and the vehicular cases are appropriately tested.

The emulator should have the following three properties.

- *Controllability*: The user should be able to precisely control the emulation scenario.
- *Repeatability*: The user should be able to repeat any desired sequence of events in the emulation scenario.
- *Representability*: The emulated RF scene should represent as well as possible the real environment that the CR system will experience. This is guaranteed through the MME vertical approach.

Besides the above desirable properties, the emulator should also provide a deep enough memory for the deterministic-case emulation, whereas a WB system is typically required for both deterministic as well as model-based cases.

Conclusions

We have presented an integrated vertical approach involving MME. This approach enables the reproduction of the

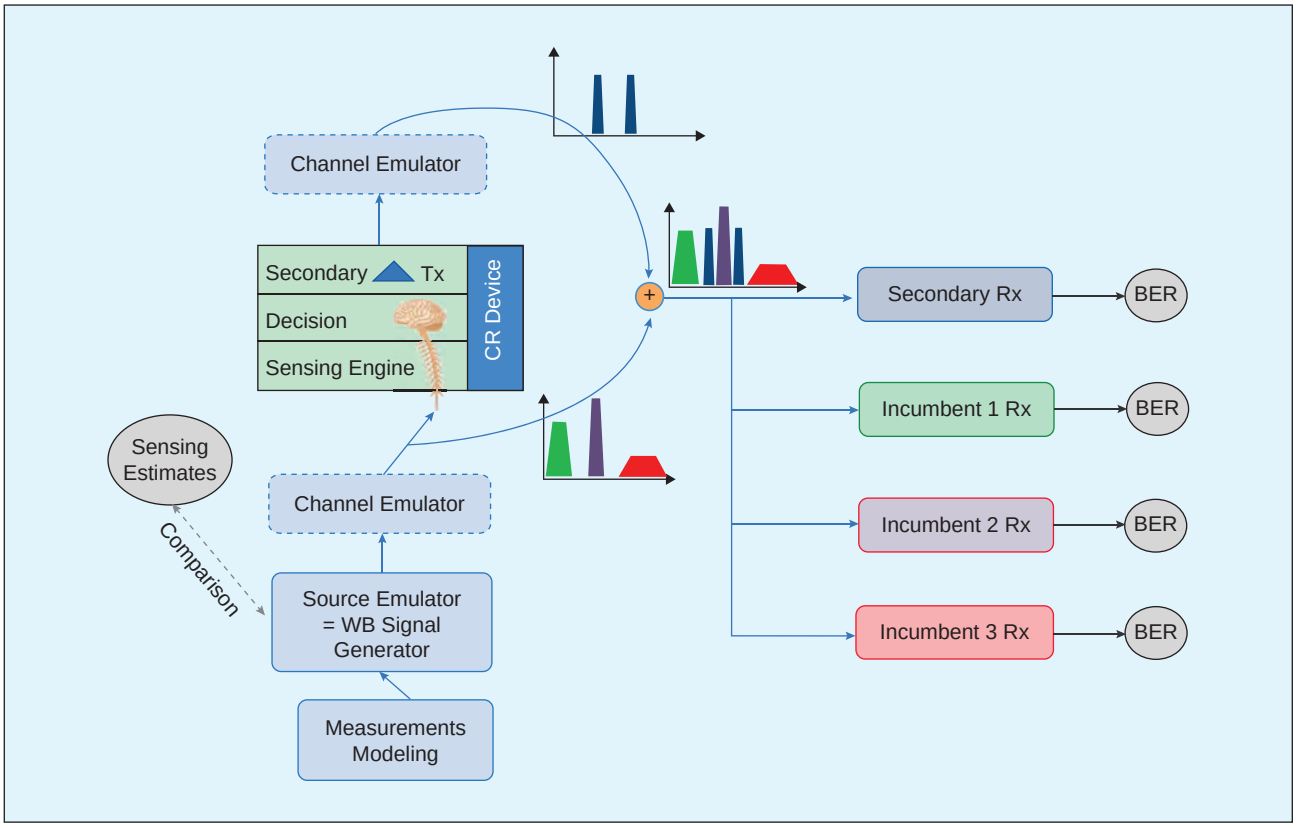

FIGURE 9 MME-based CR test bed.

radio environment in laboratory conditions and offers fully trustworthy results to the various CR stakeholders.

Acknowledgments

The research leading to these results was derived from the European Community's Seventh Framework Programme (FP7) under grant agreement no. 248454 [Quality of service and mobility driven cognitive radio systems (QoSMOS) http://www.ict-qosmos.eu/]. The authors thank the panOULU consortium for their support.

Author Information

Deepaknath Tandur (deepaknath_tandur@agilent.com) received his bachelor of engineering degree in electronics and communications from Bangalore University, India, his master of engineering degree in embedded systems design from the University of Lugano, Switzerland, and his Ph.D. degree in electrical engineering from Katholieke Universiteit (KU) Leuven, Belgium. Since 2010, he has been working as a technical staff member at the Measurement Research Labs of Agilent Technologies, Belgium. His research interests include digital signal processing techniques for telecommunications, specifically, the technological development of test and measurement instruments and their associated software for various radio access technologies (RATs).

Jonathan Duplicy received his bachelor of engineering and master of science degrees in electrical engineering from the Université Catholique de Louvain (UCL), Belgium. From 2003 to 2008, he was with telecom laboratory of UCL focusing on multiantenna, multiuser systems. In 2006, he was a visiting researcher for one semester at Hong Kong University of Science and Technology (HKUST), Hong Kong. He joined the Measurement Research Labs of Agilent Technologies in 2008. He is strongly involved in the European Union (EU) collaborative research arena. His research interests include digital signal processing techniques for fourth generation (4G) and beyond RATs.

Kamran Arshad received both his bachelor of engineering and master of science degrees in electrical engineering with distinction and his Ph.D. degree in computing science in 2007. He is a senior lecturer of communications engineering at the University of Greenwich, United Kingdom. He has more than 60 publications in peer-reviewed journals and conferences. He received three best paper awards and is a regular reviewer of several prestigious journals and conferences. His research work includes channel modeling and characterization, spectrum sensing, spectrum and radio resource management for third-generation (3G)/4G systems, and he contributed in several European integrated projects [E3, QoSMOS, and Advanced Coexistence Technologies for Radio Optimisation in Licensed and Unlicensed Spectrum (ACROPOLIS)].

David Depierre received his degree in signal processing from the Ecole Nationale Supérieure de l'Electronique et de ses Applications (ENSEA), Paris, in 1997. After two years in the research team of ArrayComm, San Jose, California, he joined Thales Communications signal processing department. He was involved in several French and European projects on antenna processing on universal mobile telecommunications system (UMTS), WiMAX, long-term evolution [Advanced Network Radio Identification Equipment for Universal Mobile (ANTIUM) communications, Système d'Evaluation par une Métrologie Avancée des Formes d'Ondes et des Réseaux (SEMAFOR), and cognitive radio experimentation world (CREW)], and sensing [QoSMOS and Cognitive Radio for Dynamic Spectrum Management (CORASMA)].

Klaus Moessner received his Dipl.-Ing. (FH) from the University of Applied Sciences, Offenburg, Germany, his M.Sc. degree from Brunel University, and his Ph.D. degree from the University of Surrey, United Kingdom. He is a professor of cognitive networks and services in the Centre for Communication Systems Research at the University of Surrey, United Kingdom. His research interests include dynamic spectrum allocation, cognitive networks, reconfiguration management, service platforms, and adaptability of multimodal user interfaces.

Janne Lehtomäki received his M.Sc. (Tech.) and Ph.D. (Tech.) degrees in telecommunications from the University of Oulu in 1999 and 2005, respectively. Currently, he is a project research fellow at the Centre for Wireless Communications (CWC), University of Oulu. In 2008, he was a visiting researcher at the University of Agriculture and Technology, Tokyo, Japan. His research interests include spectrum measurements, energy detection, and CR networks.

Keith Briggs received his B.Sc. degree in physics and Ph.D. degree in applied mathematics. He worked in the mathematics of dynamical systems and biomathematics before joining the BT Research complexity research team in 2000. Since then he has worked for BT Research in areas including network topology, distributed algorithms, optimal route planning in transport systems, media access control (MAC) layer design, and propagation modeling. He also works in historical linguistics.

Luis Gonçalves received his Licenciatura (five-year degree) in electronics engineering and telecommunications and his Ph.D. degree in electrical engineering from the University of Aveiro in 1991 and 2009, respectively. He worked for companies including Texas Instruments and Blaupunkt from 1991 until 1999. Since 1999, he has been a researcher at Telecommunications Institute, Aveiro, where he is doing a postdoctoral project on CR. He was an invited assistant at the University of Madeira in the Department of Mathematics and Engineering from 2004 to 2008.

Atílio Gameiro received his licenciatura degree and his Ph.D. degree from the University of Aveiro in 1985 and 1993, respectively. He is currently a professor in the Department of Electronics and Telecommunications at the University of Aveiro and a researcher at the Instituto de Telecomunicações, Pólo de Aveiro, where he is the head of the group. His research interests include signal processing techniques for digital communications and communication protocols, and within this research line, he has done work for optical and mobile communications, either at the theoretical or experimental level, and has published more than 120 technical papers in international journals and conferences.

References

[1] J. Mitola and G. Q. Maguire, Jr., "Cognitive radio: Making software radios more personal," *IEEE Pers. Commun.*, vol. 6, no. 4, pp. 13–18, Aug. 1999.

[2] F. H. Sanders, "Broadband spectrum survey in Denver, CO, San Diego, CA and Los Angeles, CA: Methodology, analysis and comparative results," in *Proc. IEEE Symp. Electromagnetic Compatibility*, 1998, pp. 988–993.

[3] M. Islam, C. L. Koh, S. W. Oh, X. Qing, Y. Y. Lai, C. Wang, Y. C. Liang, B. E. Toh, F. Chin, G. L. Tan, and W. Toh, "Spectrum survey in Singapore: Occupancy measurements and analyses," in *Proc. CROWNCOM*, Singapore, July 2008, pp. 1–7.

[4] R. I. C. Chiang, G. B. Rowe, and K. W. Sowerby, "A quantitative analysis of spectral occupancy," in *Proc. IEEE Veh. Technol. Conf.*, Apr. 2007, pp. 3016–3020.

[5] M. Wellens, J. Wu, and P. Mähönen, "Evaluation of spectrum occupancy in indoor and outdoor scenario in the context of cognitive radio," in *Proc. CROWNCOM*, FL, Aug. 2007, pp. 420–427.

[6] M. Lopez-Benitez and F. Casadevall, "Methodological aspects of spectrum occupancy evaluation in the context of cognitive radio," in *Proc. 15th European Wireless Conf.*, Aalborg, Denmark, May 2009, pp. 199–204.

[7] M. Biggs, A. Henley, and T. Clarkson, "Occupancy analysis of the 2.4 GHz ISM band," *IEE Proc. Commun.*, vol. 151, no. 5, pp. 481–488, Oct. 2004.

[8] L. Mendes, L. Gonçalves, and A. Gameiro, "GSM downlink spectrum occupancy modeling," in *Proc. IEEE Int. Symp. Personal, Indoor and Mobile Radio Communications*, Toronto, Canada, Sept. 2011, pp. 10–14.

[9] M. Wellens, J. Riihijärvi, and P. Mähönen, "Empirical time and frequency domain models of spectrum use," *Phys. Commun.*, vol. 2, no. 1–2, pp. 10–32, Mar.–June 2009.

[10] Z. Wang and S. Salous, "Spectrum occupancy statistics and time series models for cognitive radio," *J. Signal Process. Syst.*, vol. 62, no. 2, pp. 145–155, 2011.

[11] C. Ghosh, S. Pagadarai, D. Agrawal, and A. Wyglinski, "A framework for statistical wireless spectrum occupancy modeling," *IEEE Trans. Wireless Commun.*, vol. 9, no. 1, pp. 38–44, Jan. 2010.

[12] M. Wellens and P. Mähönen, "Lessons learned from an extensive spectrum occupancy measurement campaign and a stochastic duty cycle model," in *Proc. TridentCom*, Apr. 2009, pp. 1–9.

[13] C. Ghosh, "Innovative approaches to spectrum selection, sensing, and sharing in cognitive radio networks," Ph.D. thesis, Univ. Cincinnati, Cincinnati, OH, May 2009.

[14] M. Wellens, J. Riihijärvi, and P. Mähönen, "Spatial statistics and models of spectrum use," *Comput. Commun.*, vol. 32, no. 18, pp. 1998–2011, Dec. 2009.

[15] M. Lopez-Benitez and F. Casadevall, "Statistical prediction of spectrum occupancy perception in dynamic spectrum access networks," in *Proc. IEEE Int. Conf. Communications*, June 5–9, 2011, pp. 1–6.

[16] K. Arshad and K. Moessner, "Statistical models for spectrum opportunities for cognitive radio," in *Proc. PIMRC, WS-Cognitive Radio Networking: Challenges and Solutions Ahead*, Toronto, Canada, Sept. 2011, pp. 11–14.

[17] H. Mark Gibson. (2010, Jan.) Comsearch comments to Ofcom Consultation document on implementing geolocation [Online]. Available: http://stakeholders.ofcom.org.uk/binaries/consultations/geolocation/responses/Comsearch.pdf.

[18] Spectrumbridge. (2011). TV white space database: Protected entity registration and data portal [Online]. Available: http://spectrumbridge.com/whitespaces.aspx. ***VT***

The spectrum scarcity faced by the operators can be significantly alleviated by employing CR technology.

The most commonly used measurement method is the energy/power detection scheme.

The criterion for threshold selection is dependent on the application use case.

It is critical that all stakeholders interested in CR, such as operators, device manufacturers, and regulators, have a clear understanding of the limitations and possibilities of this technology.

It is also crucial to understand and model incumbent user behavior.

In static radio environments, CR systems are envisaged to have access to a database of incumbent spectrum occupancy to minimize the risk of interference and reduce the sensing requirements.

Emulation is the third pillar of the MME-integrated approach.

The emulator should have the following three properties: controllability, repeatability, and representability.

The approach consists of three pillars: measurement, modeling, and emulation.

GSM Downlink Spectrum Occupancy Modeling

Luís Mendes*,Luís Gonçalves*,Atílio Gameiro†
*Instituto de Telecomunicações, Campus Universitário de Santiago,
3810-193 Aveiro, Portugal, Email: mendes@av.it.pt, lgoncalves@av.it.pt
†Universidade de Aveiro, Departamento de Electrónica, Telecomunicações e Informática,
3810-193 Aveiro, Portugal, Email: amg@ua.pt

***Abstract*—In this article the spectrum occupancy of a GSM900 and a DCS1800 band as an analog power or binary quantized power is modeled. In the case of analog power it is presented histograms of the power distribution during one working day. In the case of quantized power it presents the two time statistics, the time period of opportunities distribution and the time between opportunities distribution. The measurement setup is standing in line of sight with the base station. Also, the measurement setup in terms of maximum sensitivity is described and analyzed. Spectrum non occupancy, for a working day, in terms of total time for the GSM900 band and for the DCS1800 band is given.**

***Index Terms*—Cognitive Radio, Spectrum Occupancy Models, Measurement Setup**

I. Introduction

Cognitive Radio Systems will be used in order to maximize the full potential of the allocated to and unutilized spectrum of primary systems. The study of the technology associated to these systems are in an initial stage despite of several years of evolution and one standard already set (IEEE 802.22, for packet use in rural areas using the holes of TV spectrum).

The Power Spectral Statistics must be characterized in order to find channel occupational models. Each sample of these occupational models functions could be analog or quantized. The quantized model could be associated to one (two levels) or more thresholds depending of the resolution necessary to it description. These models could be used in the study of sensor fusion in secondary networks. In this article the analog and quantized (one threshold) occupational model for GSM900 and DCS1800 in a standing line of sight reception scenario is described and analyzed. The analog occupational model is presented by the histograms (distribution) of the powers levels during one day for one GSM900 band and one DCS1800 band. The binary quantized model is presented by the time between opportunities distribution and the time period of opportunities distribution.

The measurements are described in the Portuguese frequency allocation context. This work complements the one presented in [1] which presents the period of time of opportunities distribution for a GSM900 band in a mobile situation. This work goes beyond other spectrum occupational articles [2]–[6] in the way that it tries to model the spectrum occupancy.

Also, it presents and mathematically analyzes the measurement setup used. Spectrum non occupancy, for a working day, in terms of total time for a GSM900 band and a for DCS1800 band is presented.

The Section II describes the Measurement Setup. In Section III the best sensitivity achievable by the measurement setup is determined. In Section IV, the measurements and correspondent statistics and distributions are presented. And finally in Section V, the main conclusions are stated.

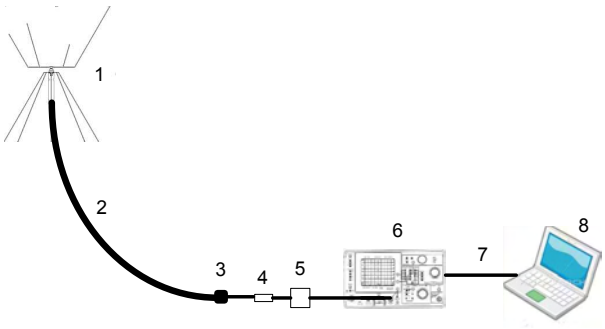

Figure 1. Measurement Setup, 1 - M-POL Antenna, 2 - Low Attenuation Cable, 3 - N-SMA Adapter, 4 - Filter, 5 - Pre-Amplifier, 6 - Spectrum Analyser, 7 - Ethernet LAN Cable, 8 - Portable Computer

II. Setup Description

The measurement setup is pictured in Figure 1. It is composed of a high bandwidth omnidirectional antenna ($25MHz-6GHz$) from MP Antenna with typical $3dBi$ gain. A semi-rigid low attenuation cable (typical < 0.12 dB/meter at $5GHz$) with about 8 meters, a high steeply passband filter ($500MHz-1GHz$ for GSM900, $1GHz-2GHz$ for DCS1800), a high bandwidth preamplifier ($15dB$ gain at $950MHz$), a Spectrum Analyser (SA) and a Portable Computer with an Acquisition Program. From the low attenuation cable, to the SA, the components are connected with thin cable with SMA connectors. The preamplifier gain is such that the GSM signal ($-102dBm$ in $200KHz$, sensitivity level) is brought above the noise level of the SA but not enough to generate visible intermodulation products due to non linearity of the input mixer of the SA. The SA is set in the highest sensitivity *i.e.* with $0dB$ attenuation of the input attenuator. The total signal in $500MHz-1GHz$ band (pass band of the filter) at the input of the SA was about $-17dBm$. The secure signal level in terms of intermodulation is below $-10dBm$. Another criterion in choosing the filter is: that the higher passband frequency is not more than one octave from the lower passband frequency. This avoids the second order intermodulation products to be inside the passband.

The measurements took place at the top roof of the Department of Electronics, Telecommunications and Informatics of the University of Aveiro as shown in Figure 2.

III. Setup Analysis

Figure 3 shows the equivalent circuit of the measurement setup from the preamplifier to inside the Spectrum Analyzer (SA) including the sum of the internal noise. S_i is the input

Figure 2. Antenna deployment

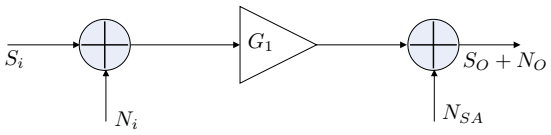

Figure 3. Equivalent circuit of the measurement setup from the preamplifier to the inside of the Spectrum Analyzer

signal, N_i is the noise signal at the input. These two signals are already combined before the preamplifier, despite showing the combination at the input. $\mathbf{G_1}$ is the Power Gain of the preamplifier, N_{SA} is the internal noise signal of the SA, S_0 is the output signal resulting from S_i, and N_0 is the output noise signal. Also, there is one variable, the noise figure of the preamplifier $\mathbf{NF}$, which is not shown. The power of the signals described previously is represented with the same letters of the signals, but in boldface. The power of these signals is measured in logarithm form (dBm/Hz), and the noise figure $\mathbf{NF}$, as well as the gain $\mathbf{G_1}$ in dB. $\mathbf{N_i}$ depends on the environment noise caught by the antenna and the noise added by the lossy elements before the preamplifier. $\mathbf{S_i}$ is the power of the signal caught by the antenna at the measured frequency, attenuated by the lossy elements before the preamplifier.

How much $\mathbf{S_i}$ must be above $\mathbf{N_i}$ in dB (or the signal to noise relation in linear) in function of the gain $\mathbf{G_1}$, considering the limit case of $\mathbf{S_0} = \mathbf{N_0}$ is then calculated. This last condition limits the point which can separate signal from noise. The minimum of that function could be described by Equation 1

$$\begin{cases} \left\{\widehat{\mathbf{G_1}}\right\} = \arg\min\limits_{\{\mathbf{G_1}\}} \left[\mathbf{S_i} - \mathbf{N_i}\right] \\ \mathbf{S_0} = \mathbf{N_0} \\ \mathbf{S_0} = \mathbf{S_i} + \mathbf{G_1} \\ \mathbf{N_0} = 10\log\left(10^{(\mathbf{N_i}+\mathbf{NF}+\mathbf{G_1})/10} + 10^{\mathbf{N_{SA}}/10}\right) \end{cases} \quad (1)$$

$\mathbf{S_i}$ is given by

$$\mathbf{S_i} = -\mathbf{G_1} + 10\log\left(10^{(\mathbf{N_i}+\mathbf{NF}+\mathbf{G_1})/10} + 10^{\mathbf{N_{SA}}/10}\right) \quad (2)$$

Considering $\mathbf{N_i} = -174dBm/Hz$ (best case), $\mathbf{NF} = 3.5dB$ and constant with the preamplifier gain, $\mathbf{N_{SA}} = -155dBm/Hz$, then the Figure 4 presents $\mathbf{S_i} - \mathbf{N_i} = f(\mathbf{G_1})$. Looking at Figure 4, it is concluded that the solution of Equation 1 for $\mathbf{G_1}$ is infinity. And the value reached at infinity for $\mathbf{S_i} - \mathbf{N_i}$ is $\mathbf{NF}$ (by the limit of Equation 2 minus $\mathbf{N_i}$ in both sides with $\mathbf{G_1}$ to infinity).

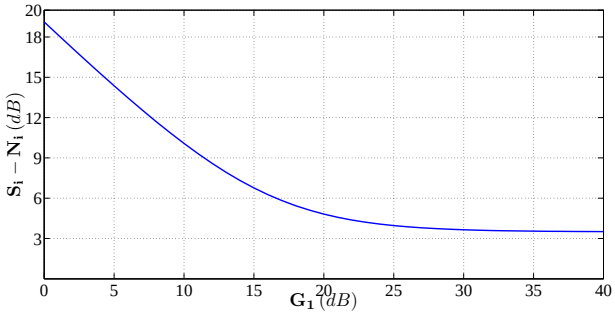

Figure 4. $\mathbf{S_i} - \mathbf{N_i}$ in function of $\mathbf{G_1}$

The lossy elements before the amplifier will be taken into account in order to calculate the minimum GSM signal that can be detected with this setup. The antenna gain is also taken into account. The lossy elements mentioned above, will amplify (or add in dB) the noise induced by the antenna. This amplification is equal to the attenuation induced to the signal (Cable attenuation times Filter Attenuation - plus if in dB). This attenuation amount in dB, is represented by $\boldsymbol{\alpha_{dB}}$. The Figure 5 represents the operations made to the signal and to the noise from the antenna to the preamplifier input. In an ideal scenario the noise at the antenna output will be the thermal noise (N_{th}) and equal to $-174dBm/Hz$ ($10^{\mathbf{N_{env}}/10} = 0$, environmental noise power equal zero). Considering a gain $\mathbf{G_1}$ equal to infinity and that the antenna catches the lowest detectable power. Then

$$\begin{cases} \mathbf{S_i} - \mathbf{N_i} = \mathbf{NF} \\ \mathbf{N_i} = -174dBm/Hz + \boldsymbol{\alpha_{dB}} \\ \mathbf{S_i} = \mathbf{S_{Ain}} + \mathbf{G_A} - \boldsymbol{\alpha_{dB}} \end{cases} \quad (3)$$

which is equivalent to

$$\mathbf{S_{Ain}} = -\mathbf{G_A} + 2\boldsymbol{\alpha_{dB}} - 174dBm/Hz + \mathbf{NF} \quad (4)$$

It was considered the attenuation of the cable connecting the antenna, plus the pass band filter attenuation to be $\boldsymbol{\alpha_{dB}} = 1.5dB$. The antenna gain is $3dBi$ and considering the noise figure $3.5dB$, then $\mathbf{S_{Ain}} = -170.5dBm/Hz$ or

$\mathbf{S_{Ain}} = -117.5dBm/(200KHz)$. This is the lowest GSM signal detectable with this setup.

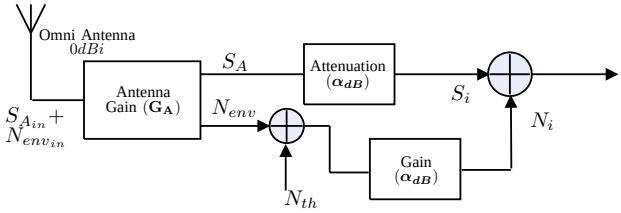

Figure 5. Equivalent circuit of the measurement setup from antenna to preamplifier input

IV. Measurements and Statistics

The measures were taken at a distance of 250 meters (measured with GPS) from the nearest GSM base station during school period. This base station covers, the University Campus with a population of approximately 15000 students, using GSM900 and DCS1800 bands. Two GSM operators are co-located in this base station belonging the studied GSM900 band to one operator and the studied DCS1800 band to the other.

The measurements were done with a resolution bandwidth of $100KHz$ at 501 points covering in excess all GSM900 downlink band (Figure 6) and the allocated part of the DCS1800 band (Figure 8). Each measured $100KHz$ covers one side of the $200KHz$ GSM band. In the case of single frequency, the 501 points were measured in a specific frequency with a span equal to zero. The measured power was adjusted to reflect the power received at the output of the equivalent unit gain antenna (see Figure 5, at output of the Omni-Antenna) and for the bandwidth of 200KHz it was added 3dB. The time at each measurement point was set to the frame period (about $4.62ms$) giving a sweep time about $2.4s$. There is practically no delay between consecutive measurements.

Figure 6 shows the spectrum occupancy of GSM900 band at 5H19 of a working day. The frequency axes ticks are the limits of the bands of the three Portuguese GSM operators. Figure 7 shows the spectrum occupancy of GSM900 band at 13H in the same 24H. The City of Aveiro is a plane region and because of that the antenna is at line of sight of several base stations, hence the high occupancy. In that situation two base stations with a decade of distance (in relation to the setup antenna) one from another could originate a diference (in dB) on the received power as low as $20dB$ (assuming that the same power is being transmitted). The power measurements done for this sectorized base station shows that the power received from the other sectors, is not more than 20dB below (measured in the Broadcast Control Channels (BCCH) which has no frequency hopping).

Figure 8 shows the spectrum occupancy of the DCS1800 band at 5H19 of a working day. The Portuguese Communications Regulator (ANACOM) allocates spectrum according to the operators needs and requirements. For this reason, there are two bands for each of two operators and a larger band for one operator only. Figure 9 shows the spectrum occupancy of the DCS1800 band at 13H in the same 24H.

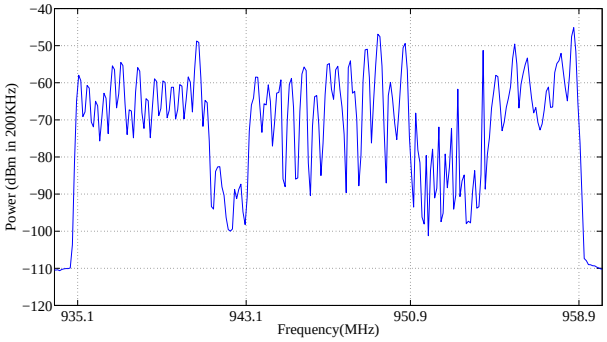

Figure 6. Typical Power Spectrum Density at 5H19 for GSM900

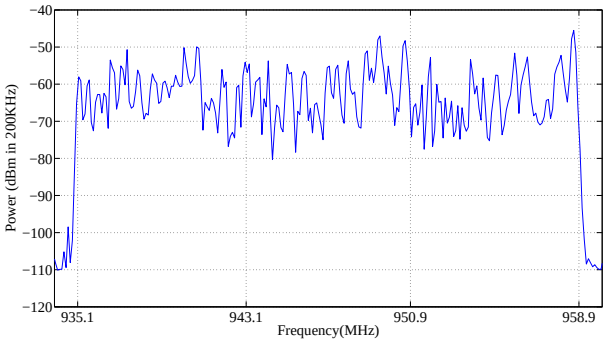

Figure 7. Typical Power Spectrum Density at 13H for GSM900

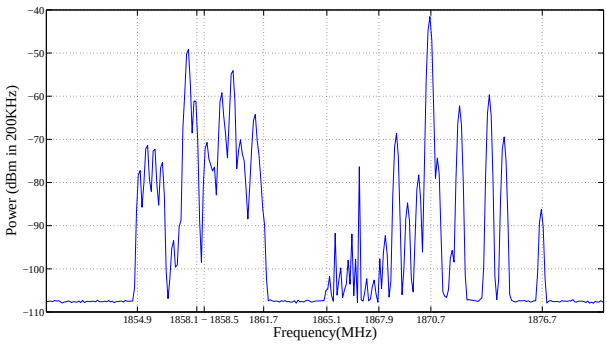

Figure 8. Typical Power Spectrum Density at 5H19 for DCS1800

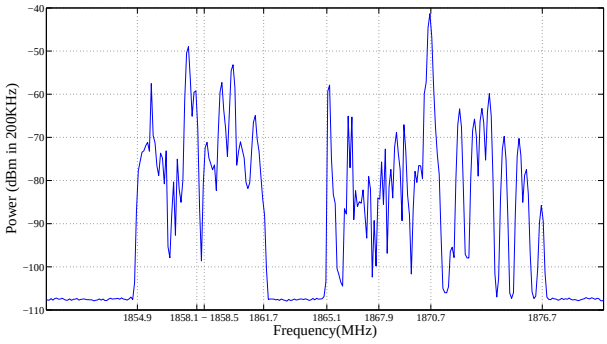

Figure 9. Typical Power Spectrum Density at 13H for DCS1800

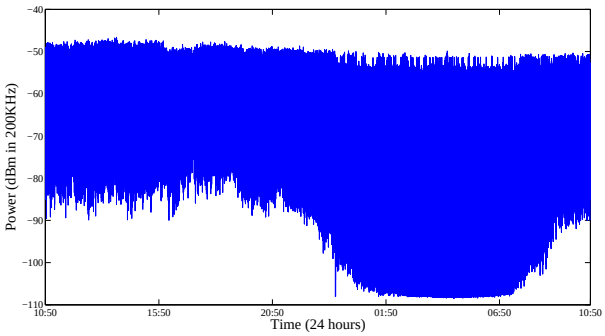

Figure 10. Power in the $953.9 - 954.1MHz$ band during one day

Measurements were made during four consecutive working days and the power profile was similar between days. Figure 10 presents the power variation at the $953.9 - 954.1MHz$ band in one of the four days measured. The correspondent power occurrence is presented in Figure 11.

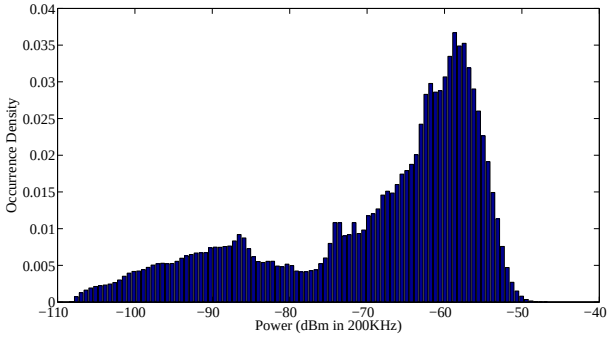

Figure 11. Power Occurrence Density in the $953.9 - 954.1MHz$ band during one day

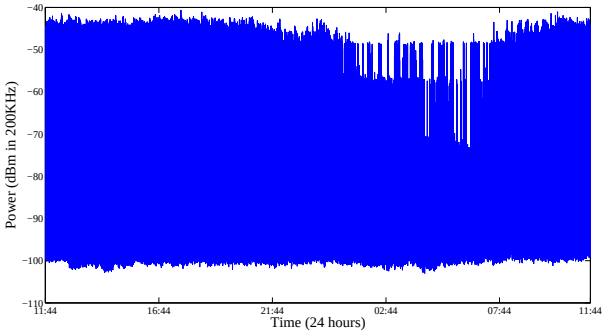

Figure 12. Power in the $1856.9 - 1857.1MHz$ band during one day

In Figure 12 is presented the power variation during a working day in the band of $1856.9 - 1857.1MHz$. The correspondent histogram is presented Figure 13.

For the time statistics a threshold must be defined. The threshold was set approximately $10dB$ above the noise level, just a few dBs below the minimum level needed to detect the signal with an adequate error probability. The decision level for GSM900 was $-98dBm/200KHz$ and $-90dBm/200KHz$ for DCS1800.

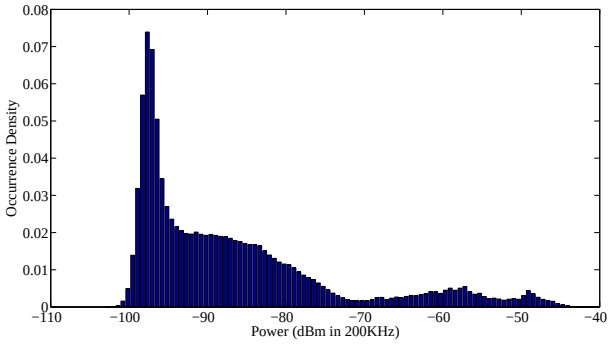

Figure 13. Power Occurrence Density in the $1856.9 - 1857.1MHz$ band during one day

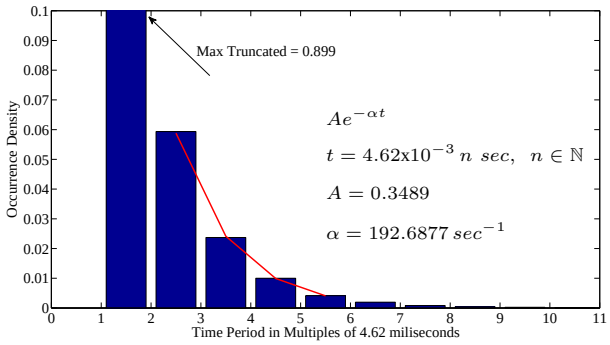

Figure 14. Time period of opportunities distribution of the measured GSM900 band

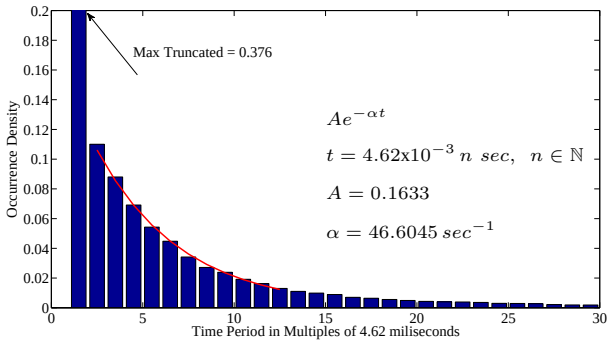

Figure 15. Time between opportunities distribution of the measured GSM900 band

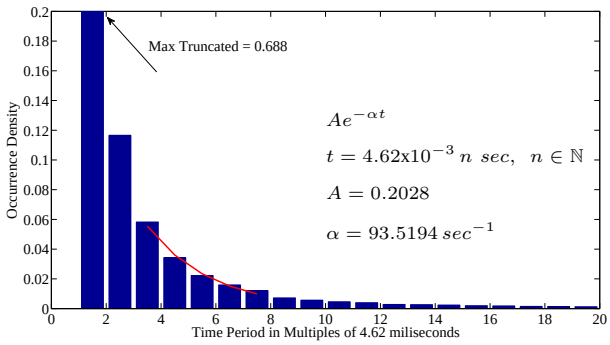

Figure 16. Time period of opportunities distribution of the measured DCS1800 band

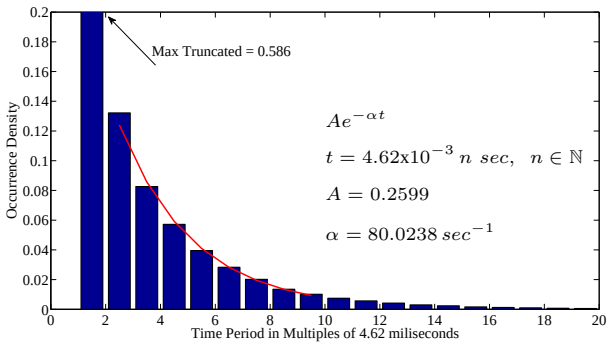

Figure 17. Time between opportunities distribution of the measured DCS1800 band

Figure 14 shows the time period of opportunities distribution for the measured GSM900 band. By doing the logarithmic of the vertical axes (turns an exponential in a straight line) it can be concluded that this distribution has an exponential behavior with the first bin ill-conditioned. An approximated straight line is obtained by the least square method. The parameters of the this straight line provide the parameters of the exponential by reverting the logarithm of the vertical axes. Figure 14 also presents the exponential approximation function (in red) and the correspondent parameters for the well conditioned bins. The total time of the opportunities is about 50 minutes in 24 hours which indicates high occupancy. About 39 minutes (of 50) is one frame opportunities. This particular band was one with lowest traffic of the entire GSM900 spectrum. Thus it can be concluded that the GSM900 spectrum is not usable for opportunistic use due to high occupancy. Figure 15 represents the correspondent time between opportunities distribution. This distribution has an exponential behavior with the first bin ill-conditioned.

Figure 16 shows the time period of opportunities distribution for the measured DCS1800 band. This distribution presents an exponential behavior with the first and second bin ill-conditioned. The total time of the opportunities is about 10 hours in 24 hours, which indicates relative low occupancy. About 2.4 hours (of 10) is one frame opportunities. It is found opportunities as long as 28 seconds (outside the horizontal axes represented in Figure 16). Figure 17 represents the correspondent time between opportunities distribution. This distribution has an exponential behavior with the first bin ill-conditioned.

V. Conclusions

In this article a measurement setup was presented and analyzed. Measurements were taken in GSM900 and DCS1800 frequency. Concerning the time period of opportunities for the measured GSM900 band from the statistic analysis, it can be concluded that the distribution has an exponential behavior with the first bin ill-conditioned. The correspondent time period between opportunities distribution (estimation) also has an exponential behavior, with first bin ill-conditioned. This GSM900 frequency has a high occupancy. The time period of opportunities distribution for the measured DCS1800 band has an exponential behavior with the first and second bin ill-conditioned. The correspondent time period between opportunities distribution has an exponential behavior, with the first bin ill-conditioned. This DCS1800 frequency has enough low occupancy to enable opportunistic use.

Acknowledgments

We would like to thank the Portuguese Communications Regulator (ANACOM) and Vodafone Portugal for the information provided. The research leading to these results was derived from the European Community's Seventh Framework Programme (FP7) under Grant Agreement number 248454 (QoSMOS) and Foundation for Science and Technology (FCT) project AGILE.

References

[1] P. Marques, H. Marques, J. Ribeiro, and A. Gameiro, "Coexistence Analysis and Cognitive Opportunities Selection in GSM Bands," in *IEEE 69th Vehicular Technology Conference. VTC Spring*, (Barcelona, Spain), 26-29 April 2009.

[2] M. López-Benítez and F. Casadevall, "Spectrum Occupancy in Realistic Scenarios and Duty Cycle Model for Cognitive Radio," *Advances in Electronics and Telecommunications*, vol. 1, pp. 26–34, April 2010.

[3] M. López-Benítez, F. Casadevall, A. Umbert, J. Pérez-Romero, R. Hachemani, J. Palicot, and C. Moy, "Spectral Occupation Measurements and Blind Standard Recognition Sensor for Cognitive Radio Networks," in 4^{th} *International Conference on Cognitive Radio Oriented Wireless Networks and Communications (CROWNCOM)*, (Hannover, Germany), 22-24 June 2009.

[4] A. Carniani, L. Giupponi, and R. Verdone, "Evaluation of Spectrum Opportunities in the GSM Band," in *European Wireless Conference (EW)*, (Lucca, Italy), 12-15 April 2010.

[5] R. Schiphorst and C. H. Slump, "Evaluation of Spectrum Occupancy in Amsterdam Using Mobile Monitoring Vehicles," in *IEEE* 71^{st} *Vehicular Technology Conference (VTC2010-Spring)*, (Taipei, Taiwan), 16-19 May 2010.

[6] V. Blaschke, H. Jaekel, T. Renk, C. Kloeck, and F. K. Jondral, "Occupation Measurements Supporting Dynamic Spectrum Allocation for Cognitive Radio Design," in 2^{nd} *International Conference on Cognitive Radio Oriented Wireless Networks and Communications (CROWNCOM)*, (Orlando, Florida, USA), 1-3 Aug. 2007.

EUROPEAN TRANSACTIONS ON TELECOMMUNICATIONS
Eur. Trans. Telecomms. 2008; **19**:495
Published online 21 April 2008 in Wiley InterScience
(www.interscience.wiley.com). DOI: 10.1002/ett.1297

Erratum: Multi-Sensor frequency domain multiple access interference canceller for DS-CDMA systems

(*Eur. Trans. Telecomms.* 2007; **18**:263–273)

Luis Gonçalves and Atílio Gameiro

In the article [page 264] ''. . . to situations where signals with different code lengths coexist'' should read ''. . . to situations where signals with different channelization code lengths coexist''.
In the article [page 267] equation (19) should read

$$s(t) = \sum_{l=0}^{\frac{Q_{\max}}{Q}-1} \sum_{k} a_k^l g_l(t - kT_{max})$$

and equation (22) should read

$$r(t) = \sum_{u=1}^{U} \sum_{l=0}^{\frac{Q_{\max}}{Q_u}-1} \sum_{k} a_k^{l,u} g_l^{(u)}(t - kT_{max}) + n(t)$$

where T_{max} is the symbol period of the users of spreading factor Q_{max}. Q_{max} is the maximum spreading factor in the system.

Multi-Sensor Frequency Domain Multiple Access Interference Canceller for DS-CDMA Systems

Luis Gonçalves [1,3], Atílio Gameiro[2,3]
[1]Departamento de Matemáticas e Engenharias, Universidade da Madeira, Portugal
[2]Departamento de Electrónica e Telecomunicações, Universidade de Aveiro, Portugal
[3]Instituto de Telecomunicações, Campus Universitário de Santiago, 3810-193 Aveiro, Portugal
email: *luisgo@uma.pt*, *amg@det.ua.pt*
DOI Link: http://doi.wiley.com/10.1002/ett.1146

Abstract

Direct Sequence Code Division Multiple Access (DS-CDMA) signals exhibit cyclostationary properties which imply redundancy between frequency components separated by multiples of the symbol rate. In this paper a Multiple Access Interference (MAI) Canceller (Frequency Shift Canceller (FSC)) that explores this property is presented. The linear frequency domain canceller operates on the spreaded signal so as to minimise the interference and noise at the output (Minimum Mean Squared Error Criterium). The performance of multi-sensor configurations for the cases of beamforming and uncorrelated spatial channels was evaluated considering both synchronous (UMTS-TDD) and time misalignment systems. The FSC configurations were concatenated with 2D-PIC structure and evaluated. The simulation results show considerable improvement relative to the conventional 2D-RAKE and 2D-PIC receiver. A performance close to the single-user RAKE case was achieved when it was evaluated jointly with 2D-PIC.

1 Introduction

Direct sequence Code Division Multiple Access (DS-CDMA) has emerged as one of the most promising techniques to implement various radio communication systems. It presents significant advantages over Time Division Multiple Access (TDMA), in terms of its adoption, frequency diversity, multipath diversity and enhanced spectrum efficiency in multi-cell systems [1]], which led as the candidate choice for third generation cellular systems. The first version of third generation CDMA systems is based on the conventional RAKE receiver, which is known to be limited by multiple access interference (MAI) and requires very precise power control. To overcome these limitations, joint detection of the received DS-CDMA signals has been proposed at the base station (BS) or at the user equipment. The optimum joint detector [2] , although well known, results in prohibitively high computational complexity, and consequently effort has been made to devise suboptimum algorithms [3–7] with good tradeoff between performance and complexity that can be implemented at low cost in future CDMA systems. In this paper, we propose a low complexity MAI canceller whose approach can be considered a feasible solution for broadband DS-CDMA signals.

A DS-SS signal is a particular case of a random pulse amplitude modulation. It is well known [8] that these signals exhibit cyclostationary properties which imply redundancy (diversity) between frequency components separated by multiples of the symbol rate. This characteristic is explored in the proposed MAI canceller, named hereafter as the Frequency Shift Canceller (FSC) detector.

The canceller fits in the category of frequency shift (FRESH) filters [9] which are structures that use the correlation between bands inherent in most man made signals. The use of FRESH filters has been proposed for signal extraction of Multi-user Direct Sequence signals [10, 11].

Most of the work on such type of structures reported in the literature follows a time domain approach. In this paper, we explore the correlation between frequency bands to remove the MAI in Multi-user Direct Spread Spectrum Signals, but in terms of implementation consider a frequency domain approach, and extend the algorithm to situations where signals with different code lengths coexist. The frequency domain approach enables digital implementation using fast fourier transform (FFT) modules, allowing significant complexity savings, while the generalisation to variable length spreading codes allows direct application of the canceller with UMTS systems. Approximately the complexity of the algorithm per user and antenna requires the inversion of an Hermitian Definite positive matrix per symbol. The size of the matrix is equal to the number of redundant frequency bands considered and must be at least equal to the number of users if perfect signal extraction is to be achieved in the absence of noise. Considering noise, the performance can be improved by using a higher number of frequency bands, whose maximum number depends on the code length and excess bandwidth of the pulse shaping filter. Currently the implementation of real time matrix inversion is not a constrain in the advent of specific ASIC processors that accelerates this function.

It is consensual that the use of antenna arrays is a key component to increase the capacity cellular systems [12, 13]. The performance and complexity of a multi-sensor detector is dependent on the array/multipath processing and multi-user detection units [14] and therefore we investigate several array processing configurations for the multi-sensor FSC, and consider the cases of high correlation between antenna elements channels (beamforming) and low correlation (diversity).

The paper is outlined as follows: in Section 2 we present the theoretical framework and show that in a DS-SS signal non-overlapping frequency bands separated by a multiple of the baud rate are linearly related; in Section 3 the architecture and design principles of a MAI canceller are presented; in Section 4 several configurations involving the detector FSC are presented; in Section 5 simulation results are presented for a given scenario in a UMTS-TDD system and in a time misalignment system; Finally in Section 6 the main conclusions of this work are outlined.

2 Theoretical Background

A DS-SS signal is represented as

$$s(t) = \sum_k a_k g(t - kT) \tag{1}$$

where $\{a_k\}$ is the sequence of information symbols, $\frac{1}{T}$ the symbol rate and $g(t)$ is the signature waveform, which assuming a spreading factor Q_{max} can be written as

$$g(t) = \sum_{q=0}^{Q_{\max}-1} c_h p(t - qT_c) * h(t) \tag{2}$$

where $\{c_h\}$ is the code sequence, $p(t)$ the normalized elementary pulse, T_c the chip period, $h(t)$ is a linear filter that may represent a channel impulse response and the symbol * stands for convolution.

The Fourier Transform of $s(t)$ is

$$S(f) = \sum_k a_k G(f) e^{-j2\pi fkT} = G(f)A(f) \tag{3}$$

with

$$\begin{aligned} A(f) &= \sum_k a_k e^{-j2\pi fkT} \\ G(f) &= P(f)H(f) \sum_{v=0}^{Q_{\max}-1} c_v e^{-j2\pi f\, vT_c} \end{aligned} \tag{4}$$

From (4) it is easy to verify that

$$A(f + \tfrac{i}{T}) = A(f)\ \forall i \in \mathbb{Z} \tag{5}$$

Assuming that the elementary pulse $p(t)$ has a bilateral bandwidth $\frac{\alpha}{T_c}$, where typically (for pulse of the raised cosine family) α is a number between one and two, we can say that the signal bandwidth is $\frac{\alpha Q_{max}}{T}$ *i.e.* from (5) we have a αQ_{max} order frequency diversity.

Let us define

$$\begin{aligned} S_{mB}(f) &= S\left(f + \frac{m}{T}\right) rect\,(fT) \\ G_{mB}(f) &= G\left(f + \frac{m}{T}\right) rect\,(fT) \end{aligned} \tag{6}$$

where

$$rect(f) = \begin{cases} 1 & \text{if } f \in \left[-\frac{1}{2}, \frac{1}{2}\right[\\ 0 & \text{if } f \notin \left[-\frac{1}{2}, \frac{1}{2}\right[\end{cases} \tag{7}$$

and m is the index of the band. Hereafter the subscript $_B$ means a signal frequency shifted to baseband. Then using (6) for two bands of index m_1 and m_2 and assuming $G_{m_1B}(f)$ has no singularities, it can be concluded that in the interval $f \in \left[-\frac{1}{2T}, \frac{1}{2T}\right[$ we have that

$$S_{m_2B}(f) = \frac{G_{m_2B}(f)}{G_{m_1B}(f)} S_{m_1B}(f) \tag{8}$$

that is the signal information in non-overlapping frequency bands spaced by a multiple of the baud rate are related through a linear transformation.

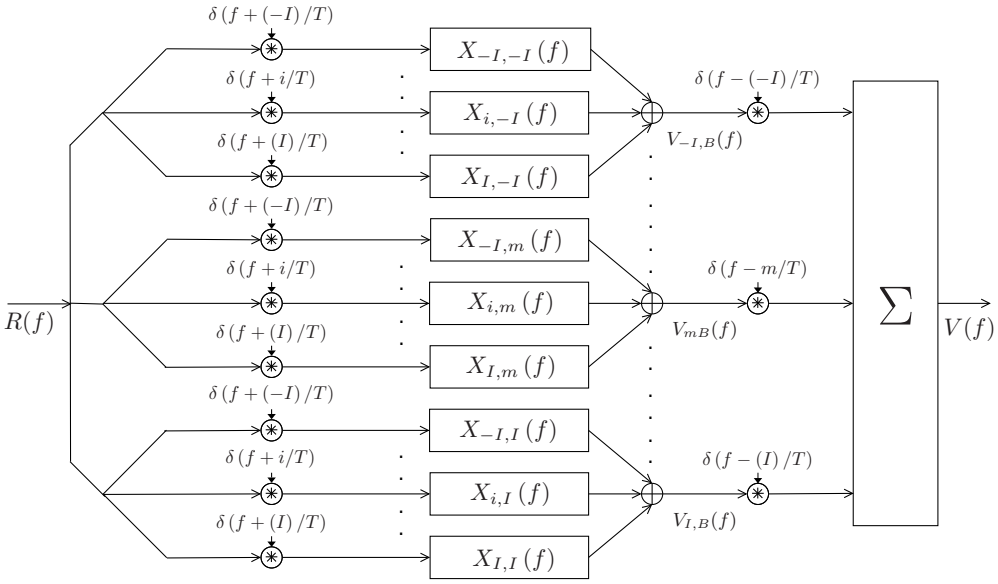

Figure 1: Conceptual Schematic of the Canceller.

3 Canceller Architecture

The canceller operates in the frequency domain but in practical implementation or simulation, the time to frequency domain conversion will be performed digitally through a FFT. However, in the derivations we shall use a continuous representation for the functions

The architecture of the canceller is shown in Figure 1, for a given user. The symbol * stands for convolution and δ is the Dirac impulse.

Assuming U users, the input signal in the frequency domain is given by

$$R(f) = \sum_{u=1}^{U} S^{(u)}(f) + N(f) \tag{9}$$

where $N(f)$ is the Fourier transform of the additive noise, with power spectral density $\eta_{in}(f)$ and $S^{(u)}(f)$ is the Fourier transform of $s^{(u)}(t)$ where the superscript $^{(u)}$ refers to the user.

In the base station where all the signals have also to be recovered, the canceller consists of the replica of this basic receiver for each user. However, it can be applied to the mobile station provided the codes for the different users are known.

We shall start by considering the case where all the users have the same spreading factor and then proceed with the generalization for multirate.

3.1 Identical Spreading Factor

Let us consider without loss of generality that user one is the user of interest. From (8) this constraint implies that the filters $X_{i,m}(f)$ be of the form

$$X_{i,m}(f) = \alpha_{i,m}(f)\frac{G^{(1)}_{mB}(f)}{G^{(1)}_{iB}(f)}\text{[1]} \tag{10}$$

where $\alpha_{i,m}(f)$ are complex weight functions.

Using (10), the baseband shifts of the output signal $V(f)$ are given by

$$V_{mB}(f) = S^{(1)}_{mB}(f)\left(\sum_{i=-I}^{I}\alpha_{i,m}(f)\right) + \sum_{u=2}^{U}\left[\sum_{k} a_k^{(u)} e^{-j2\pi fkT}\beta^{(u)}_{mB}(f)\right] + N'_{mB}(f) \tag{11}$$

where $S^{(1)}_{mB}(f)$ is defined in (6) and

$$\beta^{(u)}_{mB}(f) = \sum_{i=-I}^{I}\alpha_{i,m}(f)\frac{G^{(1)}_{mB}(f)}{G^{(1)}_{iB}(f)}G^{(u)}_{iB}(f) \tag{12}$$

[1]In case of a singularity with $G^{(1)}_{iB}(f) = 0$ for a particular $f = f_1$ then is considered $X_{i,m}(f_1) = 0$.

From (11) we conclude that the condition that the signal of interest is not distorted is verified provided $\sum_i \alpha_{i,m}(f) = rect(fT)$. The power spectral density of additive noise disturbance at the output $N'_{mB}(f)$ is given by

$$\eta_{out_{mB}}(f) = \sum_{i=-I}^{I} |\alpha_{i,m}(f)|^2 \left| \frac{G^{(1)}_{mB}(f)}{G^{(1)}_{iB}(f)} \right|^2 \eta_{in_{iB}}(f) \tag{13}$$

The minimization of the output overall disturbance can be achieved, minimizing the power spectral density of the error term in (11) assuming that the information data sequences $\{a^{(u)}_k\}$ are sequences of *i.i.d.* random variables with $E[a^{(u)}_k] = 0$ and $E\left[\left|a^{(u)}_k\right|^2\right] = 1$. Defining the error function as $e(f) = \left(V_{mB}(f) - S^{(1)}_{mB}(f)\right)$ in (11) assuming that $\sum_i \alpha_{i,m}(f) = rect(fT)$ we get

$$C_m(f) = E\left[|e(f)|^2\right] = L_s \sum_{u=2}^{U} \left|\beta^{(u)}_{mB}(f)\right|^2 + \eta_{out_{mB}}(f) \tag{14}$$

where L_s correspond to the number of symbols existing in one burst. The quantity $E\left[|e(f)|^2\right]$ is the Mean Square Error to be minimized.

The objective and design criteria for the canceller is to minimize the overall disturbance (MAI+noise) subject to the condition that $S^{(1)}(f)$ is not distorted. Therefore if for each frequency f and output band m we minimize the power spectral density of the disturbance, then the overall power is minimised and can be expressed as

$$C_m(f) = \left|G^{(1)}_{mB}(f)\right|^2 \left[L_s \sum_{u=2}^{U} \left| \sum_{i=-I}^{I} \left(\alpha_{i,m} \frac{G^{(u)}_{iB}(f)}{G^{(1)}_{iB}(f)} \right) \right|^2 + \sum_{i=-I}^{I} \left(|\alpha_{i,m}(f)|^2 \frac{\eta_{in_{iB}}(f)}{\left|G^{(1)}_{iB}(f)\right|^2} \right) \right] \tag{15}$$

This is equivalent to minimising the terms inside the rectangular brackets in (15) and consequently the optimum values of $\alpha_{i,m}$ are identical for each m, that is $\widehat{\alpha}_{i,m} = \widehat{\alpha}_i \quad \forall m$. Under these conditions we get

$$\begin{cases} \{\widehat{\alpha}_i(f)\} = \arg \min\limits_{\{\alpha_{i,m}(f)\}} [F_m(f)] \\ \sum\limits_{i=-I}^{I} \alpha_{i,m}(f) = rect(fT) \end{cases} \tag{16}$$

where $F_m(f) = \frac{C_m(f)}{\left|G^{(1)}_{mB}(f)\right|^2}$.

Let us consider (16) for a particular f, where for simplicity of notation we drop the frequency variable in the different functions and the subscript m in the variables $\alpha_{i,m}$.

The function F in (16) can be represented by the Hermitian form

$$F(\{\alpha_i\}) = \boldsymbol{\alpha}^{\boldsymbol{H}} \mathbf{He}\, \boldsymbol{\alpha} \tag{17}$$

The matrix $\mathbf{He}$ is the Hessian Matrix (Appendix A) and $\boldsymbol{\alpha} = [\alpha_i]_{i \in \{-I,\ldots,I\}}$.

The optimum weights $\{\alpha_i\}$ are found by the minimum of F with the restriction $\sum\limits_{i=-I}^{I} \alpha_i(f) = 1$. Applying the method of Lagrange multipliers the minimum of F is found at

$$\boldsymbol{\alpha} = \mathbf{He}^{-\mathbf{1}} \boldsymbol{\varphi} \tag{18}$$

where $\boldsymbol{\varphi}$ is a $2I+1$x1 vector with equal elements given by $1 \Big/ \sum\limits_{l=1}^{2I+1} \sum\limits_{c=1}^{2I+1} \mathrm{He}^{-1}_{l,c}$ being $\mathrm{He}^{-1}_{l,c}$ the element of line l^{th} and column c^{th} of the inverse of the Hessian.

The Hessian matrix is Hermitian definite positive (Appendix A) and it can be inverted through the Cholesky decomposition.

3.2 Multi-rate Generalization

Let us consider now the case of users with different spreading factors, which is of interest for UMTS-TDD. This standard was designed to accommodate multiple symbol rates by using different spreading factors. In the standard the spreading code is defined as the product between the channelization and the scrambling code. The channelisation code is used to spread a data symbol, whilst the scrambling code lasts for Q_{max} chips or during $\frac{Q_{max}}{Q}$ symbols where Q is the

spreading factor. Then to construct the spreading code, the channelization code must be repeated $\frac{Q_{max}}{Q}$ and multiplied by the scrambling code. The spreading code extends for more than one symbol when $Q \neq Q_{max}$.

The extension of the canceller to multi-rate can be easily performed by considering that a DS signal with spreading factor $Q = \frac{Q_{max}}{Z}$ can be decomposed as the sum of Z signals with spreading factor Q_{max}, where Z is a divisor of Q_{max}, and since in commercial systems as UMTS-TDD, Q_{max} is a power of two, then Z can be any power of 2 lower than Q_{max}.

The time domain representation of an information sequence using a spreading factor of Q is given by then

$$s(t) = \sum_{l=0}^{\frac{Q_{\max}}{Q}-1} \sum_{k} a_k^l g_l \left(t - \tfrac{Q_{\max}}{Q} kT\right) \tag{19}$$

where $\{a_k^l\}$ are the sequences of information symbols, $\frac{1}{T}$ the symbol rate and $g_l(t)$ the components of signature waveform. The components of the signature waveform at the receiver are given by

$$g_l(t) = \sum_{q=0}^{Q_{\max}-1} c_q^l p(t - qT_c) * h(t) \tag{20}$$

where $p(t)$ is the normalized elementary pulse, $h(t)$ is a linear filter and $\{c_q^l\}_{q=0}^{Q_{max}-1}$ is given by

$$\{c_q^l\}_{q=0}^{Q_{max}-1} = (\underbrace{0, ..., 0}_{Ql \text{ zeros}}, \widetilde{c}_{Ql}, ..., \widetilde{c}_{Q(l+1)-1}, \underbrace{0, ..., 0}_{Q_{\max}-Q(l+1) \text{ zeros}}) \tag{21}$$

where $\{\widetilde{c}_q\}_{h=0}^{Q_{max}-1}$ is the spreading sequence.

The composite signal at the receiver is given by

$$r(t) = \sum_{u=1}^{U} \sum_{l=0}^{\frac{Q_{\max}}{Q_u}-1} \sum_{k} a_k^{l,u} g_l^{(u)} \left(t - \tfrac{Q_{\max}}{Q_u} kT\right) + n(t) \tag{22}$$

where Q_u is the spreading factor of user u, and therefore assuming the information data sequences for each user consist of *i.i.d.* random variables, the signal of (22) can be interpreted as a composite signal consisting of $Z_U = \sum_{u=1}^{U} \frac{Q_{max}}{Q_u}$ DS-SS signals all of them with spreading factor of Q_{max}. Therefore the canceller will operate as the single rate case for a total of Z_U users where $Z_U \leq Q_{max}$.

4 Application of the Canceller to UMTS-TDD

To evaluate the canceller performance a simulation chain was implemented. Consisting of transmitters compliant with 3GPP specs of UMTS-TDD [15], a channel block and a multiuser receiver that can take several configurations. The processing is made in burst by burst basis and in the discrete domain. The channel parameters are assumed to be constant within each burst and assumed to be known.

The discrete impulse response of the channel for each burst is given by

$$w^{(u,a)}(n) = \sum_{l'=1}^{L} \alpha_{u,l',a} \gamma \left(\theta_{u,l'}; a\right) \delta_{kr} \left(n - \tau_{u,l',a}\right) \tag{23}$$

where $\alpha_{u,l',a}$ is the complex amplitude of the tap, $\tau_{u,l',a}$ is the delay of the tap in samples, δ_{kr} is the Kroneker impulse and $\gamma(\theta_{u,l'}; a)$ is in case of beamforming a complex amplitude of unitary modulus and phase dependent of the angle of arrival of the tap $\theta_{u,l'}$, on the geometry and antenna element of the array (24). The variable u is the index of the user, l' the index of the tap and a the index of the antenna. In beamforming configuration we drop the dependency on antenna a in $\alpha_{u,l',a}$ and $\tau_{u,l',a}$ because those parameters are equal in all antennas for the same user and tap. In the configurations with beamforming, the receptor sensor is a circular array of four antennas with 0.45λ spacing between elements (with 0.5λ arc between elements). In that case [16]

$$\gamma \left(\theta_{u,l'}; a\right) = e^{-j\frac{2\pi}{\lambda} R_c cos\left(\theta_{u,l'} - \frac{2\pi(a-1)}{A}\right)} \tag{24}$$

where A is the number of elements of the array, $a \in \{1, ..., A\}$ is the index of the antenna, R_c is the radius of the antenna and λ is the wavelength. In space diversity, the antennas are spaced sufficiently apart that the channel of each other are uncorrelated. In that case $\gamma(\theta_{u,l'}; a) = 1$.

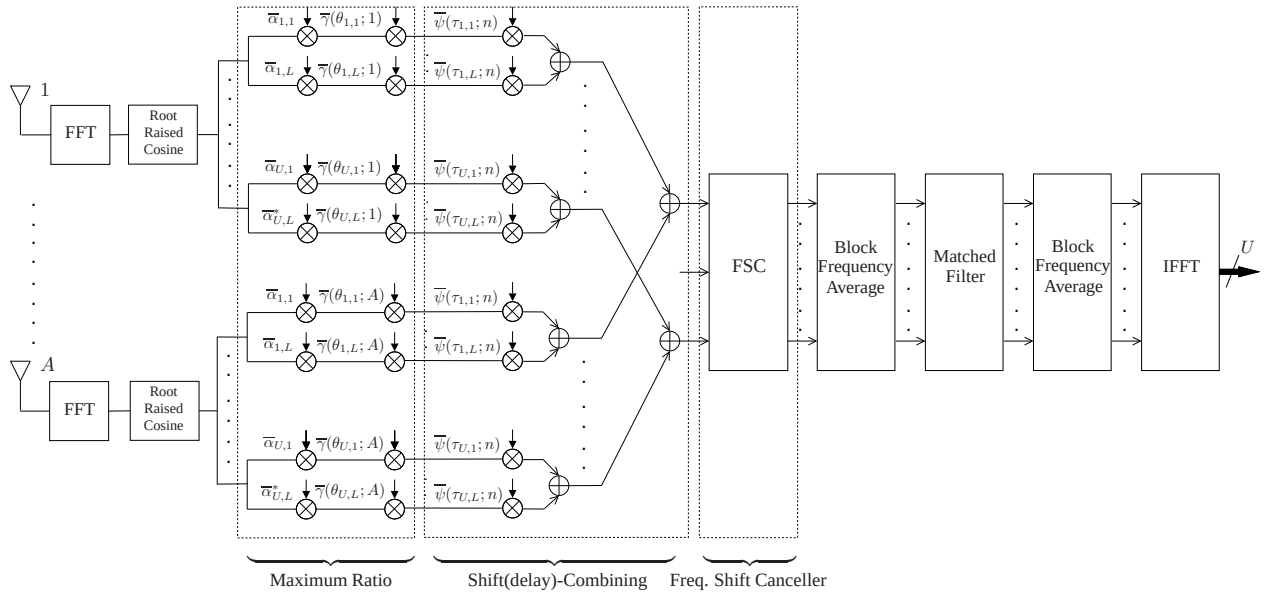

Figure 2: Configuration MaxRat-ShiftComb-FSC with multiple antennas and beamforming.

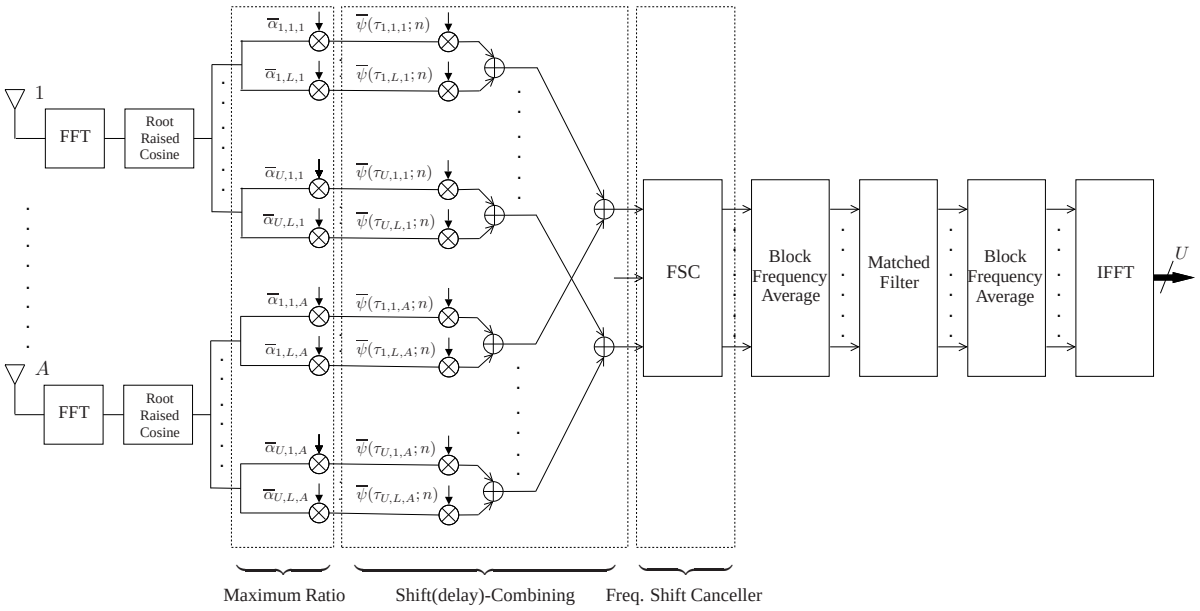

Figure 3: Configuration MaxRat-ShiftComb-FSC with multiple antennas and spatial diversity.

The corresponding channel frequency response is

$$W^{(u,a)}(n) = \sum_{l'=1}^{L} \alpha_{u,l',a} e^{-j2\pi\tau_{u,l',a} n/M} \gamma\left(\theta_{u,l'}; a\right) = \sum_{l'=1}^{L} \alpha_{u,l',a} \psi\left(\tau_{u,l',a}; n\right) \gamma\left(\theta_{u,l'}; a\right) \tag{25}$$

where M is the number of points of the FFT.

The channel model used in this work was the Geometrical Based Single Bounce Elliptical Model (GBSBEM) proposed by Liberti [17]. This model was developed for microcell and picocell environments. The propagation channel is characterized by one line of sight (LOS) tap and $L-1$ taps for each user arriving from remote reflectors located randomly within an ellipsis where the base station and the mobile unit are at the foci.

The delay of each tap including the LOS tap is a random variable characterized by a probability density function whose expression can be found in [17]. After evaluating the delays of the taps, all LOS taps delays of all users are synchronized and the others shifted accordingly. The phase of the tap is uniformly distributed in $[0, 2\pi[$. The amplitude of the tap is obtained from a constant, dependent of the distance followed by the tap (it is proportional to $1/d_i^{pl}$ where d_i is the distance and pl is the pathloss exponent) and normalized (such that the sum of the power of all taps of that user is equal to one; in case of spatial diversity is equal to the number of antennas instead of one) times a random variable with

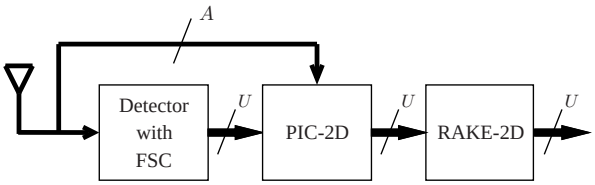

Figure 4: Receiver including FSC plus PIC-2D.

Table 1: Configurations simulated

	Operation Order			
Name	Unit 1	Unit 2	Unit 3	Unit 4
MaxRat-ShiftComb-FSC	Maximum Ratio	Shift(delay)-Combining	Freq. Shift Canceller	
MaxRat-FSC-ShiftComb	Maximum Ratio	Freq. Shift Canceller	Shift(delay)-Combining	
FSC-MaxRat-ShiftComb	Freq. Shift Canceller	Maximum Ratio	Shift(delay)-Combining	
MaxRat-ShiftComb-FSC+PIC	Maximum Ratio	Shift(delay)-Combining	Freq. Shift Canceller	PIC
MaxRat-FSC-ShiftComb+PIC	Maximum Ratio	Freq. Shift Canceller	Shift(delay)-Combining	PIC
FSC-MaxRat-ShiftComb+PIC	Freq. Shift Canceller	Maximum Ratio	Shift(delay)-Combining	PIC

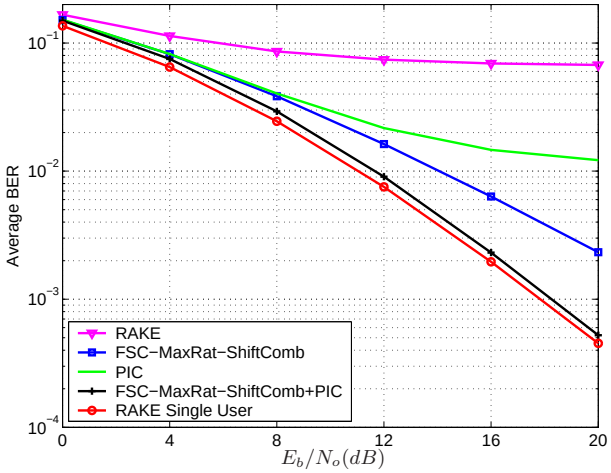

Figure 5: Single Antenna, UMTS-TDD System

Rayleigh distribution. The complex amplitude (amplitude and phase of the tap) is Doppler filtered.

In this model the angle of arrival (AOA) of the LOS tap of each user is fixed for one simulation and the angles of the other taps are random variables with mean equal to the AOA of LOS tap and a distribution given by [17]. Figures 2 and esquema2 each present a configuration including the FSC with beamforming and spatial diversity respectively. All other configurations presented in Table 1 are obtained by reordering the macro-blocks: Maximum Ratio, Shift(delay)-Combining and Frequency Shift Canceller

All configurations reduce to the RAKE-2D when the FSC operation is removed. In figures 2 and 3 the Block Frequency Average corresponds to a downsampling in time domain. The first downsampling factor is equal to the number of samples per chip, as the second downsampling aims to provide one sample per symbol and is thus equal to Q_{max}. So the length of the IFFT performed at the end of the chain is smaller than the FFT performed at the beginning. The transfer function of the matched filter is given by $FFT\left[\overline{o}\left(\Delta - n\right)\right]$ [18] where $o\left(n\right)$ is the user spreading code (discrete). The constant Δ is such that $\overline{o}\left(\Delta - n\right)$ is causal. The functions $\overline{\psi}(\tau_{u,l'}; n)$ and $\overline{\psi}(\tau_{u,l',a}; n)$ in Figures 2 and 3 respectively corresponds to a delay of $-\tau_{u,l'}$ and $-\tau_{u,l',a}$ in the time domain (Table 1).

Following (20) the FSC requires as parameters the discrete version of the linear response of the link up to its input, that is the concatenation of the channel impulse response, the root raised cosine filter and the blocks Maximum Ratio, Shift(delay)-Combining. For example for the configuration of Fig. 3 we get

$$h^{(b,u)}(n) = \sum_{a=1}^{A} \sum_{f=1}^{F} \sum_{l'=1}^{L} \alpha_{u,l',a} \overline{\alpha}_{b,f,a} \delta_{kr} \left(n - \tau_{u,l',a} + \tau_{b,f,a} \right) * Irrc(n) \tag{26}$$

Table 2: Simulation parameters settings

Redundant Bands	18
Number of Taps (per user and antenna)	2
Velocity	50 Km/h
Path Loss Exponent	3.7
Maximum Delay Spread	2.0 μs
Number of samples per chip	4
Line of Sight Distance	300m
Number of Array Elements	4

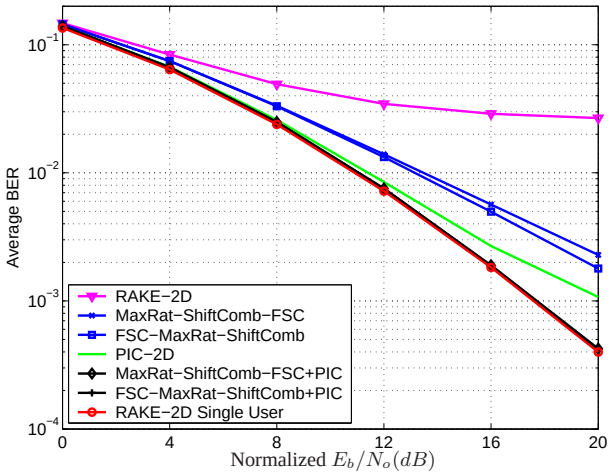

Figure 6: Beamforming, Circular Array, four antennas (A), UMTS-TDD System

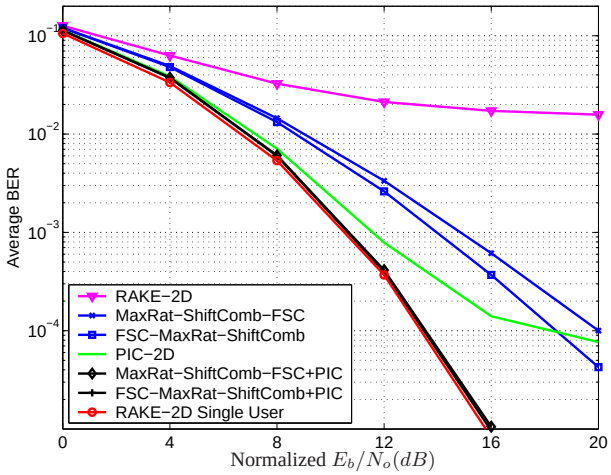

Figure 7: Spatial Diversity, four antennas (A), UMTS-TDD System

where b could take the values $b \in \{1, \ldots, U\}$ representing each input burst in the FSC corresponding to each user to be recovered. Each burst have also signal components of all users. Each user in each burst is represented by $u \in \{1, \ldots, U\}$. The letter L represents the number of taps of the transmission channel (for each user and antenna) and F represents the number of fingers of Maximum Ratio and Shift(delay)-Combining blocks (for each antenna and burst). In figure 3 $F = L$. The $Irrc(n)$ function is the impulse response of the root raised cosine. The discrete fourier transform of $h^{(b,u)}(n)$ is straight forward to calculate.

For configuration of figure 3 the power spectral density of the noise is given

$$\eta_{in}^{(b)} = \sum_{a=1}^{A} \left| W^{(b,a)}(n) \right|^2 |RRC(n)|^2 \eta^{(a)}(n) \tag{27}$$

where $\eta^{(a)}(n)$ is the power spectral density of noise in each antenna, $RRC(n)$ is the frequency domain root raised cosine and $W^{(b,a)}(n)$ is defined in (25). For the other cases the expressions equivalents to (26) and (27) can be easily derived.

The other detector configurations to be evaluated are the detectors with FSC concatenated with a single stage hard 2D-PIC (fig. 4). The reference configurations are the conventional 2D-RAKE and the conventional single stage 2D-PIC.

5 Simulation Results

In this section some numerical results are presented illustrating the performance of the proposed detector configurations with UMTS-TDD system and with time misalignment system. The simulations, whose results are presented in Figures 5, 6 and 7 were made with the parameters shown in Table 2 and considering the following scenario

- Number of users equal to eight, of which four use a spreading factor of 16, two a spreading factor of 8 and two a spreading factor of 4. This corresponds to a fully loaded system.
- The power assigned to each user is such that the Energy per Bit over the Spectral Density of Noise ($\frac{E_b}{N_0}$) is identical for all and therefore the power assigned to the users with spreading factor of eight and four is respectively 3 db and 6 db above the power assigned to the user with spreading factor of 16.

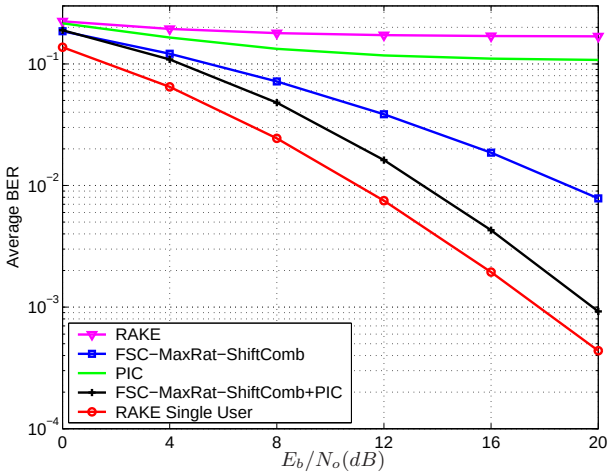

Figure 8: Single Antenna with time misalignment system

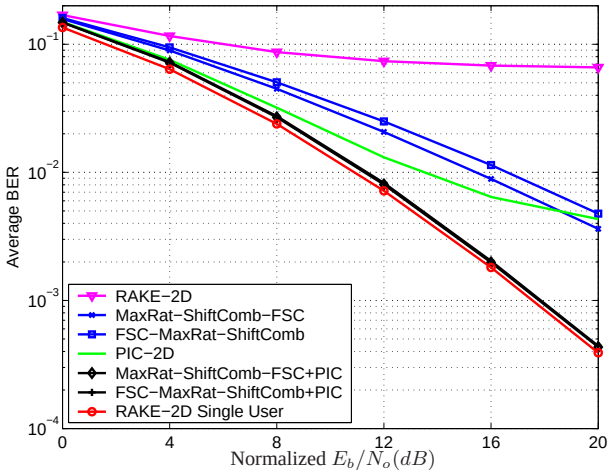

Figure 9: Beamforming, Circular Array, four antennas (A) with time misalignment system

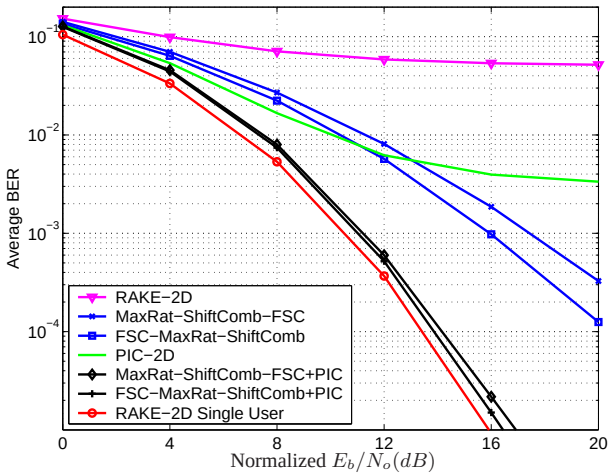

Figure 10: Spatial Diversity, four antennas (A) with time misalignment system

The results presented are only for the users with a spreading factor equal to 16. For the users with spreading factor of four the performance is slightly worst due interpath interference. The results of Fig. 6 and 7 are presented in terms of the normalized $\frac{E_b}{N_o}$ in dB, which is defined as the actual power efficiency minus the diversity antenna array gain $10log_{10}A$ where A is the number of array elements. This is done to ensure that the algorithm is compared on a fair basis and to be able to separate the performance gains due to the algorithm and configuration from the gains due to the existence of diversity only.

For the single antenna case, all configurations exhibit the same performance. For the case of multi-element array the performance differs according to the relative positions of the Shift(delay)-Combining and FSC. Then the configurations FSC-MaxRat-ShiftComb and MaxRatFSC-ShiftComb have the same performance. Although the configuration MaxRat-ShiftComb-FSC gives the worst performance, in terms of complexity this configuration only needs 1/A the amount of matrix inversions in relation to the FSC-MaxRat-ShiftComb configuration (A is the number of antennas).

From Fig. 5, 6 and 7 we observe that either for the cases of beamforming or diversity, the use of the FSC provides considerable gains relatively to the 2D-RAKE and namely eliminates the bit error rate (BER) floor.

For the single antenna case the use of the FSC outperforms the PIC for moderate to high values of $\frac{E_b}{N_o}$. The same behavior is observed with multiple antennas but for higher values of $\frac{E_b}{N_o}$ (not shown in the plots of Fig. 6 e 7).

The use of the FSC with multiple antennas leads to gains compared to the single antenna case a 1.5 dB gain for a uncoded BER of 10^{-2} for the beamforming case, and up to 6 db for the diversity case.

The concatenation of the FSC and 2D-PIC detector nearly eliminates all the interference and the performance observed is almost coincident with the single-user 2D-RAKE performance.

In figures 8, 9 and 10 are presented the simulation results for system with time misalignment. In relation to synchronous system (UMTS-TDD), the channel profile for each user and burst suffers a delay with a uniform distribution from 0 to $1\mu s$.

As expected the results are worst than in UMTS-TDD system, but for multi-antenna scenario the performance approaches the 2D-RAKE single-user case.

6 Conclusions

In this paper we proposed a frequency domain, linear multiuser canceller able to operate with multi-rate signals. The canceller takes advantage of the frequency redundancy inherent in DS-SS signals, and the multi-rate extension was done by verifying that with UMTS-TDD like systems a signal with spreading factor which is a submultiple of the maximum spreading factor can be decomposed in several DS-SS signals each one with maximum spreading factor.

The performance of the canceller was evaluated for several configurations, either as a stand alone unit or concatenated with a PIC. The results have shown considerable improvements relatively to the 2D-RAKE, and with the application of multiple antennas in diversity case a considerable performance improvements was achieved. Furthermore when concatenated with a 2D-PIC, the performance achieved for both beamforming and diversity case is very close to the single-user bound and thus the FSC turns out to be a feasible candidate for interference cancellation and as a mean to provide clean signals to a low complexity PIC that can remove all the interference.

Acknowledgement

The authors would like to acknowledge Dr Cipriano Lomba and Dr Jonathan Rodriguez for their help in the preparation of the paper. This work was supported by a PhD Grant from PRAXIS XXI, Fundação para a Ciência e Tecnologia and the projects ASILUM and VISEF.

A Computation of the Gradient and Hessian

The function to be minimized in (16) is

$$F\left(\{\alpha_i\}_{i\in\{-I,\ldots,I\}}\right) = L_s \sum_{u=2}^{U} \left| \sum_{i=-I}^{I} \left(\alpha_i \frac{G_{iB}^{(u)}}{G_{iB}^{(1)}} \right) \right|^2 + \sum_{i=-I}^{I} \left(|\alpha_i|^2 \frac{\eta_{in_{iB}}}{\left|G_{iB}^{(1)}\right|^2} \right) \tag{28}$$

Assume the following complex constant and positive real constant

$$Z_i^u = \frac{G_{iB}^{(u)}}{G_{iB}^{(1)}} \tag{29}$$

$$X_i = \frac{\eta_{in_{iB}}}{\left|G_{iB}^{(1)}\right|^2} \tag{30}$$

Given a complex function P then $|P|^2 = P\overline{P}$ (It could be identified such functions in (28)) then by inspection of (28) F is a real function dependent on the complex variables $\{\alpha_i\}$ and $\{\overline{\alpha_i}\}$. In this type of functions the stationary points could be taken by the gradient in relation to $\{\alpha_i\}$ or $\{\overline{\alpha_i}\}$ [19]. The gradient in relation to $\{\overline{\alpha_i}\}$ is preferable because the resultant gradient is dependant on the variables α_i.

It is given the following formula $\frac{\partial K(\{z_i,\overline{z_i}\}_i)}{\partial \overline{z_k}} = \frac{1}{2}\left[\frac{\partial K}{\partial x_k} + j\frac{\partial K}{\partial y_k}\right]$ where $z_k = x_k + jy_k$ [19] and K is a real function of complex variables.

Each element of the gradient vector is

$$\frac{\partial F\left(\{\alpha_i\}_{i\in\{-I,\ldots,I\}}\right)}{\partial \overline{\alpha_k}} = L_s \sum_{u=2}^{U} \left(\overline{Z_k^u} \sum_{i=-I}^{I} \left(Z_i^u \alpha_i \right) \right) + \alpha_k X_k \tag{31}$$

where the gradient vector is $\nabla F\left(\{\alpha_i\}_{i\in\{-I,\ldots,I\}}\right) = \left[\frac{\partial F\left(\{\alpha_i\}_{i\in\{-I,\ldots,I\}}\right)}{\partial \overline{\alpha_k}}\right]_{k\in\{-I,\ldots,I\}}$.

The Hessian Matrix is given by

$$\mathbf{He} = \left[\frac{\partial F\left(\{\alpha_i\}_{i\in\{-I,\ldots,I\}}\right)}{\partial \alpha_c \partial \overline{\alpha_k}}\right]_{k\in\{-I,\ldots,I\}, c\in\{-I,\ldots,I\}} \tag{32}$$

The coefficients of the Hessian Matrix are

$$\frac{\partial F\left(\{\alpha_i\}_{i\in\{-I,\ldots,I\}}\right)}{\partial\alpha_c\partial\overline{\alpha_k}} = L_s\sum_{u=2}^{U} Z_c^u\overline{Z_k^u} + X_k \qquad c = k \tag{33}$$

and

$$\frac{\partial F\left(\{\alpha_i\}_{i\in\{-I,\ldots,I\}}\right)}{\partial\alpha_c\partial\overline{\alpha_k}} = L_s\sum_{u=2}^{U} Z_c^u\overline{Z_k^u} \qquad c \neq k \tag{34}$$

The proof that the Hessian is positive definite is implied by the definition of Matrix positive definite. Then given the vector, $\mathbf{x} = [x_{-I},\ldots,x_0,\ldots,x_I]^T$ the following inequality is always true for $\mathbf{x}\in\mathbb{C}^{2I+1}/\mathbf{0}$

$$\left[\mathbf{x^H}\left[\mathbf{He}\right]\mathbf{x}\right] = L_s\sum_{u=2}^{U}\left|\sum_{k=-I}^{I} x_k Z_k^u\right|^2 + \sum_{k=-I}^{I} X_k\left|x_k\right|^2 > 0 \tag{35}$$

when the superscript $^{\mathbf{H}}$ means transpose-conjugate. Then the matrix **He** is Hermitian definite positive and can be inverted by Cholesky decomposition. The Hessian matrix is Hermitian definite positive in all the domain of $\{\alpha_i\}$ and therefore the function F is strictly convex [20]. By the same process can be proved that the Hessian matrix of the function F with the restriction $\sum_{i=-I}^{I}\alpha_i(f) = 1$ (we proved only for F) is strict convex, and the minimum at (18) is global.

References

[1] R. Kohno, R. Meidan, and L. B. Milstein, "Spread Spectrum Access Methods for Wireless Communications," *IEEE Communications Magazine*, vol. 33, pp. 58–67, January 1995. 1

[2] S. Verdú, "Minimum Probability of Error for Asynchronous Gaussian Multiple-Access Channels," *IEEE Transactions of Information Theory*, vol. 32, pp. 85–96, January 1986. 1

[3] Z. Xie, R. T. Short, and C. K. Rushforth, "A Family of Suboptimum Detectors for Coherent Multiuser Communications," *IEEE Journal of Selected Areas in Communications*, vol. 8, pp. 683–690, May 1990. 1

[4] A. Klein and P. W. Baier, "Linear Unbiased Data Estimation in Mobile Radio Systems Applying CDMA," *IEEE Journal of Selected Areas in Communications*, vol. 11, pp. 1058–1066, September 1993. 1

[5] A. Duel-Hallen, "A Family of Multiuser Decision-Feedback Detectors for Asynchronous Code-Division Multiple-Access Channels," *IEEE Transactions on Communications*, vol. 43, pp. 421–434, February/March/April 1995. 1

[6] D. Guo, *Linear Parallel Interference Cancellation in CDMA*. M.Eng. Thesis, National University of Singapore, Dec. 1998. 1

[7] D. Divsalar, M. K. Simon, and D. Raphaeli, "Improved Parallel Interference Cancellation for CDMA," *IEEE Transactions on Communications*, vol. 46, pp. 258–268, February 1998. 1

[8] W. A. Gardner, *Cyclostationarity in Communications and Signal Processing*. IEEE PRESS, 1994. 1

[9] W. A. Gardner, "Cyclic Wiener Filtering: Theory and Method," *IEEE Transactions on Communications*, vol. 41, pp. 151–163, January 1993. 1

[10] J. Zhang, K. M. Wong, Z. Q. Luo, and P. C. Ching, "Blind Adaptative FRESH Filtering for Signal Extraction," *IEEE Transactions on Signal Processing*, vol. 47, pp. 1397–1402, May 1999. 1

[11] J. Whitehead and F. Takawira, "Blind Adaptative Multiuser Detection for Periodically Time Varying Interference Suppression," in *IEEE Wireless Communication and Networking Conference*, (New Orleans, LA, USA), 13-17 March 2005. 1

[12] J. H. Winters, "Smart Antennas for Wireless Systems," *IEEE Personal Communications*, vol. 5, pp. 23–27, February 1998. 2

[13] L. C. Godara, "Applications of Antenna Arrays to Mobile Communications, Part I: Performance Improvement, Feasibility, and System Considerations," *Proceedings of IEEE*, vol. 85, pp. 1031–1060, July 1997. 2

[14] H. C. Huang, *Combined Multipath Processing, Array Processing, and Multiuser Detection for DS-CDMA Channels*. Ph. D. Thesis, Faculty of Princeton, Princeton, USA, 1996. 2

[15] "3GPP TS 25.223," *"Spreading and modulation (TDD)"*, Jan 2004. 5

[16] J. Litva and T. K.-Y. Lo, *Digital Beamforming in Wireless Communications*. Artech House Publishers, Boston, USA, First ed., 1996. 5

[17] J. C. Liberti and T. S. Rappaport, *Smart Antennas for Wireless Communications: IS-95 and Third Generation CDMA Applications*. Prentice Hall, New Jersey, USA, 1999. 6, 7

[18] G. L. Turim, "An Introduction to Matched Filters," *IRE Transactions on Information Theory*, vol. 6, pp. 311–329, June 1960. 7

[19] B. A. D. H. Brandwood, "A Complex Gradient Operator and its Application in Adaptative Array Theory," *IEE Proc., Pts. F and H*, vol. 130, pp. 11–16, February 1983. 10

[20] B. Pchénitchny and Y. Daniline, *Méthodes Numériques dans les Problèmes D'Extrémum*. Éditions MIR, Moscou, 1977. 11